

**Investigating the role of Vasoactive Intestinal Peptide interneurons in the  
mouse Medial Entorhinal Cortex**

Saishree Badrinarayanan

Integrated Program in Neuroscience

McGill University, Montreal

October 2023

A thesis submitted to McGill University in partial fulfillment of the requirements of the degree  
of Doctor of Philosophy in Neuroscience

© Saishree Badrinarayanan 2023

For appa and amma

## Table of Contents

Abstract.....	7
Résumé.....	9
Acknowledgements.....	11
Contribution to Original Knowledge .....	13
Contribution of Authors.....	14
List of Figures and Tables.....	16
List of Abbreviations .....	18
Other Notes.....	20
Introduction: General overview of the thesis.....	21
Chapter 1: A comprehensive review of the literature.....	24
1. 1 Studying spatial navigation in rodents: .....	24
1.1.1 The theory of the cognitive map: Place vs response learning .....	24
1.2 The Hippocampal – Entorhinal circuit:.....	26
1.2.1 The hippocampus and its subdivisions: .....	26
1.2.2 The Medial Entorhinal Cortex (MEC): .....	27
1.3 Spatially tuned cells within the MEC circuitry: .....	29
1.3.1 Grid cells: .....	29
1.3.2 Head Direction cells: .....	30
1.3.3 Border cells:.....	31
1.3.4 Object vector cells: .....	31
1.3.5 Aperiodic/Non grid cells: .....	32
1.4 Input-Output organization of the MEC and its different cell types: .....	33
1.4.1 Laminar organization in the MEC:.....	33
1.4.2 Connectivity between excitatory cells in the MEC: .....	35
1.4.3 Inhibitory cells:.....	35
1.4.4 Connectivity between interneurons and excitatory cells in the MEC: .....	36
1.5 How do the cell types contribute to the functional properties of the MEC?.....	38
1.5.1 Manipulating the excitatory cells in the MEC:.....	39
1.5.2 Manipulating the inhibitory cells in the MEC:.....	40
1.6 Bridging anatomical findings with computational models: .....	41

1.7 A brief overview on VIP interneurons .....	42
1.8 VIP mediated disinhibition and its implications in other cortical structures .....	43
1.9 Integrating sensory inputs and navigational strategies:.....	44
2.0 Rationale of study and specific aims:.....	45
Chapter 2: A characterization of the electrophysiological and morphological properties of vasoactive intestinal peptide (VIP) interneurons in the medial entorhinal cortex (MEC).....	46
Abstract .....	46
1 Introduction .....	47
2 Materials and Methods .....	49
2.1 Animals.....	49
2.2 Immunohistochemistry (IHC).....	49
2.3 Image acquisition and Data analysis for quantification.....	50
2.4 In Vitro Electrophysiology .....	51
2.5 Morphology of VIP cells .....	52
2.6 Data analysis and statistics .....	53
3 Results .....	55
3.1 Molecular characterization of VIP cells in the MEC .....	55
3.2 Electrophysiological properties of VIP neurons vary between superficial and deep layers of the MEC .....	56
3.3 Electrophysiological properties of VIP cells vary along the Dorsal-Ventral (D-V) axis of the MEC.....	57
3.4 VIP cells show heterogeneity in their firing patterns .....	58
4 Discussion .....	59
4.1 VIP cells show heterogeneity in their electrophysiological and morphological properties .....	60
5 Functional implications .....	63
6 Acknowledgements .....	63
7 References .....	64
Figure and figure legends:.....	72
Supplementary figures.....	78

Foreword to Chapter 3 .....	85
Chapter 3: Investigating monosynaptic inputs and behavioural correlates of Vasoactive Intestinal Peptide (VIP) interneurons in the Medial Entorhinal Cortex (MEC) .....	86
Abstract .....	86
1. Introduction .....	87
2 Materials and Methods .....	89
2. 1 Animals.....	89
2.2 Stereotaxic surgeries for viral transfection:.....	90
2. 3 Habituation and handling for behavior experiment:.....	92
2.4 Memory testing using novel object location paradigm .....	92
2.5 Immunohistochemistry .....	94
2.6 Tracing of input regions for rabies circuit tracing experiments: .....	95
2.7 Image acquisition and Data analysis for c-Fos quantification.....	97
2.8 Data analysis and statistics .....	97
3 Results .....	98
3.1 Monosynaptic tracing of inputs to VIP cells in the MEC.....	98
3.2 VIP cells show c-Fos activation in a novel object location task .....	101
3.3 Inhibition of VIP cells prior to sampling results in behavioural deficits in a novel object location task .....	103
4 Discussion .....	104
4.1 VIP interneurons are in a unique position in the MEC to receive and transmit input from various spatial processing centers in the brain .....	107
4.2 VIP interneurons in the MEC are involved in a novel object location paradigm.....	107
5 References .....	109
6 Figures and Figure legends .....	123
Chapter 4. Discussion .....	134
4.1 Connecting the dots: Characterization, Inputs and Spatial Functions of VIP cells in the MEC .....	134
4.2 Potential circuit-level mechanisms for VIP mediated inhibition/disinhibition:.....	135
4.3 Critical considerations:.....	137

4.3.1 Characterization of VIP cells across the different layers of the MEC: .....	137
4.3.2 Monosynaptic retrograde tracing of inputs to VIP cells:.....	138
4.3.3 Using c-Fos as an activity marker: .....	139
4.3.4 Inhibition of VIP cells using DREADDs virus: .....	140
4.4 Future Directions:.....	142
Conclusion and Summary .....	144
Figures and Figure Legends .....	145
References.....	147

## Abstract

The medial entorhinal cortex (MEC) is a crucial brain region involved in both episodic memory and spatial navigation. The MEC microcircuit achieves its functions through a delicate balance of excitation and inhibition (E/I), giving rise to a multitude of spatially modulated cells that collectively form a map of the animal's environment. These spatially modulated cells are predominantly found in the superficial layers of the MEC, and a subset of them directly transmit spatial information to the hippocampus, forming a vital anatomical pathway essential for memory.

The MEC comprises of various types of excitatory and inhibitory cells such as Parvalbumin (PV) and somatostatin (SOM) GABAergic cells. The role of these cells in spatial navigation has been extensively studied. In this context, interneurons expressing Vasoactive Intestinal Peptide (VIP) play a significant role in maintaining E/I balance by disinhibiting excitatory cells, including other interneurons and some excitatory cells. However, compared to other excitatory and inhibitory neuron types, VIP cells remain insufficiently characterized, and their specific contributions to MEC physiology and functionality remain elusive.

To address this gap, our study aimed to thoroughly characterize the electrophysiological and morphological properties of VIP cells in the MEC using *in vitro* electrophysiology. Our findings revealed a concentration of VIP cells in the superficial layers of the MEC, suggesting their indirect involvement in transmitting memory-related information to and from the hippocampus. Additionally, we observed distinct electrophysiological and morphological properties of VIP cells across both superficial and deep MEC layers. Subsequently, we investigated the inputs received by VIP cells in the MEC through retrograde trans-synaptic tracing, revealing connections from essential spatial coding centers in the brain, including the hippocampus CA1, subiculum, retrosplenial cortex, and anterodorsal thalamic nucleus. To further assess the role of VIP cells, we

employed the novel object location paradigm to evaluate their involvement in spatial memory. Combining behavioral analysis and immunohistological detection of the c-Fos protein, we found that VIP cells are recruited during this paradigm. Moreover, employing chemogenetic inhibition via DREADDs, we observed that inhibiting VIP cells before sampling led to poor behavioral performance in the novel object location task, indicating the essential role of VIP cells in spatial memory.

In conclusion, our study demonstrates that VIP cells within the MEC form a heterogeneous population and receive inputs from key spatial coding centers in the brain. Additionally, our results highlight the pivotal role of these cells in the MEC circuitry, where they gate incoming information for spatial memory. These findings enhance our understanding of the functional significance of VIP cells in the MEC and their contributions to spatial memory processes.

## Résumé

Le cortex entorhinal médian (CEM) est une région du cerveau cruciale à la fois pour la mémoire épisodique et pour la navigation spatiale. Grâce à un équilibre délicat entre excitation et inhibition, les microcircuits neuronaux au sein du CEM donnent naissance à des neurones spécialisés dans le codage de l'espace, qui, tous ensemble, permettent l'émergence d'une carte mentale spatiale d'un environnement particulier. Ces neurones spécialisés dans le codage de l'espace se situent en très grande majorité dans les couches superficielles du CEM, et une partie d'entre eux transmettent les informations spatiales à l'hippocampe, formant ainsi une voie anatomique essentielle pour la mémoire.

Le CEM contient des neurones excitateurs et inhibiteurs de différentes classes, dont les cellules GABAergiques de type somatostatine (SOM) ou parvalbumine (PV) qui ont été largement étudié dans le cadre de leur fonction dans le traitement des informations spatiales. Dans ce contexte, les interneurones exprimant le Peptide Intestinal Vasoactif (PIV) jouent un rôle significatif dans le maintien de l'équilibre excitation/inhibition en désinhibant d'autres cellules, telles que des neurones excitateurs et des interneurones. Toutefois, en comparaison d'autres types de cellules excitatrices ou inhibitrices, les interneurones PIV restent beaucoup moins étudiés, et leur contribution au rôle du CEM sur le plan fonctionnel et physiologique est largement incomprise.

Pour répondre à ce manque de connaissances, notre étude tend à caractériser en profondeur les propriétés morphologiques et physiologiques des interneurones PIV grâce à l'électrophysiologie *in vitro*. Nos résultats montrent une concentration importante de ces interneurones dans les couches superficielles du CEM, suggérant un rôle essentiel dans la transmission d'informations à l'hippocampe en lien avec la mémoire. De plus, nous avons observé des propriétés électrophysiologiques et morphologiques distinctes entre les interneurones PIV des couches

superficielles et profondes du CEM. Par la suite, nous nous sommes intéressés aux connexions reçues par les interneurons PIV du CEM grâce au traçage rétrograde trans-synaptique. Cette approche a révélé des connexions provenant de structures essentielles au codage de l'espace par notre cerveau, tels que le CA1 de l'hippocampe, le subiculum, le cortex rétrospeñial et le noyau antérodorsal du thalamus.

Pour évaluer plus précisément le rôle des interneurons PIV, nous avons utilisé le paradigme comportemental dit *du nouvel emplacement d'un objet* pour déterminer leur potentielle implication dans la mémoire spatiale. En combinant des analyses comportementales avec la détection par immunohistochimie de la protéine c-Fos, nous avons montré l'implication de ces interneurons dans cette tâche comportementale. Par ailleurs, l'inhibition chémozénétique grâce à l'utilisation de DREADDs des interneurons PIV avant la phase d'apprentissage est associée à de faibles performances comportementales dans ce *paradigme du nouvel emplacement d'un objet*, indiquant un rôle certain des interneurons PIV dans la mémoire spatiale.

En conclusion, notre étude démontre que les interneurons PIV au sein du CEM forment une population hétérogène et reçoivent des informations de centres cérébraux clé dans le traitement des information spatiales. Nos résultats soulignent également le rôle pivot de ces cellules dans les microcircuits du CEM, où ils jouent un rôle de relais des informations nécessaires à la mémoire spatiale. Ces résultats nous éclairent sur la fonction des interneurons PIV dans le CEM et sur leur contribution aux processus de la mémoire spatiale.

## Acknowledgements

"In the end, the only sure criterion is to have fun. And I have had fun."

- Edward Chace Tolman, (1959)

I am deeply grateful to everyone who has made this journey as enjoyable as it could be. I want to express my sincere gratitude to Dr. Mark Brandon, my supervisor, for his mentorship, patience, invaluable feedback, and constant encouragement. Mark's enthusiasm for science has been immeasurable in my journey. Thank you, Mark, for providing an intellectually stimulating environment that fostered my academic growth, allowing me to become the scientist I am today.

Additionally, I would like to thank my advisory committee members, Drs. Sylvain Williams and Adrien Peyrache, for their guidance and insightful discussions throughout my PhD. I am grateful to all my former and current colleagues in the Brandon lab for their support, encouragement, and lively discussions on all aspects of science and beyond. I also want to thank them for patiently tolerating my love for animal videos. A special thank you to Drs. Robert Rozeske, Justin Quinn Lee, Jennifer Robinson, Zaki Ajabi, Johnson Ying, Hyun Choong Yong, Cecilia Kramer, Coralie Anne-Mosser, Andrés Nieto Posados and Frédéric Manseau.

I am also thankful to Leonie Runtz, Etienne Maes and Raphael Lavoie for our engaging discussions in the office and lab, which made the arduous days of conducting experiments more interesting. My sincere gratitude goes to Dr. Marie Oulé, whose patience, kindness, and encouragement have been invaluable throughout this process.

Outside of the lab, I've received tremendous support from friends and family. A special shoutout to Suzanne van der Veldt, Isabelle Groves, Kirsten Wilson, Malosree Maitra, Eamon Fitzgerald, and Alexandra Keinath. Our endless chats about science, life, and animals have made this journey

more enjoyable, and they've played a crucial role in helping me maintain my sanity outside the lab. For the past seven years, you've been my home away from home, and I am deeply grateful for that. I will always cherish the time I've spent with all of you. To my friends Akshara Gopinath, Nethra Gomatheswaran, and Keerthana Kumar, who have been my cheerleaders from the very beginning, I thank you for patiently enduring both the highs and lows of this thesis journey with me

Above all, I am thankful beyond words for my family, not just for their love and support for the past few years but for always helping me find ways to foster and nurture my love for science. Thank you, Amma, for everything. You have always been an infinite source of love, motivation, strength, and comfort for us all. Your unwavering support and belief in me are something I always cherish. Thank you, Appa, for your love and protection; you may not be around physically, but I know you are always with me, cheering me on. Your presence is always felt. To my sister Anju, I can't thank you enough for introducing me to the wonders of science. You are my constant source of love and inspiration for all that I set out to do. Conversations with you are vital to keep me going. You truly are the best sister in the whole wide world. And to Kris, thank you for your affection and calmness. You are easily the coolest brother-in-law, and you have been an integral part of my journey. Your sense of humor also helps.

Finally, to all my mentors both past and present, the individuals mentioned above, and those I may have unintentionally omitted, I extend my sincere gratitude.

## **Contribution to Original Knowledge**

1. The research work described in this thesis involves an in-depth characterization of Vasoactive Intestinal Peptide (VIP) interneurons in the Medial Entorhinal Cortex (MEC).
2. In the thesis, we show that VIP cells in the MEC constitute a heterogeneous population of interneurons with diverse electrophysiological and morphological properties.
3. Through our experiments, we demonstrate that VIP cells are involved in spatial tasks, such as novel object location.
4. Additionally, these cells are uniquely positioned to relay incoming spatial information from various regions, including the hippocampus, subiculum, and the anterior dorsal thalamic nuclei, to downstream regions.

The characterization of VIP cells extends our knowledge on this class of interneurons in the MEC. Through these experiments, we predict that these cells play a pivotal role within the microcircuit of the MEC.

## Contribution of Authors

### Chapter 1

Suzanne van der Veldt provided feedback and suggestions to Chapter 1

### Chapter 2:

Badrinarayanan, S *et al* (2021). “**A Characterization of the Electrophysiological and Morphological Properties of Vasoactive Intestinal Peptide (VIP) Interneurons in the Medial Entorhinal Cortex (MEC).**” *Frontiers in Neural Circuits*: 653116.

Mark P Brandon, Frederic Manseau, Sylvain Williams and Saishree Badrinarayanan planned this study. In this work, Saishree Badrinarayanan conducted the immunohistochemical experiments, performed the electrophysiological recordings and subsequently analyzed all the electrophysiology and morphology data. Saishree Badrinarayanan wrote the initial draft of the manuscript; Mark P Brandon contributed to editing and revising the manuscript.

### Chapter 3:

Badrinarayanan, S\*, Oulé, M\* *et al* (2023) “**Investigating monosynaptic inputs and behavioural correlates of Vasoactive Intestinal Peptide (VIP) interneurons in the Medial Entorhinal Cortex (MEC)**” *In preparation*

\* Equal first author

Mark P Brandon, Marie Oulé and Saishree Badrinarayanan conceived the project and planned the study design. Saishree Badrinarayanan performed all stereotaxic surgeries for the rabies mediated viral tracing experiment and the chemogenetic inhibition experiment. Saishree Badrinarayanan collected and analyzed all the data for the rabies mediated tracing experiments. Marie Oulé and

Saishree Badrinarayanan performed all the behavioral testing in animals. Marie Oulé and Saishree Badrinarayanan performed all the behavior analysis. Marie Oulé gathered histology data for the c-Fos experiments. Marie Oulé and Saishree Badrinarayanan trained undergraduate volunteers Rosa – Sundar Maccagno and Michaela Hirsch to conduct stereology counting on the brain sections. Saishree Badrinarayanan wrote the first draft of the manuscript. Marie Oulé and Mark P Brandon provided valuable feedback.

#### **Chapter 4**

Marie Oulé provided feedback and suggestions to Chapter 4

Mark P Brandon provided advice and guidance throughout the thesis.

## List of Figures and Tables

### Chapter 1

Figure 1. Edward Tolman's sunburst maze

Figure 2. The Hippocampal – Entorhinal circuit.

Figure 3. Properties of grid cells

Figure 4. Head direction and other spatially tuned cells in the MEC

Figure 5. Laminar organization of inputs and output in the MEC

Figure 6. Connectivity between different excitatory and inhibitory cells in Layer 2 of the MEC

### Chapter 2

Figure 1. Specificity of cre-driven fluorescence for VIP in VIPcre/tdTom mice and presence of colocalization with other molecular markers.

Figure 2. Comparison of electrophysiological properties between LI-LIII and LIV-LVI VIP cells

Figure 3. Passive and Active properties as a function of layer and location along the Dorsal-Ventral axis.

Figure 4. Variability in firing patterns of VIP cells from layers I-III and IV-VI.

Figure 5. Morphometric analysis of VIP cells

Supplementary Figure 1

Supplementary Figure 2

Supplementary Figure 3

## Supplementary Figure 4

Table 1. Tabulation of all passive and active membrane properties measured for VIP cells located in superficial (LI-LIII) and deep (LIV-LVI) layers in the MEC

Table 2. Tabulation of all passive and active membrane properties measured for all VIP cells located across all layers

## Chapter 3

Figure 1. Rabies viral strategy and confirmation of starter cells

Figure 2. Generating and quantifying brain wide inputs to VIP cells in the MEC

Figure 3. Local and long-range connectivity from distinct regions of the brain to VIP cells in the MEC

Figure 4. Detecting c-Fos expression in VIP cells

Figure 5. Inhibition of VIP cells causes a behavioural deficit during a novel object location task

Supplementary Figure 1

Supplementary Figure 2

## Chapter 4

Figure 1 Potential circuit level-mechanisms mediating disinhibition/inhibition via VIP cells

Figure 2 Identifying post-synaptic targets of VIP cells in the MEC

## List of Abbreviations

5HT3aR	5-hydroxytryptamine	DREADDs	Designer Receptors Activated by Designer Drugs
AAV	Adeno-associated virus	VIP	Vasoactive Intestinal Peptide
CLA	Clastrum	RM	Retromammillary nucleus
CNA	Continuous non-adapting	CA	Continuous Adapting
CR	Calretinin	IS	Irregular Spiking
DB	Diagonal Band	DG	Dentate Gyrus
DS	Dorsal subiculum	ADN	Anteriodorsal thalamic nuclei
GFP	Green Fluorescent protein	SOM	Somatostatin
IAD	Interanterodorsal thalamic nuclei	VA	Ventral anterodorsal thalamic nuclei
IEG	Immediate early gene	GABA	$\gamma$ -aminobutyric acid
IMSC	Intermediate stellate cell	IMPC	Intermediate pyramidal cell
L2/LII	Layer 2	L3/LIII	Layer 3
LPLR	Lateral posterior thalamic nuclei	LDVL	Lateral dorsal thalamic nuclei
MEC	Medial Entorhinal Cortex	PV	Parvalbumin
MS	Medial Septum	Sub	Subiculum
NOL	Novel object location	NOR	Novel object recognition

PERI	Perirhinal cortex	AuD	Auditory cortex
PIR 2	Piriform cortex	BLA	Basolateral amygdala
RFP	Red Fluorescent Protein	ChAT	Choline acetyltransferase
Rt	Reticular nucleus	HD	Head direction cell
SC	Stellate cell	PC	Pyramidal cell
V2L	Secondary visual cortex, lateral	V1	Primary visual cortex
V2MM/V2ML	Secondary visual cortex, medial	RSP/A30	Retrosplenial cortex

## **Other Notes**

The thesis is organized in a manuscript-based structure, where each individual manuscript comprises its unique set of figures. Figure numbers are chapter-specific, enabling references to figures like Figure 1 across various chapters. Additionally, the citation numbering and style vary based on the journals where the manuscripts were published or intended for submission. Chapter 2 and 3 include their respective reference section to accommodate the citations relevant to those specific chapters. The order of sections may slightly differ depending on the target journal for each manuscript. The reference section at the end of the thesis is applicable only to chapters 1 and 4, which include the literature review and discussion.

The work conducted in this thesis was supported by a Healthy Brains for Healthy Lives Doctoral Fellowship.

## **Introduction: General overview of the thesis**

A sense of place and the ability to navigate is crucial for our existence. A sense of place provides us with a perception of our environment and our ability to find our way in a complex and changeable environment depends on the brain's capacity to integrate various information. Interestingly, the fundamental neural mechanisms to know where we are and to find our way from one place to another is conserved between humans (Jacobs et al. 2010), mammals (Geva-Sagiv et al. 2015) and other mobile species (Wehner 2003). This inner GPS system makes use of information about the location, the distance we have travelled, the speed with which we are moving and the direction we are moving in (Barry and Burgess 2014). Understanding how the brain processes and stores such information has been of interest to scientists for many years and recent advances in neuroscience has shed light on the entorhinal–hippocampal complex which is not only implicated for spatial navigation but is also vital for the formation and storage of episodic memory. Interestingly, each component of this circuit has specialized cell types that respond differently to spatial locations but work in conjunction to enable an organism to navigate in an environment.

Of the various spatially tuned cells present in this network, grid cells present in the medial entorhinal cortex (MEC) and place cells present in the hippocampus have been extensively studied. The firing rate of grid cells peaks when an animal reaches specific locations in the environment. These peaks of high activity form the vertices of a regular triangular grid thus spanning the entire environment the animal navigates (Hafting et al. 2005). While a single grid cell has multiple firing fields (known as grid fields), place cells in CA1 of the hippocampus have a single field and code for a specific location the animal traverses (J. O'Keefe and Dostrovsky 1971). Many studies have focused on the interaction of these two cell types, often questioning how the neural code generated by one controls the output of the other (Kanter et al. 2017; Moser, Kropff, and Moser 2008). With

these studies, we have learned that the MEC can provide the hippocampus with a rigid spatial framework of the environment (Moser et al. 2014; Nilssen et al. 2019). This framework is generated through a careful balance between the excitatory and inhibitory cells in the circuit which generate grid cells along with a multitude of other spatially tuned cells (Zutshi et al. 2018; Fuchs et al. 2016). These cells help encode for geometric information with implications for how organisms estimate distance in their environments, often by integrating local cues and sensory information (e.g. proprioceptive feedback and vestibular information). The mechanisms used by the MEC to integrate such information to construct this network remains unknown. Recent studies investigating the anatomical structure have suggested that the micro-circuitry of the MEC can support this assimilation sources (Witter et al. 2017; Caputi et al. 2022). While the role of excitatory and certain inhibitory cell populations has been studied extensively, the interplay required to generate and maintain this excitation-inhibition (E/I) balance remains elusive (Witter et al. 2017).

A class of interneurons - the Vasoactive Intestinal Peptide (VIP)-expressing interneurons are known to inhibit other interneurons in various cortical structures (Pi et al. 2013). Their mechanism of action places them as potential contenders in maintaining the E/I balance by disinhibiting excitatory cells in the MEC from ongoing inhibition in a temporally specific manner. Thus, in this thesis, **we aim to unravel the role of VIP interneurons in the MEC and investigate how their activity could be implicated in spatial memory tasks.**

Beginning with a comprehensive literature review in Chapter 1, I delve into various aspects of spatial memory and explore the properties of the entorhinal cortex. This includes an examination of its connections with different brain structures and a detailed analysis of the neuroanatomical

organization of the region. Additionally, I thoroughly discuss VIP interneurons and their significant role as disinhibitory interneurons in various cortical structures.

Moving on to Chapter 2, we investigate the electrophysiological and morphological properties of VIP cells across different layers and along the Dorsal-ventral axis of the MEC. Our findings revealed that these cell types are primarily GABAergic and form a heterogeneous population. While these diverse properties offer intriguing insights into the characteristics of VIP cells, they also leave room for interpretation regarding their functional roles.

In Chapter 3, we performed retrograde monosynaptic tracing of inputs to VIP cells in the MEC, with the primary objective of identifying inputs that influence their behavior. Subsequently, we examined their role in a spatial memory task and manipulated these cells to uncover their specific contributions to the novel object location paradigm.

In a conclusive effort to summarize our findings and highlight their significance, I provide a comprehensive general discussion in Chapter 4. Within this chapter, I also present critical considerations and propose exciting ideas for future experiments that aim to deepen our understanding of the crucial role VIP cells may play in the MEC.

# Chapter 1: A comprehensive review of the literature

## 1.1 Studying spatial navigation in rodents:

Mammals exhibit remarkable navigational abilities, employing a diverse range of strategies to find their way through the world (Geva-Sagiv et al. 2015). One of the most fascinating navigation techniques used by mammals is the concept of cognitive maps, a term popularized by the psychologist Edward C. Tolman. Cognitive maps refer to the mental representations of the environment that animals create, allowing them to form an internalized understanding of spatial relationships and locations. Unlike simple stimulus-response behaviors, cognitive maps enable mammals to plan and execute complex routes, anticipate obstacles, and make adaptive decisions based on past experiences and learned associations with specific locations.

### *1.1.1 The theory of the cognitive map: Place vs response learning*

In the early 1900s, the dominant view of learning was based on stimulus-response associations, as proposed by Clark L. Hull. According to Hull's perspective, all behaviors were learned through active processes, reducible to specific stimuli evoking corresponding responses in the brain (Hull 1943). Tolman's observations were a significant departure from the prevailing stimulus-response view (Tolman, Ritchie, and Kalish 1946). While Hull focused on investigating over trained and habitual behaviors, Tolman's interest lay in studying early and novel behaviors. Tolman was further influenced by the research of Karl Lashley and Shepherd Franz, who explored the effects of brain lesions on learning and memory using experimental psychology methods. Tolman made additional observations from Lashley's incidental findings (Lashley 1929), where rats displayed shortcut behavior in the alley maze to reach the goal location. Tolman repeated these experiments in a modified version and observed that animals, when trained on a specific path to reach a reward, could find the closest non-rewarded path to the reward when the initial path was

closed off. This suggested that rats develop wider spatial maps that encompass more than the specific path they were trained on (Tolman, Ritchie, and Kalish 1946). Tolman proposed a complex and integrated approach to understanding animal behavior. He argued that animals develop expectancies through their interactions with the environment, creating a cognitive map of their surroundings based on cues present in the environment (Goodman 2021; Edward C. Tolman 1948). This cognitive map was not limited to simple stimulus-response connections but encompassed a broader representation of the environment.

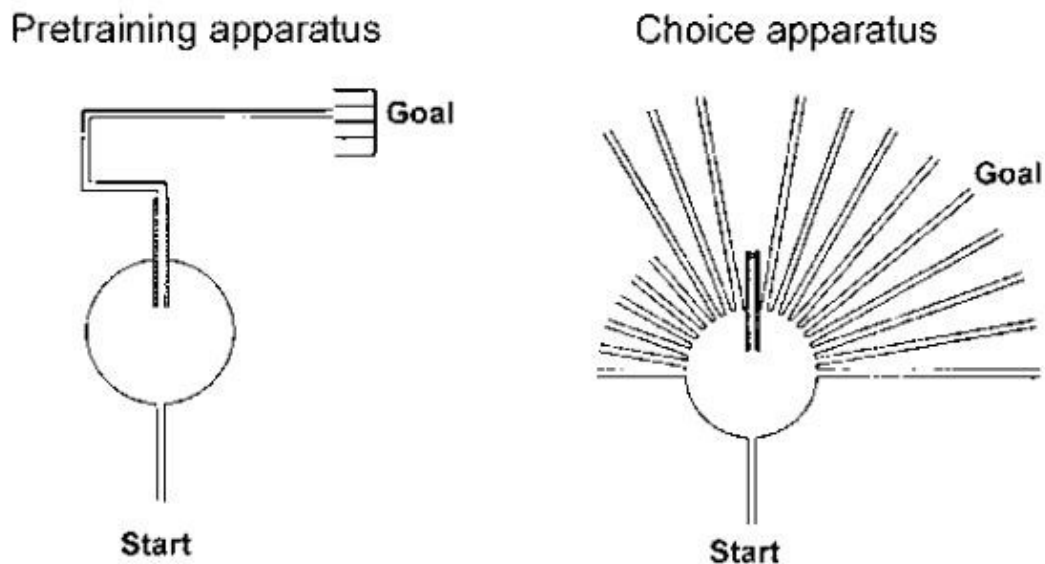


Figure 1. Edward Tolman's sunburst maze

(Left) The schematic illustrates the training apparatus used for rats to learn a stereotyped path from the starting platform to the goal location. (Right) The schematic depicts the sunburst maze, which comprises multiple paths radiating from the starting platform. Figure taken from (Tolman, Ritchie, and Kalish 1946)

This finding revolutionized our understanding of animal cognition and spatial memory. Thus, it can be said that the cognitive map-based navigation strategy relies on the animal's ability to utilize both self-motion and distal landmarks to navigate surroundings. Behaviour paradigms like novel

object location (NOL) and object recognition (NOR) are examples of tasks that require animals to remember and update their mental representation of the environment. Successful performance in these tasks suggests that animals have formed a cognitive map of the familiar environment and can use it to recognize changes in the location of objects, for example, detecting if the object has been moved to a novel location in the same arena (Chao et al. 2022). Furthermore, the presence of cells with spatially selective firing fields in the hippocampus and the entorhinal cortex has led many researchers to believe that the neural basis of cognitive maps in mammals lies in these brain regions (John O’Keefe and Nadel 1978; Poulter, Hartley, and Lever 2018).

## **1.2 The Hippocampal – Entorhinal circuit:**

According to Santiago Ramón y Cajal's seminal work, extensive connections exist between the hippocampus and the entorhinal cortex. Cajal's meticulous neuroanatomical studies included intricate diagrams that unveiled the hippocampus's complex architecture, including the dentate gyrus (DG) and various Cornu Ammonis (CA) regions. Moreover, Cajal's investigations into the entorhinal cortex's connectivity revealed the critical perforant pathway, responsible for carrying information from the entorhinal cortex to the hippocampal formation, which plays a crucial role in memory processing and spatial navigation. His work also delved into the organization of diverse neuronal types present in the entorhinal cortex, providing insights into excitatory and inhibitory connections within the local circuitry (Ramón y Cajal 1968; Ramón y Cajal 1909). It is through his studies that the importance of this circuit and its anatomical position has gained prominence, highlighting its crucial role in the spatial navigation system of the mammalian brain.

### *1.2.1 The hippocampus and its subdivisions:*

The hippocampus is organized into distinct layers, such as the stratum oriens, housing the basal dendrites of glutamatergic pyramidal cells and serving as a conduit for afferent and efferent fibers.

Positioned above the stratum oriens is the stratum pyramidale, where the cell bodies of pyramidal cells reside, distributed across both superficial and deep layers. Extending into the stratum radiatum are the apical dendrites of these pyramidal cells. The most superficial layer, the stratum lacunosum-moleculare, comprises two sublayers, the lacunosum and the moleculare. Notably, pyramidal cell somas, representing the principal excitatory cells, are exclusively localized within the stratum pyramidale, while interneurons are dispersed across all layers, playing essential roles in regulating neural activity.

The external inputs are paramount in shaping the information flow within the hippocampus. Sensory information from the neocortex comes through layer II neurons of the entorhinal cortices, specifically targeting the molecular layer of the dentate gyrus and CA3. This pathway, known as the perforant path, originates in the entorhinal cortex, and is pivotal for relaying sensory inputs to these specific hippocampal regions. Axons from the MEC terminate in the middle portion of the molecular layer, facilitating the integration of entorhinal cortex signals into the hippocampal circuitry. Additionally, layer III of the entorhinal cortex also projects directly to CA1 and the subiculum, establishing synaptic connections at the level of the stratum lacunosum. Subsequently, CA1 pyramidal cells project to both the subiculum and the deep layers of the entorhinal cortex, forming a robust reciprocal connection between these structures.

### *1.2.2 The Medial Entorhinal Cortex (MEC):*

The MEC integrates various sensory information received from the entire cortical mantle before sending it to various telencephalic regions (Tsoi et al. 2022; Swanson and Kohler 1986; Lu et al. 2022). It acts as a central nodal point for relaying information to and from the hippocampal formation through reciprocal connections. Along with the hippocampus, the MEC has extensive connections with other cortical structures such as the presubiculum, parasubiculum, retrosplenial

cortex (RSC), postrhinal cortex, claustrum and the basolateral amygdala (BLA) (Witter et al. 2017; Sürmeli et al. 2015). Using *in vivo* recordings in rodents, numerous cell types exhibiting spatial, directional, or speed tuning have been extensively described in the MEC.

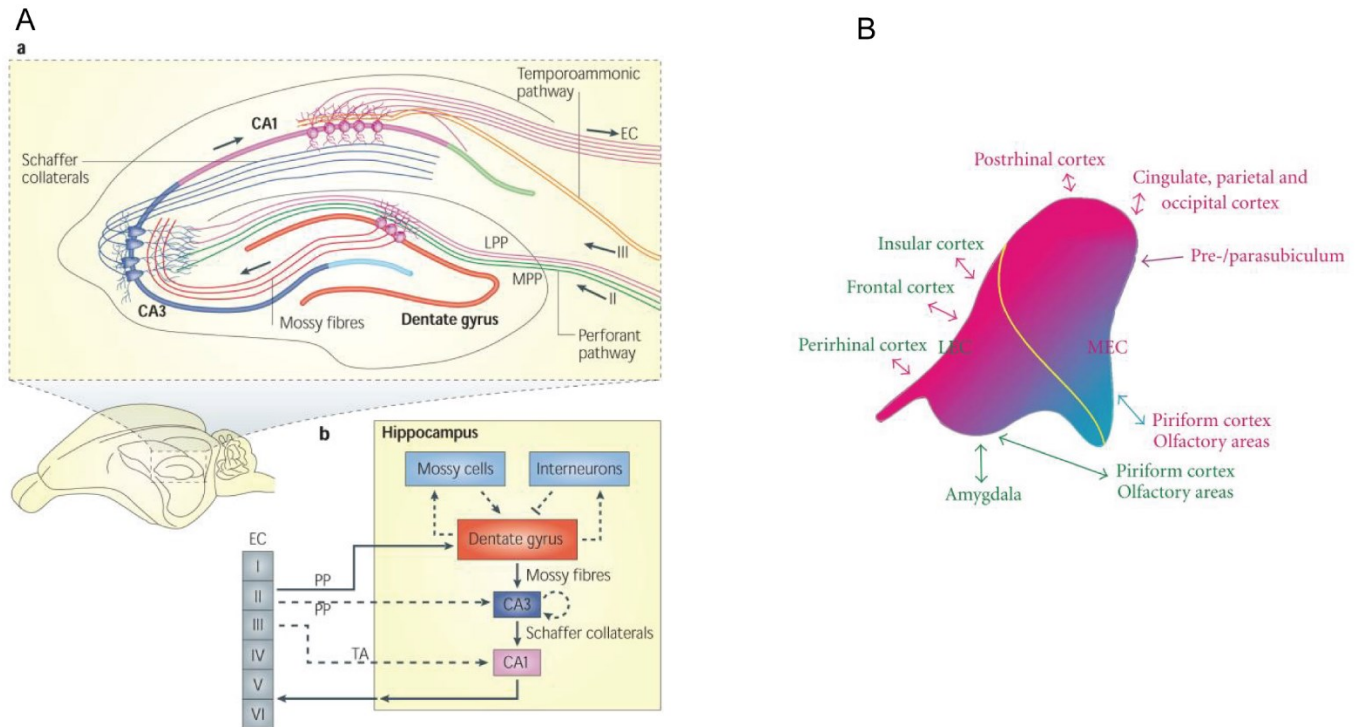


Figure 2. The Hippocampal – Entorhinal circuit.

Panel A (Left) is from (Deng, Aimone, and Gage 2010). In the entorhinal cortex, both Layer 2 and Layer 3 have connections to the hippocampus, but they follow different pathways. Layer 2 projects to the hippocampal regions, DG, CA3, and CA2, through the perforant pathway. On the other hand, Layer 3 connects to the hippocampal regions, CA1, and subiculum, via the temporoammonic pathway.

In the dentate gyrus (DG), granule cells receive inhibitory signals from mossy cells and interneurons present in the polymorphic layer. These DG granule cells then send information to CA3 through specialized axonal projections known as mossy fibers.

The CA3 region of the hippocampus exhibits recurrent connectivity, and its pyramidal cells communicate with CA1 via the Schaffer collaterals pathway.

Panel B (right) from (Canto, Wouterlood, and Witter 2008) shows the main connectivity of the different portions of the medial (MEC) and lateral (LEC) portions of the entorhinal cortex. In green are the brain areas connected to the LEC and those connected with the MEC are in magenta.

## **1.3 Spatially tuned cells within the MEC circuitry:**

### *1.3.1 Grid cells:*

The firing rate of grid cells exhibits peaks when an animal reaches specific locations in the environment (Figure 3A). These peaks of high activity give rise to a regular triangular grid pattern that spans the entire navigable area of the animal (Hafting et al. 2005). Thus, a single grid cell can have multiple firing fields, referred to as grid fields. Studies in the past have noted that the organization of grid cells is partly topographic: Grid cells with smaller scales (distance between adjacent grid fields) are more enriched near the dorsal border of the MEC while cells with a larger scale are found more ventrally (Brun et al. 2008). Grid phase (the x-y location of grid fields) do not follow a topographic organization and are instead known to cover all locations in the MEC (Hafting et al. 2005). Like grid phase, grid orientation (the rotation of grid axis) does not show changes depending on location from the dorsal border (Figure 3B).

Along with this, grid cells are found to compute for the animal's position, direction and velocity using self-motion cues (Sargolini et al. 2006), thereby suggesting that they perform a function known as path integration - a neural process by which an animal is able to update its position from a starting point using self-motion cues and in the absence of any visual landmarks (Mittelstaedt and Mittelstaedt 1980; McNaughton et al. 2006).

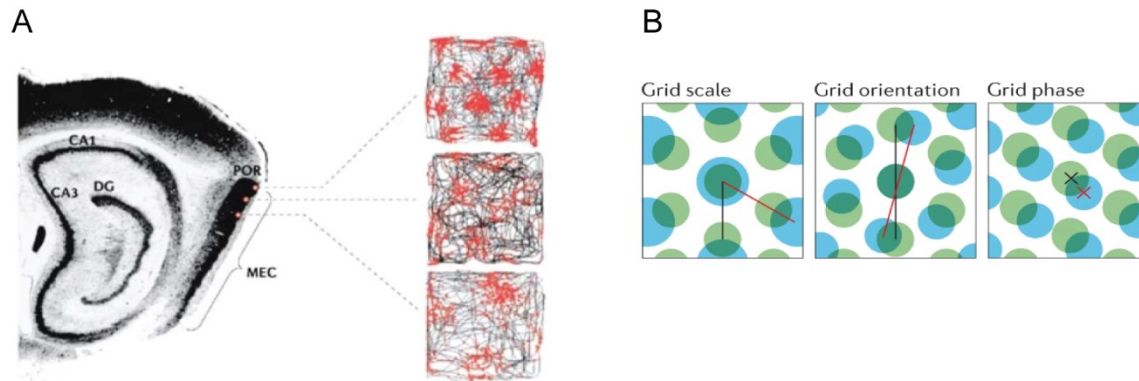


Figure 3. Properties of grid cells.

In panel A, the recording region is visualized on a sagittal brain section passing through the medial entorhinal cortex (MEC). Each panel represents the grid field of an individual neuron located in Layer 2 of the MEC. The locations where these neurons emit spikes are depicted using red dots, while the path of the rat's movement is shown as grey lines. Notably, the grid scale becomes larger as the distance from the MEC's border with the postrhinal cortex (POR) increases. Image taken from (McNaughton et al. 2006)

Panel B contains schematics representing grid scale, grid orientation, and grid phase. These schematics portray the firing patterns of pairs of grid cells using blue and green cartoons, revealing the differences in grid scale, grid orientation, and grid phase between the two cells. The left and middle panels display lines that denote the two axes of the grid pattern, defining the grid orientation. In contrast, the panel on the right exhibits crosses that indicate the grid phase, representing the x-y location of grid fields. Image taken from (Moser et al. 2014)

### 1.3.2 Head Direction cells:

Head direction cells (HD cells) exhibit alignment to compass directions, meaning that each HD cell has a preferred firing direction that corresponds to a specific heading of the animal (Jeffrey S. Taube 1998; Sargolini et al. 2006). These cells were first recorded from the anterodorsal thalamic nuclei (Jeffrey S. Taube 1998) and were subsequently found in the subiculum, the parasubiculum and the MEC (J S Taube, Muller, and Ranck 1990; Winter, Clark, and Taube 2015; Boccara et al. 2010)

In the MEC, conjunctive head direction cells are also present. These cells represent a unique hybrid of two distinct types of cells: head direction cells and grid cells. Like head direction cells, conjunctive head direction cells encode the heading direction of the animal, but they also exhibit grid-like firing fields reminiscent of the spatially modulated firing patterns observed in grid cells (Sargolini et al. 2006; Boccara et al. 2010). This intriguing combination suggests that these neurons may play a crucial role in integrating information about both head direction and spatial location, possibly contributing to the animal's ability to navigate its surroundings effectively (Gerlei et al. 2021). Head direction cells and conjunctive cells are found in all layers of the MEC, except for layer 2 (Sargolini et al. 2006) (Figure 4A)

### *1.3.3 Border cells:*

These neurons play a vital role in encoding an animal's environment's boundaries and edges during spatial navigation. As the animal explores its surroundings, border cells selectively fire at the geometric boundaries, such as walls or borders, in the environment. In addition to this, border cells are relatively sparse, making up less than 10% of the local cell population (Solstad et al. 2008) (Figure 4B)

### *1.3.4 Object vector cells:*

Object vector cells (Figure 4C) in the MEC fire selectively when the animal is at specific distances and directions relative to the objects in the environment. The 'object-vector cells' demonstrate equal tuning to a diverse range of discrete objects, independent of their location in the test arena. These results strongly suggest that vector coding serves as a prominent form of position coding in the medial entorhinal cortex (Høydal et al. 2019)

### 1.3.5 Aperiodic/Non grid cells:

Aperiodic spatially tuned cells are cells with discrete aperiodic firing fields (Figure 4D), unlike grid cells which are periodic. Close to 67.5% of spatially tuned cells are non-grid cells in the MEC (Diehl et al. 2017)

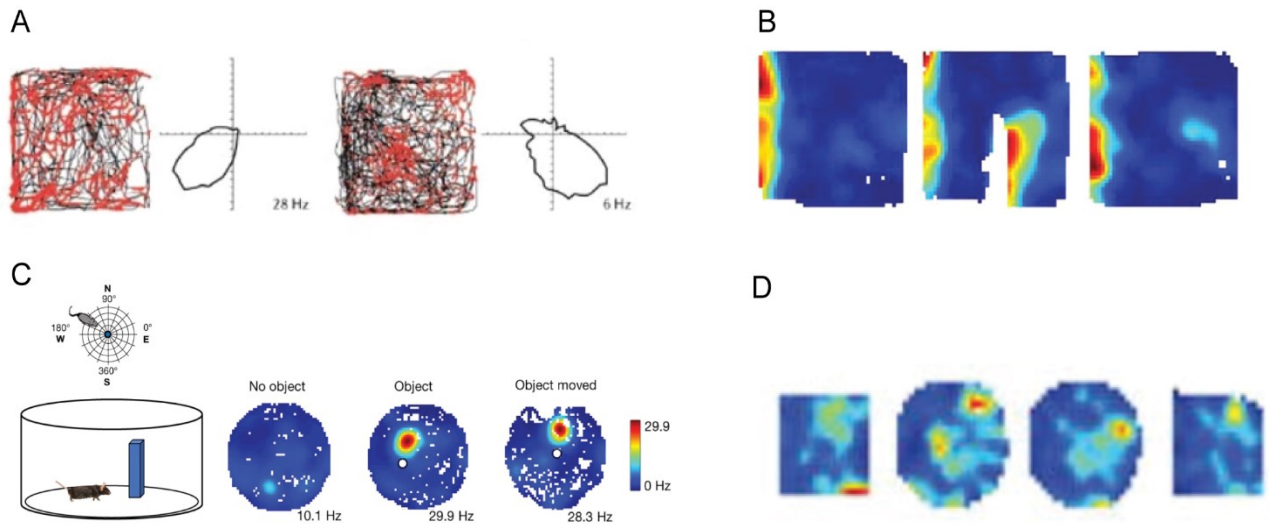


Figure 4. Head direction and other spatially tuned cells in the MEC

In panel A, the red dots illustrate the locations where the neurons emit spikes for both cells, while the rat's movement path is represented by grey lines. The cells represented in this figure are recorded from the deeper layers of the MEC. On the left panel is a head direction cell, which is not influenced by location. On the right side, is a recording of a conjunctive cells. The firing properties of these cells depend on both location and head orientation. For both cells the directional firing rate is represented in polar plots (McNaughton et al. 2006)

Panel B contains an example of a recording from a border cells from (Solstad et al. 2008). On the left, a border cell fires to existing boundaries of an environment, in addition to added boundaries as seen in the middle panel.

In Panel C, is an example of an object vector cell from (Høydal et al. 2019). The recording environment is illustrated, and the distances and orientations are defined in an allocentric frame, with the central circle serving as the reference point (0° orientation is East). On the left is a colour coded firing rate map of an object-vector cell. The firing is modulated by the presence of an object (white dot). Moving this object changes the cell's firing representation.

Panel D shows an aperiodic spatially tuned cell. The cell displays consistent firing within the same environment and respond to box manipulations by reorganizing their spatial firing. Image taken from (Diehl et al. 2017)

In all panels warmer colors in rate maps indicate high firing rates.

## **1.4 Input-Output organization of the MEC and its different cell types:**

To understand how the MEC generates and maintains the neural properties of these various spatially tuned cells, many studies have closely examined the cytoarchitecture and the different classes of excitatory and inhibitory cell populations present within the structure.

### *1.4.1 Laminar organization in the MEC:*

Like most cortical structures, the MEC is comprised of 6 distinct layers, each distinguishable by the expression of a specific transcription factor. Layers I, II, and III constitute the input layer, while layers IV, Va, Vb, and VI form the output layer (Ramsden et al. 2015). The superficial layers (LI-III) receive inputs from the ventral part of the orbitofrontal cortex, postrhinal cortex, and pre- and para-subiculum. All layers of the MEC receive extensive glutamatergic, GABAergic, and cholinergic projections from the medial septum (MS) (Canto, Wouterlood, and Witter 2008; Gonzalez-Sulser et al. 2014).

In the deep layers (LIV-VI), LVa projects to the Nucleus accumbens, retrosplenial cortex, perirhinal cortex, the secondary visual area, and the amygdala (Sürmeli et al. 2015; Tsoi et al. 2022). Inputs from the MEC to the hippocampus originate via two pathways: the perforant pathway (from LII) to the dentate gyrus and the temporo-ammonic pathway (TA) (from LIII) to CA1. In return, the hippocampus sends back projections to LVb of the MEC. Within the MEC, LVb and LII have reciprocal connections with each other (Bonnievie et al. 2013; Sürmeli et al. 2015).



#### *1.4.2 Connectivity between excitatory cells in the MEC:*

The MEC contains two main types of excitatory cells: Pyramidal cells (PC) found in all layers, and stellate cells (SC) exclusively found in layer II (L2SCs). L2SCs play a role in the perforant pathway, while pyramidal cells found in layer II (L2PCs) project to CA1 via the temporo-ammonic pathway (TA). These two cell types express different calcium-binding proteins: reelin for L2SCs and calbindin for L2PCs (Witter et al. 2017). Apart from their distinct projection patterns, L2SCs can be differentiated from L2PCs by their morphologies and electrophysiological profiles. L2SCs express the HCN1 channel, giving them a characteristic sag when subjected to hyperpolarizing current (Klink and Alonso 1997; Alonso and Klink 1993; Pastoll, Ramsden, and Nolan 2012).

Interestingly, recent research has further subdivided excitatory cells into intermediate pyramidal cells (IMPCs) and intermediate stellate cells (IMSC) (Fuchs et al. 2016). However, a study by (Winterer et al. 2017) investigating excitatory connections within L2 of the MEC found no obvious difference between SC and IMSC, and PCs and IMPCs. Excitatory connections between these different cell populations have been reported. Specifically, L2PCs (13.5%) and L3PCs (7%) target L2SCs respectively, but the reverse is not observed. Instead, L2SCs send dense projections to PCs in the deep layers (L5b) (Sürmeli et al. 2015; Witter et al. 2017), forming an important route for information transfer between the input and output layers of the MEC.

#### *1.4.3 Inhibitory cells:*

Over a century ago, Ramón y Cajal observed the remarkable diversity and heterogeneity of interneurons, speculating in his *Recollections of My Life* that the exceptional functional superiority of the human brain is closely intertwined with the abundance and unprecedented richness of what he termed “neurons with short axons” (1989). Despite comprising only a minority (20%) of neurons in the brain, interneurons play a crucial role as the primary source of inhibition,

critically modulating and refining the flow of information throughout the nervous system (Kepecs and Fishell 2014; Rudy et al. 2013). Interneurons form an incredibly heterogeneous cell population, displaying distinct morphologies, connectivity, neurochemical markers, and electrophysiological properties (Kepecs and Fishell 2014).

#### *1.4.4.1 Types of inhibition in the MEC:*

The major types of inhibition in the MEC include:

1. **Local Inhibition:** This refers to inhibitory connections between neighboring neurons within the MEC. GABAergic interneurons like Parvalbumin (PV) and Somatostatin (SOM) play a crucial role in providing local inhibition to regulate the activity of PCs and SCs (Fuchs et al. 2016)
2. **Recurrent Inhibition:** Recurrent inhibition occurs when excitatory neurons in the MEC excite inhibitory interneurons, and these interneurons, in turn, inhibit the same excitatory neurons that initially activated them (Buetfering, Allen, and Monyer 2014; Couey et al. 2013)
3. **Disinhibition:** Disinhibition is a process by which inhibitory interneurons inhibit other inhibitory neurons, effectively releasing the inhibition on excitatory neurons. This can lead to a net increase in excitatory activity and enhance the representation of spatial information in the MEC (Schmidt-Hieber and Nolan 2017). In the MEC, long-range disinhibitory projections from the MS have been reported (Gonzalez-Sulser et al. 2014; Schlesiger et al. 2021)

#### *1.4.4 Connectivity between interneurons and excitatory cells in the MEC:*

Studies on GABAergic cells in the MEC show us that the cells can be sub-divided into three main categories, namely: PV, SOM and 5-hydroxytryptamine (5HT3a) expressing cells (Witter et

al. 2017; Gonzalez-Sulser et al. 2014). Using this classification, (Fuchs et al. 2016) reported the following connectivity profile between the interneurons and excitatory cells in the MEC. PV cells displayed a fast spiking physiological profile and targeted both IMPCs (36.6%, 15 of 41 pairs) and SCs (35.7%, 10 of 28 pairs) and IMSCs (45.5%, 10 of 22 pairs) but not PCs. In the same study, SOM interneurons were characterized by a low threshold firing and a prominent sag potential. SOM cells were found to contact SCs (5 of 37 pairs) and IMPCs (5 of 41 pairs) but not IMSCs and PCs. They next investigated 5HT3a expressing cells. This cell type encompasses cells that can co-express Calretinin (CR), Vasoactive Intestinal Peptide (VIP) and Cholecystokinin (CCK), however in the above study they did not make a distinction between any of these cell classes and treated it as one big population. All recorded 5HT3a cells made contact to all four types of excitatory cells, with preferences to PCs and IMPCs.

For excitatory → inhibitory cell connections, SCs synapse onto all 3 interneuron classes, with a preference for PV and SOM. For PCs and IMPCs, the preferred interneuron to connect with are 5HT3a and SOM respectively (Fuchs et al. 2016).

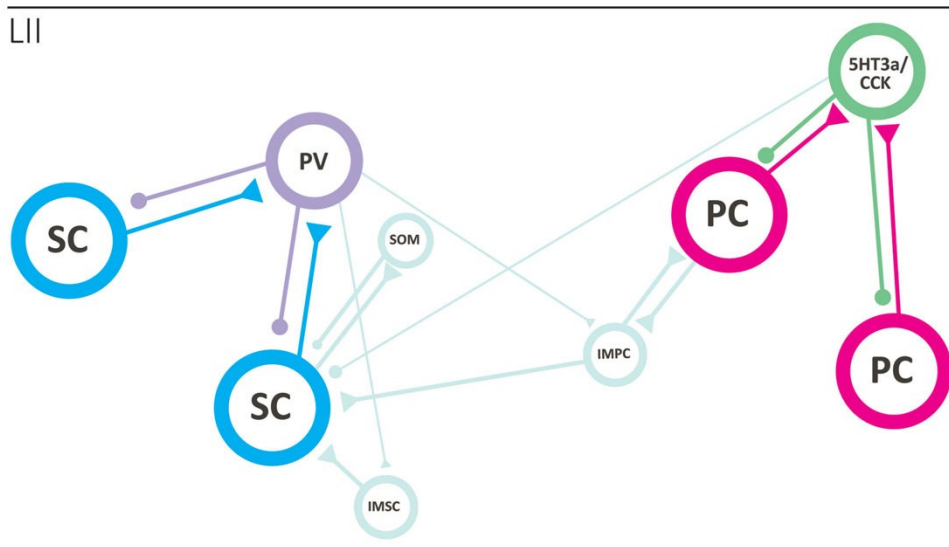


Figure 6. Connectivity between different excitatory and inhibitory cells in Layer 2 of the MEC

The local circuits within Layer II of the MEC consist of two main types of principal neurons: stellate cells (as seen in cyan; left side) and pyramidal cells (as seen in magenta; right side), forming distinct networks. These neurons do not exhibit direct monosynaptic connections with each other. Instead, they are linked disynaptically, with a preference for different subtypes of interneurons. Stellate cells are connected via fast-spiking PV cells, while pyramidal neurons are connected through 5HT3a/CCK-type basket cells.

The two networks are thought to be interlinked through intermediate pyramidal neurons (light blue). Furthermore, PV interneurons may target both intermediate pyramidal cells and stellate cells. Image taken from (Witter et al. 2017)

### **1.5 How do the cell types contribute to the functional properties of the MEC?**

Understanding the role of this intricate connectivity in spatial navigation and the generation of various spatially tuned cells involves a thorough examination of the functional properties of various cell types within the MEC. Previous studies have mainly focused on the circuits in Layer 2, as it contains a high percentage of grid cells (Sargolini et al. 2006). Conjunctive grid cells are found in Layer 3 and beyond, while other spatially tuned cells are dispersed throughout the MEC layers. Afferent inputs from the hippocampus, medial septum, and thalamic nucleus (via the pre and para-subiculum) are known to be essential for maintaining the spatial periodicity of grid cells (Bonnievie et al. 2013; Brandon et al. 2011; Winter, Clark, and Taube 2015). Without these inputs, grid cells lose spatial information, speed modulation, theta rhythmicity, and/or directional tuning.

However, the circuits within the MEC responsible for integrating such information have only recently gained attention. To investigate the mechanistic basis of grid cell formation and other spatially tuned cells, researchers have attempted to manipulate specific populations of cells or circuits within the MEC to observe the functional consequences of these disruptions.

### *1.5.1 Manipulating the excitatory cells in the MEC:*

Several studies have assessed the effects of manipulating excitatory cells in L2 of the MEC, especially with regard to the formation of different spatially tuned cells and the maintenance of its firing characteristics. In one study where the authors used a knockout model that rendered the loss of HCN1 channel specifically in the MEC (thus hindering L2SCs) showed no effect on the generation of grid patterns but instead had effects on grid spacing (Giocomo et al. 2011). In another study, Kanter et al. 2017, the authors selectively perturbed L2SCs by crossing a Cre-driver mouse for SCs with a Designer Receptors Exclusively Activated by Designer Drugs (DREADDs) constituent mouse line expressing the depolarizing receptor hm3Dq or the inhibitory receptor hm4Di (Roth 2016). Interestingly, only on depolarization of L2SCs, they noticed significant changes in relative firing rates of individual grid fields. This further caused drastic changes (artificial re-mapping) in place fields in CA1.

To investigate the contribution of L2PCs in grid cell functions, Zutshi et al. 2018 activated L2PCs using optogenetics and recorded from different cell types. Upon photo-stimulation, they noticed that some cells exhibited excitation, inhibition, showed no response or showed a combination of excitation and inhibition. This indicates that in addition to SCs, various interneurons were also activated, thus recruiting feed-back inhibition. On looking at the different spatially tuned cells, they found that the properties of sharply tuned HD cells remained unaltered while speed cells, grid cells and conjunctive cells showed minor disruption in their properties during the period of feed-back inhibition. This interesting observation goes on to show that the circuits responsible for processing sharply tuned HD signal is separate from the ones involved in integrating speed and broad HD signals for grid cells.

In the past, studies have tried to ascertain if grid cells have a cellular identity. To explore this question, two landmark papers investigated stellate and pyramidal cells using optogenetics and juxta-cellular recordings respectively. In (Rowland et al. 2018), stellate cells were optogenetically tagged using the inhibitory opsin ArchT. From their results we see that stellate cells can belong to multiple functional cell classes and that, approximately 1 in 4 stellate cells are grid cells. These findings are in stark contrast to (Tang et al. 2014) where they find using juxta-cellular labelling that grid and border cells are preferentially contributed by pyramidal and stellate cells, respectively. It is important to note that the criteria to classify cells was not the same across the two studies. In the latter, theta-locking-based classification was used to determine if a cell passed criteria for a grid cell, while in (Rowland et al. 2018), they noticed that the stellate cells which were grid cells were not strongly theta rhythmic when compared to non-grids.

#### *1.5.2 Manipulating the inhibitory cells in the MEC:*

Numerous studies have investigated the impact of manipulating inhibitory cells in Layer 2 of the MEC. In Miao et al. 2017, the authors use DREADDS to inhibit PV and SOM interneurons while recording from various spatial cell types. While the expression of DREADDS wasn't restricted to any layer, the recording electrodes were placed in the superficial layers. Upon inhibition of PV, firing rate of grid cells outside of grid fields increased while the grid centers remained unaltered. Thus, suggesting that grid patterns could be maintained by recurrent pathways in a separate sub-circuit mediated by a different class of neurons. There was also a reduction in speed-coding upon PV cell inactivation. Interestingly, when SOM cells were inhibited, aperiodic spatial cells were the only type of cells that were disrupted. Grid cells and speed cells remained unaltered. Border cells and HD cells were not affected by the inactivation of PV or SOM. However,

when PV cells were inhibited using optogenetics robust silencing (decreased firing rates) of all spatial cell types was observed (Buetfering, Allen, and Monyer 2014).

## **1.6 Bridging anatomical findings with computational models:**

Through these studies we learn that each cell type in the MEC contributes to different aspects of spatial functions within the MEC. Furthermore, from the *in vitro* and *in vivo* studies we learn that excitatory coupling in L2 is present but sparse and instead, the excitatory cells are embedded in a network of inhibitory cells. Excitation or inhibition of any of these cells types shows us that in addition to grid cells, other cell classes show impaired functional properties. However, border cells and sharply tuned HD cells remain unaffected by any manipulation to the circuit. This observation suggests that these cells might be created by a distinct sub-circuit within the MEC. This could potentially account for the fact that specific features of grid cells are affected when stellate, pyramidal, or PV cells are manipulated, yet the overall grid pattern remains unchanged. Since the feedback from sharp head direction (HD) and border signals remains unaffected, the information transmitted from these intact signals may sufficiently compensate for some of the altered grid tuning.

To generate the grid pattern, computational attractor models (Kang and Balasubramanian 2019) and experimental data (Fuchs et al. 2016; Schmidt-Hieber and Nolan 2017) suggest that in a network, where grid cells are constantly under inhibition, an increase in the cell's firing in a spatially periodic manner could be a result of a disinhibitory mechanism, thus resulting in a hexagonal periodic structure. Furthermore, previous studies also indicate that grid cells along with other spatially tuned cells in MEC are generated through a careful balance of excitation-inhibition (E/I), which when disturbed can lead to abrupt changes in the firing properties of some cells.

## 1.7 A brief overview on VIP interneurons

Vasoactive Intestinal Peptide (VIP) neurons play a significant role in providing transient and selective breaks in the excitatory-inhibitory (E/I) balance by disinhibiting excitatory cells in various cortical regions (Letzkus, Wolff, and Lüthi 2015). These neurons primarily target SOM interneurons and, to a lesser extent, PV interneurons (Pi et al. 2013; Kepecs and Fishell 2014). Additionally, VIP interneurons also exhibit minor monosynaptic connections with pyramidal cells (Batista-Brito et al. 2017; Rhomberg et al. 2018).

In most cortical structures, VIP interneurons express other protein markers such as Calretinin (CR) or Cholecystokinin (CCK) or 5HT3a (Rhomberg et al. 2018; Karnani et al. 2016; Tremblay, Lee, and Rudy 2016). For instance, in the hippocampus, VIP cells that express CR have been shown to possess disinhibitory properties (Gulyás, Hájos, and Freund 1996; Tyan et al. 2014). In specific cortical regions like the barrel and visual cortex, VIP interneurons tend to cluster in the superficial layers, which are major input regions of the cortex (Prönneke et al. 2015; Batista-Brito et al. 2017).

Along with diverse molecular characteristic, VIP interneurons also have heterogenous electrophysiology and morphological properties. Past studies have shown that VIP interneurons have low-threshold firing characteristics and display diverse firing patterns. Typically, they exhibit a bi-polar morphology and extend their axons and dendrites across the cortical column (Rhomberg et al. 2018; Prönneke et al. 2015, 2020). Various stimuli can activate VIP interneurons, including long-range projections (M1) (S. Lee et al. 2013), neuromodulatory inputs (Paspalas and Papadopoulos 2001; Prönneke et al. 2020), aversive (Krabbe et al. 2019), rewarding (Pi et al. 2013), or locomotory stimuli (Fu et al. 2014). In this regards, VIP cells are considered to be versatile contributors to associative learning via disinhibition (Letzkus, Wolff, and Lüthi 2015).

## 1.8 VIP mediated disinhibition and its implications in other cortical structures

A defining feature of VIP-mediated disinhibition is its recruitment by a wide range of salient stimuli, indicating the adaptability of VIP circuitry. For example, in the visual cortex, activity of VIP cells is highly correlated to locomotion, even in the absence of visual stimuli. Surprisingly, VIP cells in superficial layers of V1 don't receive input from the motor cortex but instead have high amounts of input originating from the nucleus of the diagonal band of Broca (NDB), a region enriched with cholinergic neurons. Interestingly, when VIP cells are activated in awake stationary mice, there is an increase in visual response gain, similar to what one would see if the animal was running (Batista-Brito et al. 2017; Karnani et al. 2016)

In the basolateral amygdala (BLA), during auditory fear conditioning, VIP interneurons are activated by aversive events (Unconditioned stimulus (US)). The source of VIP activation during US presentation remains unknown. Upon the acquisition of fear memory, VIP cells shift from being instructive to predictive of the tone (Krabbe et al. 2018). A similar circuit motif is observed in CA3 of the hippocampus. When mice undergo training in the Morris Water Maze task, there is a decrease in PV cell activity (measured using c-Fos) during the training period. Simultaneously, there is an increase in the number of VIP boutons on PV cells. A reduction in boutons is observed once the animal learns the task, and the network then shifts to an increase in PV cell activity. This period of disinhibition mediated by the VIP → PV connectivity during training is thought to provide enhanced structural plasticity, thus facilitating memory consolidation and retrieval (Donato, Rompani, and Caroni 2013). While it remains unknown whether the reduction of VIP boutons is indicative of reduced VIP activity, it is interesting to note that VIP activity is increased and is important during the acquisition phase of a learning task.

In CA1 of the hippocampus, VIP cells that are negative for CCK show negative velocity modulation, while most VIP cells (positive for CR) are positively modulated by velocity. Along with this, VIP interneurons were also modulated by presence of reward and this activity is strongly correlated with task demands. A significant proportion of VIP cells were active in a goal-oriented spatial learning paradigm, where the animal learned to associate the reward with a location. Conversely, in the absence of a learning component, fewer VIP cells were recruited (Turi et al. 2019).

It is intriguing to note the similarities in VIP functions across these structures, even if they don't share common inputs. From these studies, it is evident that VIPs preferentially modulate responses to velocity, locomotion, and tasks involving learning components. What is most fascinating is that VIP cells seem to play a key role in integrating sensory information with local inputs to help generate the desired function of the structure.

### **1.9 Integrating sensory inputs and navigational strategies:**

Previous research on grid cells has provided insights into their modulation by sensory inputs. However, the source of this input and the circuits responsible for integrating this information remain unknown (Moser et al. 2014). Furthermore, previous studies have suggested that grid cells generate a context-independent grid code, offering a reliable estimation of the animal's location based on self-motion, orientation, and speed (Diehl et al. 2017).

Recent investigations have delved into the role of grid cells in various navigational strategies, revealing that different navigational approaches can influence both grid cells and other spatial cell types in the MEC (Aronov, Nevers, and Tank 2017). Additionally, a recent discovery proposes that the MEC activity can be modulated by the memory of reward locations (Butler, Hardcastle,

and Giacomo 2019). These findings underscore the need for a circuit mechanism in the MEC that integrates local and self-motion cues with sensory and modulatory stimuli.

## **2.0 Rationale of study and specific aims:**

As the MEC receives a plethora of input, we predict that VIP neurons play a crucial role in maintaining the excitation-inhibition balance within the circuit. These interneurons are likely involved in releasing excitatory cells from inhibition, allowing them to exceed their firing threshold in a spatially periodic manner. Additionally, VIP neurons may be instrumental in integrating essential components of sensory information with self-motion cues, contributing to the generation of spatial representations and navigation in the brain.

**Aim 1: To investigate the electrophysiological and morphological properties of VIP cells across different layers and along the Dorsal-ventral axis of the MEC.** Based on previous studies, we predict that VIP interneurons are a heterogeneous population with diverse electrophysiological and morphological properties.

**Aim 2: To identify the monosynaptic inputs to VIP cells in the MEC and explore their influence in a spatial location task.** This aim involves retrograde monosynaptic tracing to map the anatomical structures providing input to VIP interneurons, shedding light on the circuitry regulating their activity. Using a novel object location paradigm, we uncover the functional roles of VIP cells in spatial memory. We employ c-Fos to map their activity and utilize DREADDs-mediated inhibition to manipulate their activity

## **Chapter 2: A characterization of the electrophysiological and morphological properties of vasoactive intestinal peptide (VIP) interneurons in the medial entorhinal cortex (MEC)**

### **Authors:**

Saishree Badrinarayanan<sup>1,2</sup>, Frédéric Manseau<sup>1</sup>, Sylvain Williams<sup>1,2</sup>, Mark P. Brandon<sup>1,2, \*</sup>

<sup>1</sup>Department of Psychiatry, Douglas Hospital Research Centre, McGill University, Montreal, QC, Canada.

<sup>2</sup>Integrated Program in Neuroscience, McGill University, Montreal, QC, Canada.

\* Correspondence: Mark P. Brandon: mark.brandon@mcgill.ca

**Keywords:** VIP interneurons, medial entorhinal cortex, in vitro patch clamp, characterization, interneurons

### **Abstract**

Circuit interactions within the medial entorhinal cortex (MEC) translate movement into a coherent code for spatial location. Entorhinal principal cells are subject to strong lateral inhibition, suggesting that a disinhibitory mechanism may drive their activation. Cortical Vasoactive Intestinal Peptide (VIP) expressing inhibitory neurons are known to contact other interneurons and excitatory cells and are thus capable of providing a local disinhibitory mechanism, yet little is known about this cell type in the MEC. To investigate the electrophysiological and morphological properties of VIP cells in the MEC, we use *in vitro* whole-cell patch clamp recordings in VIPcre/tdTom mice. We report several gradients in electrophysiological properties of VIP cells that differ across laminae and along the dorsal-ventral MEC axis. We additionally show that VIP

cells have distinct morphological features across laminae. Together, these results characterize the cellular and morphological properties of VIP cells in the MEC.

## **1 Introduction**

The medial entorhinal cortex (MEC) is a 6-layered cortical structure involved in episodic memory and spatial navigation. Layers I–III form the input and layers V–VI form the output domain to various cortical structures (Ramsden et al. 2015; Sürmeli et al. 2015; Witter et al. 2017). Projections to the hippocampus from the MEC primarily originate from the superficial layers, while outputs from the hippocampus terminate in the deep MEC layers (Canto, Wouterlood, and Witter 2008). Through these reciprocal connections, circuits within the hippocampus and the MEC support spatial navigation and memory (Moser, Kropff, and Moser 2008). The MEC consists of several types of spatially tuned cells (Hafting et al. 2005; Solstad et al. 2008; Sargolini et al. 2006) of which, the spatial firing patterns of ‘grid cells’ are hypothesized to emerge locally. Grid cells fire in a repetitive hexagonal spatial pattern that span the environment an animal navigates. An animal’s displacement, trajectory, or angular motion can be decoded from the discharge of grid cell populations (Moser et al. 2014). It is because of these properties that grid cells are also suggested to perform a function known as path integration (Mittelstaedt and Mittelstaedt 1980; McNaughton et al. 2006).

Grid cells are particularly abundant in layer II of the MEC (Sargolini et al. 2006, Boccara et al. 2010), and in vitro experiments have shown that excitatory coupling in LII is present but sparse. Instead, the excitatory neurons are connected almost exclusively via strong lateral inhibition (Couey et al. 2013; Fuchs et al. 2016; Winterer et al. 2017). Consistent with this, in vivo optogenetic activation of parvalbumin (PV) expressing inhibitory neurons directly inhibits both

grid cells and border cells, with grid cells providing a back projection onto PV cells (Buetfering, Allen, and Monyer 2014). Finally, DREADD inactivation of the PV inhibitory cell populations, but not the somatostatin expressing inhibitory populations (SOM), disrupt the spatial firing pattern of grid cells (Miao et al. 2017). Computational attractor models have shown how excitation-inhibition-excitation (E-I-E) networks or recurrent inhibitory networks can generate grid cells (Bonnevie et al. 2013, Schmidt-Hieber and Nolan 2017; Kang and Balasubramanian 2019). Thus, several lines of evidence indicate that grid cells are under strong lateral inhibition from interneurons within the MEC. To this end, the role of excitatory and certain inhibitory cell populations has been studied extensively, but the interplay required to generate and maintain this Excitation/Inhibition (E/I) balance in the MEC remains elusive.

While studies have shown that interneurons within the MEC receive inhibitory projections from the medial septum (Gonzalez-Sulser et al. 2014; Fuchs et al. 2016), another form of disinhibition, conserved across cortical structures, is mediated by Vasoactive Intestinal Peptide (VIP) expressing interneurons. These cells are known to target both PV and SOM inhibitory cells as well as excitatory cells in various structures (Kepecs and Fishell 2014; Kuchibhotla et al., 2017; Batista-Brito et al. 2017; Rhomberg, Rovira-Esteban, et al. 2018; Krabbe et al. 2019, Garcia-Junco-Clemente, Tring, Ringach, & Trachtenberg, 2019). Thus, VIP interneurons are well-positioned to provide transient and selective breaks in the E/I balance by disinhibiting excitatory cells in other cortical regions (Letzkus, Wolff, and Lüthi 2015; Guet-McCreight, Skinner, and Topolnik 2020). The disinhibitory circuit motif has been well defined in the hippocampus (Tyan et al. 2014; Turi et al. 2019), auditory cortex (Pi et al. 2013), basolateral amygdala (Rhomberg et al. 2018; Krabbe et al. 2019), visual cortex (Batista-Brito et al. 2017; Pfeffer et al. 2013) and somatosensory cortex (Prönneke et al. 2015; Bayraktar et al. 2000; S. Lee et al. 2013). These

studies show that VIP interneurons exhibit a range of molecular, electrophysiological, and morphological characteristics, all of which remain less well-defined in the MEC. Through this study, we aim to describe both anatomical and *in vitro* physiological properties of VIP cells in the MEC, with a focus on differences across both laminae and across the dorsal-ventral extent of the MEC. Our work thus adds to the growing body of studies that describe the anatomical characteristics and functions of various interneuron populations within the hippocampal-entorhinal circuits that support spatial navigation and memory.

## **2 Materials and Methods**

### *2.1 Animals*

All animal procedures were performed in accordance with the McGill University and Douglas Hospital Research Centre Animal Use and Care Committee (protocol #2015-7725). Animals were housed in a temperature-controlled room with a 12/12 hr light/dark cycle and food and water ad libitum. Animals were housed with litter mates. For this study, we crossed homozygous *Vip-ires-cre* (*VIPtm1(cre)Zjh*, The Jackson Laboratory, Bar Harbor, ME, USA) mice with homozygous *Ai9 lox-stop-lox-tdTomato cre-reporter* strain mice (RRID: IMSR JAX:007905) to generate *VIPcre/tdTom* mice in which *tdTom* is exclusively expressed in cells that have *cre* recombinase. *tdTom* fluorescence was used to identify VIP cells. Using the three different approaches (molecular, electrophysiological, and morphological techniques) to characterize VIP cells in the MEC, we also test the specificity and efficacy of the *cre* driven mouse line.

### *2.2 Immunohistochemistry (IHC)*

*VIPcre/tdTom* mice, aged between 5-7 weeks were deeply anesthetized and intracardially perfused with 4% paraformaldehyde in PBS. Brains were dissected, post-fixed by immersion in the same fixative for at least 24 hours before slicing. Free-floating sagittal sections (40  $\mu$ m) of the

entire MEC were cut using a vibratome (VT 1200S, Leica, Wetzlar, Germany). Every fourth section was collected for IHC. After slicing, the sections were washed in 1X PBS (3x 5 min) and blocked with 1X PBS containing 0.45% fish gelatin and 0.25% Triton-X (3x 15min each). Sections were then incubated with primary antibodies for 48 hr at 4°C on a rotating shaker. The following primary antibodies were used: 1:500 rb- $\alpha$ -VIP Immunostar 722001/20077 (ImmunoStar, Dietzenbach, Germany), 1:500 Ms- $\alpha$ -PV PARV-19 monoclonal P3088 (Millipore Sigma, Saint Louis, Missouri, USA), 1:1000 Ms- $\alpha$ -SOM (H-11) sc-74556 (Santa Cruz Biotechnology, CA, USA), 1:3000 rb- $\alpha$ -Calretinin (CR) 7697 (Swant, Marly, Switzerland) and 1:2000 rb- $\alpha$ -GABA A 2052 (Millipore Sigma). The sections were then subsequently rinsed in 1X PBS (3x 5min) and then incubated in Alexa Fluor 488-conjugated Ab raised against rabbit IgG and mouse IgG at 1:1000 for 2hrs at RT. After several washes with 0.3% PBS-T the sections were then mounted, and cover slipped with mounting medium Fluoromount-G and DAPI, 0100-20 (SouthernBiotech, Birmingham, AL, USA). For IHC against VIP and CR n = 3 animals and for staining against GABA n = 2 animals. For IHC against PV and SOM n = 1 animals.

### *2. 3 Image acquisition and Data analysis for quantification*

Quantification of VIP, CR and GABA colocalization was performed using the optical fractionator method in StereoInvestigator software with a Zeiss ApoTome structured illumination device on a widefield microscope. Contours were drawn to delineate the superficial (LI-III) and deep layers (LIV-VI) of the MEC using DAPI as reference. While LIV is lamina dissecans in the MEC, we repeatedly found many tdTom cell bodies in between LIII (on the outer edge of the layer) and LV. Our observations are similar to those previously reported in Canto et al., 2008. Hence for all VIP cells located in deep layers, VIPtdTom somas found in this region (LIV) are included in the LIV-LVI category.

Using live counting, all markers were counted according to optical dissector inclusion-exclusion criteria at each cell's widest point. Separate markers were used to count the number of tdTom (RFP), VIP/CR/GABA (GFP) and colocalized or double labelled cells (yellow).

## *2. 4 In Vitro Electrophysiology*

VIPcre/tdTom (n = 17 animals), of either sex, aged between 5-8 weeks were killed by decapitation and the brain was dissected and placed in an ice cold high-sucrose solution in the following composition: 252 mM sucrose, 24 mM NaHCO<sub>3</sub>, 10 mM glucose, 3 mM KCl, 2 mM MgCl<sub>2</sub>, 1.25 mM NaH<sub>2</sub>PO<sub>4</sub>, and 1 mM CaCl<sub>2</sub>, continuously oxygenated with 95% O<sub>2</sub>/5% CO<sub>2</sub>; pH 7.3. Sagittal sections of 350 μm were cut using a vibratome, according to the method previously described by Pastoll et al (Pastoll, White, and Nolan 2012). Following this, the sections were transferred to an artificial cerebrospinal fluid (aCSF) solution at RT (solution as above with 126 mM NaCl replacing sucrose, 2.5 mM KCl and 2 mM CaCl<sub>2</sub>) for 30 min before recording. Slices were recorded in a bath aCSF heated to 35°C. VIPtdTom cells were identified by tdTom fluorescence using an upright BX51WI Olympus microscope with a 40× immersion objective (Olympus, Canada) and an X-cite Series 120Q fluorescence system (Lumen Dynamics). For whole cell patch clamp recordings, glass pipettes of 5-7MΩ resistance were filled with an intracellular composition with the following components: 144 mM K-gluconate, 10 mM HEPES, 3 mM MgCl<sub>2</sub>, 2 mM Na<sub>2</sub>ATP, 0.3 mM GTP, and 0.2 mM EGTA; adjusted to pH 7.2 with KOH. Membrane potentials were not corrected for a junction potential of approximately -10mV. VIPtdTom cells were recorded using a visually guided whole-cell patch clamp technique, a Multiclamp 700B amplifier, a DigiData 1440A digitizer and pClamp10 software.

## 2. 5 Morphology of VIP cells

For the morphology of VIP cells, cells were patched using the above intracellular solution with the addition of neurobiotin (0.4%, SP-1120-50, Vector Laboratories, ON, Canada). To obtain efficient biocytin fills, cells were subjected to a high amount of current at the end of each recording session (Jiang et al. 2015). Following this, the pipette was left undisturbed in whole-cell mode for 30 minutes to allow for the diffusion of neurobiotin through all neuronal processes. Finally, the pipette was retracted carefully to ensure that the cell membrane did not rupture, as this would result in incomplete fills or the loss of the soma. Slices were fixed in PFA (4% in PBS) at 4°C overnight. Fixed slices were incubated with streptavidin Alexa 488 (1:1000, Jackson ImmunoResearch, West Grove, PA, United States) and NeuroTrace 647 (1:1000) in 0.3% PBS-Triton overnight at room temperature. Slices were mounted on glass slides with Fluoromount G, 0100-01 (Southern Biotech). Biocytin-labelled VIP cells were imaged under the MBF Zeiss ApoTome microscope with a 20x magnification (Carl Zeiss, Germany). The cells were manually reconstructed using NeuroLucida 11 software (MBF Bioscience, Williston, United States).

Immunostaining for CR following in vitro recordings in 350µm sections: The protocol from Swietek et al., 2016 was adapted for immunostaining following a recording session. In brief, after recording, slices were fixed overnight in PFA (4% in PBS) at 4°C overnight. The following day, they were rinsed in 0.3% PBS-T (3x 15min) before incubation with primary antibody, 1:2000 rb- $\alpha$ -Calretinin (CR) 7697 (Swant, Marly, Switzerland) overnight at RT. The next day, the sections were rinsed in 0.3% PBS-T before incubating in streptavidin Alexa 647 (1:1000) and Alexa Fluor 488-conjugated Ab raised against rabbit IgG (1:500) overnight at RT. After 3x 10min washes in PBS, slices were mounted on glass slides and coverslipped with mounting medium Fluoromount-G and DAPI, 0100-20 (SouthernBiotech, Birmingham, AL, USA)

Contours between layers were marked using cells labelled with NeuroTrace or DAPI as a reference. Dendrites were distinguished from axons by the presence of spines. Initial axon segments were identified by their smooth appearance near the soma which later appeared discontinuous as the axon continued branching. Due to slicing techniques, neuronal processes may be cleaved, leaving abrupt endings visualized as ball-like structures at the end of the processes. The dendrites and axons of filled cells were noted for these abrupt endings and if present were excluded from analysis. We also note that our reconstruction includes partial trees at least in the case of axons, that are not in continuity of the initial segment.

## *2. 6 Data analysis and statistics*

Electrophysiological properties were analyzed with Clampfit10 Software. Recordings were kept for analysis if the spikes overshoot 0mV and access resistance was  $<30\text{M}\Omega$ . Membrane resistance ( $R_m$ ) and access resistance ( $R_a$ ) were measured in voltage clamp (vc) using pClamp10 software. The following properties were assessed in current clamp (cc). Resting membrane potential (RMP) and spontaneous spiking were assessed over a 30s recording with no holding current. I-V curves were generated from 20pA current pulses ranging from -80pA to +100pA at the voltage sag-peak. To assess spike properties, cells were held at a holding potential (h.p.) of -65 mV and a series of 500 ms depolarizing current steps in 10pA increment steps was applied. The step which elicited the first spike or action potential (AP) was used to assess rheobase, decay time, AP peak amplitude and AP half width, and after-hyperpolarization (AHP) amplitude and time. The AHP time (ms) was measured from the time point the repolarization of the AP reached firing threshold to maximum amplitude of the AHP.

Firing pattern generated on double the rheobase current were used to categorize the firing patterns based on the Petila convention (Ascoli et al.2008) and were also used to analyze and determine

peak interspike interval (ISI) (ISI for the first two spikes), steady state ISI (ISI for the last two spikes). Spike frequency adaptation (SFA%) was determined using the following  $[(\text{First Instantaneous Frequency} - \text{Last instantaneous frequency}) / \text{First Instantaneous Frequency}]$ . Phase plots were analyzed in Clampfit10 Software for the first AP generated at double the rheobase current. To assess the hyperpolarization-activated sag current ( $I_h$ ), if present, a series of hyperpolarizing current steps was applied at a h.p. of -65 mV. The step which hyperpolarized the cell to -120 mV was used to calculate the sag amplitude, measured as the difference between peak and steady state hyperpolarization. Procedures to measure the location of the cell along the dorsal-ventral axis and in a specific layer were modified from (Pastoll, White, and Nolan 2012). In brief, after each recording session, the pipette would be pulled out of the cell carefully from a whole-cell configuration to a cell-attached mode. Using an Olympus microscope with a 4x objective, images of the position of the pipette relative to the dorsal border of the MEC were taken and stitched together for each cell. This was performed to confirm the location of the recorded cell for a specific layer and its location along the dorsal-ventral axis of the MEC. A total of 60 VIP cells were patched and recorded.

To assess the morphological properties of the recorded cells, the reconstruction of 17 (LI-III = 11 cells; LIV-VI = 6 cells) neurons were quantified with NeuroLucida 11 software (MBF Bioscience, United States). These neurons were considered for reconstruction as they had no visualized swellings in their axonal and dendritic arbours. Dendritic and axonal complexity were assessed using Sholl analysis in which concentric Sholl segments are generated starting from the center of the cell body (radial interval: 10 $\mu$ m) and the number of process intersections per Sholl segment are recorded. Branched structure analysis was conducted to estimate the total length of

the neural process contained within each layer of the MEC (Neurotrace/DAPI was used to distinguish between the different layers of the MEC). Data were not corrected for tissue shrinkage.

Statistical analysis was carried out using GraphPad prism software (San Diego, CA, USA). Data are presented as mean  $\pm$  standard error of the mean (SEM) throughout the text and in Tables 1 and 2. Statistical significance was tested with two-tailed Mann-Whitney U test (layer differences, vertical and horizontal extent of neurite process) and linear regression (dorsal-ventral). R2 values are stated for results of linear regression. A two-way analysis of variance (ANOVA) was performed to determine the length of neurite process present within in a layer. A post hoc Bonferroni test on all pairwise comparisons was performed to determine significance.

### **3 Results**

#### *3.1 Molecular characterization of VIP cells in the MEC*

We quantified the distribution of MEC VIP neurons in layer-specific and layer-independent manners by crossing transgenic VIP-ires-cre and tdTomato cre-reporter mice. To verify the validity of the mouse model and assess if the expression of tdTom in VIP cells is an effective way to identify VIP in a consistent manner, we performed IHC against VIP antibodies and other protein markers known to colocalize with VIP positive cells (Fig 1). We found that a total of  $6219.56 \pm 607.81$  cells expressed tdTomato (tdTom), of which  $5849.51 \pm 633$  cells were labelled with VIP IHC (Fig. 1C). Thus, 94.05% of tdTom cells colocalized with VIP (VIPtdTom). When quantified by cortical layer, VIP cell bodies were not equally distributed. Superficial MEC (LI-III) had the highest proportion of VIPtdTom cell bodies (89.28%), while the deep MEC (LIV-VI) consisted of 19.71% of the cell bodies ( $4673 \pm 388.40$  cells in the superficial layer vs  $1153.43 \pm 251.21$  cells in the deep layer) (Fig. 1D). These results indicate that tdTom expression is highly specific (Fig. 1A-D) for VIP-positive cells in the VIPcre/tdTom mouse line and thus suitable for the study. To

ascertain if VIP cells express other molecular markers, we performed IHC against antibodies for GABAergic cells (Fig. 1E-E''), Calretinin (CR, Fig. 1H-H'') and estimated the percent of colocalization with tdTom. For Fig 1B-D and Fig 1H-J, n = 3 animals, for Fig 1E-G n = 2 animals. We observed that all tdTom cells colocalized with GABA ( $4945.75 \pm 685.01$  cells). Our results indicate that 11.05% of the total GABAergic population are positive for VIP ( $4945.75 \pm 685.01$  tdTom cells of  $44726.64 \pm 727.24$  GABAergic cells) (Fig. 1F), similar to previous reports in the cortex (Rudy 2013; Tremblay, Lee, and Rudy 2016; Prönneke et al. 2015). As seen in other structures, VIP cells expressed CR in the MEC. Of all the CR-expressing cells, 45.63% colocalized with tdTom ( $3922 \pm 521.05$  CR-positive tdTom cells of  $8594.54 \pm 682$  CR cells) while 67.59% of tdTom cells colocalized with CR ( $3922 \pm 521.05$  CRtdTom cells of  $5802 \pm 520.72$  tdTom cells) (Fig. 1I). This is in line with results of VIP cells in hippocampus (Tyan et al. 2014) and basolateral amygdala (Rhomberg et al. 2018), but much higher than the 35% of colocalization observed in the visual cortex (Gonchar, Wang, and Burkhalter 2008). We further looked at the distribution of CR-positive tdTom cells across the layers (Fig. 1J). A large proportion (79.27%) of CR-positive tdTom cells were found in the superficial layers ( $3109.44 \pm 534.83$  cells). Previous studies reported that VIP positive cells do not overlap with other molecularly distinct subpopulations such as PV and SOM (Prönneke et al. 2015). We observed a similar pattern in our experiments (Fig S2. A-B'').

### *3. 2 Electrophysiological properties of VIP neurons vary between superficial and deep layers of the MEC*

Next, we determined the electrophysiological properties of 60 VIP cells from all layers of the MEC (LI-III n = 35; LIV-VI n = 25). Two passive membrane properties were significantly different between the two populations (Fig. 2B): VIP neurons in LIV-VI had higher input resistance (Fig. 2B(i)) compared to neurons present in LI-III ( $511.51 \pm 28.91$  vs  $418 \pm 18.63$  M $\Omega$ ,

Mann Whitney  $U = 257.0$ ,  $p = 0.0070$ ). Consistent with this difference, the amount of current (rheobase) (Fig. 2B(ii)) required to generate an action potential (AP) in deep MEC was lesser than the superficial VIP cells ( $20.22 \pm 2.66$  vs  $36.85 \pm 3.64$  pA, Mann Whitney  $U = 222.5$ ,  $p = 0.0012$ ). Layer differences were also observed for active membrane properties (Fig. 2C): Cells in the superficial layers had a smaller AP half-width compared to VIP cells in the deep layers ( $1.25 \pm 0.008$  vs  $1.6 \pm 0.103$  ms, Mann Whitney  $U = 260$ ,  $p = 0.008$ ) (Fig. 2C(i)), accordingly significant difference was observed in the maximum rise slope of spikes (Fig. 2C(ii)) between superficial and deep VIP cells ( $174.30 \pm 10.69$  vs  $126.75 \pm 8.85$  mV/ms, Mann Whitney  $U = 215$ ,  $p = 0.010$ ). We also found deep VIP cells to have a much longer duration in AHP time compared to superficial cells ( $72.78 \pm 5.21$  vs  $56.78 \pm 9.51$  ms, Mann Whitney  $U = 207$ ,  $p = 0.0006$ ) (Fig. 2C(iii)). No significant differences were observed in properties such as resting membrane potential (population average of  $-60 \pm 1.17$  mV), voltage sag amplitude ( $4.05 \pm 0.35$  mV), firing threshold ( $-41.28 \pm 0.77$  mV), peak amplitude ( $6.62 \pm 1.3$  mV), half-amplitude ( $33.22 \pm 0.64$  mV), AHP amplitude ( $-11.10 \pm 0.67$  mV), and steady state inter-spike interval ( $37.59 \pm 3.65$  ms) (Table 1). I-V curves and phase plots for VIP cells located in superficial and deep cells are included in Fig S2.

### *3.3 Electrophysiological properties of VIP cells vary along the Dorsal-Ventral (D-V) axis of the MEC*

Grid cells in the MEC show variation in their grid scales along the D-V axis (Brun et al., 2008; Hafting et al., 2005, Sargolini et al., 2006). To understand the potential mechanism underlying this topographical organization, previous work has investigated if the active and passive membrane properties of the different classes of excitatory cells differed depending on their location from the dorsal border. Prior studies have shown that stellate cells exhibit a gradient in the input resistance (IR), membrane time constant and rheobase (Garden et al. 2008; Giacomo and

Hasselmo 2008) and hyperpolarization-activated cation current ( $I_h$ ) (Giocomo et al., 2011). We asked if VIP cells show a similar gradient in their properties along the D-V axis (Fig. 3B-D). We recorded 58 VIP-expressing cells (LI-III = 33; LIV-VI = 25 cells) along the D-V axis (we excluded 2 cells due to an inability to quantify the position of the recording pipette). Since we observed layer differences in the electrophysiological properties, we further asked if passive and active properties varied as a function of cell's laminar position. We found that for VIP cells located in deep MEC, the rheobase (Fig. 3C(ii)) was much larger for neurons located close to the dorsal border as compared to those recorded at more ventral locations (slope =  $-0.012 \pm 0.005$  pA R2 = 0.163,  $p = 0.045$ ). Interestingly, the input resistance (Fig. 3B(ii)) and firing threshold of these cells showed no dependence on the location of the cell along the D-V axis (Fig. 3D(ii)). For cells located in the superficial layers, the firing threshold (Fig. 3D(i)) steeply increased with cell's distance from the dorsal border (slope =  $0.0033 \pm 0.0011$ mV R2 = 0.213,  $p = 0.006$ ), while other properties showed no dependency on the location of the cell along the dorsal border (data not shown).

### *3. 4 VIP cells show heterogeneity in their firing patterns*

Next, we sought to investigate the firing patterns of VIP neurons in the MEC. As reported in previous studies, VIP cells were never fast-spiking, but showed the following firing patterns, according to description in the Petila convention (G. A. Ascoli 2008): irregular spiking (IS, 60%), continuous non-adapting (CNA, 30%) and continuous adapting (CA, 10%) (Fig. S1C). We further investigated the distribution of these firing patterns within the MEC layers. In the superficial layers ( $n = 35$  cells), 61% of the cells had IS firing pattern, while CNA and CA comprised of the remaining 24% and 10% respectively (Fig. 4C). In the deep layers ( $n = 25$  cells), 56% of the cells had IS firing pattern while 40% were CNA and the remaining 4% were CA (Fig. 4D).

### 3.5 Morphological features of individual VIP neurons

To study the morphological features of VIP cells, we reconstructed and analyzed the dendritic and axonal morphology of 17 VIP neurons from all layers of the MEC. We found that most VIP cells presented with a bitufted (Fig. 5A(i&ii)) or a multipolar morphology (Fig. 5A(iii)). Our reconstructions indicate that deep VIP cells exhibited dense dendritic arborization. Indeed, we found that cells in the deep layers have a greater horizontal spread of their dendritic trees (Fig. 5D(i)) ( $385.01 \pm 46.9$  vs  $202.70 \pm 16.98\mu\text{m}$ , Mann Whitney U = 8.00, p = 0.013), while the dendrites of cells in LI-III are spread across the vertical column (Fig. 5D(ii)) ( $339 \pm 16.60$  vs  $107 \pm 31.15\mu\text{m}$ , Mann Whitney U = 1.00, p = 0.001). We found no significant differences in the horizontal or vertical extent of the axonal arbours between the two groups (data not shown). Given the difference in the dendritic expanse, we asked if the location of the cell influenced its projection to different layers. Cells in the superficial layers extended their axons well into the deep layers, however deep VIP cells made almost no contact to the superficial layers (Fig. 5E(i)). Layer III had extensive dendritic arborizations from superficial cells (p<0.001, t = 4.487), while dendrites from the deep layers rarely extended beyond layer IV and thus their projections were more local (p<0.01, t = 3.573) (Fig. 5E(ii)). A Sholl analysis revealed that most dendrites and axons were found locally near the soma ( $\leq 300 \mu\text{m}$ ) for both groups (Fig. 5F). However, it appears that the dendritic spread (Fig. 5F(ii)) for cells in the deep layers is much broader, while for superficial cells, it peaked at  $100\mu\text{m}$  from the soma.

#### **4 Discussion**

Using in vitro whole cell patch clamp recordings, we investigate the distribution, morphology, active and passive membrane properties of VIP interneurons in the MEC. We validate that our VIP cre-driver mouse line is efficient and a suitable model system for studying the VIP population in the MEC. Our results confirm that VIP neurons in the MEC are a heterogenous

population of cells, similar to reports from the hippocampus (Tyan et al. 2014), barrel cortex (Prönneke et al. 2015) and the BLA (Rhomberg et al. 2018). This study also extends previous findings on VIP cells in the MEC (Ferrante et al. 2017) in the following ways: we show evidence for a gradient in both the active and passive membrane properties of VIP cells along the D-V extent of the MEC, and that these differences are preserved between VIP cells in superficial and deep layers. Our results further indicate that VIP cells present with three different firing patterns, of which, irregular spiking cells are the most prominent type. Furthermore, morphological differences between superficial and deep VIP cells indicate that the input and output domains for superficial VIP cells are different from those seen in VIP cells located in the deep layers.

#### *4.1 VIP cells show heterogeneity in their electrophysiological and morphological properties*

In our dataset we find that the heterogeneity in firing patterns in VIP cells are similar to previous reports from other cortical areas. However, the predominance of IS firing pattern in our dataset differs from some of these previous studies. This increase in IS firing pattern could be explained by the number of VIP cells that co-express CR in the MEC. Previous studies from the hippocampus (Tyan et al. 2014) and other cortical structures (Guet-McCreight, Skinner, and Topolnik 2020) report an increase in the incidence of IS firing patterns when the cell co-expresses both VIP and CR. In addition to this, previous studies have also noted that VIP cells that colocalize with CR are disinhibitory in nature (Turi et al., 2019; Tyan et al., 2014, Guet-McCreight et al., 2020). From our IHC experiments, we find that 67.59% of the total tdTom cells colocalize with CR. Interestingly, we observe that 60% of the total VIP population in the MEC exhibited IS firing patterns. Taking layers into consideration, we see that 79.27% are positive for both CR and VIP markers. This could be reflected by the 61% incidence of IS firing patterns we observe in the

superficial layers. However, it is also possible that VIP positive cells that co-express CR do not exhibit IS firing patterns as shown in (Goff and Goldberg 2019). To ascertain if this is the case in the MEC, in a subset of our recorded and biocytin-filled cells, we labelled for CR and noted if the presence or absence of this calcium binding protein made any distinction among the VIP positive cells. Of the 4 cells tested, 2 were found to be positive for CR (Fig. S3A-C''') and the presence of CR made no distinction among VIP cells with different firing patterns (2 out of 4 cells that expressed CR had IS and CNA firing pattern (Fig S3D-H), while the other two cells also showed the same firing patterns). We note that the sample size from this experiment is low and further work is required to determine if the observations hold true for a larger population of VIP cells in the MEC. In addition to this, in our recordings, we do not find VIP cells with a bursting firing pattern, a characteristic of VIP cells previously reported in (Prönneke et al. 2020). Some studies attribute that cells that exhibit this firing characteristic belong to the CCK family (He et al. 2016). The presence of high numbers of CR positive tdTom cells as seen in our IHC experiments may explain this discrepancy. While this predominance may indicate a primarily disinhibitory circuit motif in the MEC, it remains to be established if the post-synaptic targets of VIP cells in the MEC are interneurons or if excitatory cells are also targeted by this population of cells. In terms of other electrophysiological properties, our population averages for superficial VIP cells are similar to a prior report, with the exception of a higher percentage of VIP cells with IS firing patterns (Ferrante et al. 2017).

The position of VIP cells within the MEC is associated with different morphological and electrophysiological properties. In terms of morphological features, we noticed both superficial and deep VIP cells present with similar dendritic and axonal architecture. However, their location in a specific layer dictates their projection patterns. Cells in the superficial layers had either a

multipolar or vertical bitufted morphology enabling it to span the entire cortical column, similar to the observations from the barrel cortex (Bayraktar et al. 2000; Prönneke et al. 2015). These cells are well positioned to receive and transmit incoming information to the entire MEC cortical mantle, while the cells in the deep MEC are found to exclusively cater to the deeper layers of the MEC. Furthermore, we notice that as the cells are located increasingly outwards from the MEC (from LI to LVI), the tendency of the axonal fibers to innervate the superficial layers decreases. Interestingly, this similarity in the neurite processes between superficial and deep MEC is also observed in VIP cells in the barrel cortex (Prönneke et al. 2015). We also note that in some VIP cells (Fig 4B (a) & Fig 5B (b)), the dendritic and axonal morphologies are similar to those observed in the BLA (Rhomberg et al. 2018), an unlayered structure. In the BLA, VIP cells are known to target both PV, SOM interneurons and to a lesser extent pyramidal cell (Krabbe et al. 2019). It remains to be seen if a similar connectivity is observed in the MEC.

We also identified differences in several electrophysiological properties between layers, notably in input resistance and rheobase. As a population, MEC VIP cells, are highly excitable, much like their counterparts in other structures (Kepecs & Fishell, 2014; Prönneke et al., 2015; Rhomberg et al., 2018; Tyan et al., 2014, Guet-McCreight et al., 2020). From the current dataset, we found that deep VIP cells are more excitable than superficial cells. Moreover, we saw a gradient in this intrinsic excitability wherein cells located in ventral MEC require less current to fire an AP compared to cells in dorsal MEC. The gradients in excitability that we report could provide a gating mechanism that prioritizes certain outputs from the MEC as deep MEC sends projections to various intrathalamic structures and LII of the MEC (Sürmeli et al. 2015; Ohara et al. 2018) whereas superficial MEC primarily projects to the hippocampus (Canto, Wouterlood, and Witter 2008).

## **5 Functional implications**

There is a growing body of work suggesting that VIP interneurons are critical for facilitating associative learning and maintenance of the E/I balance in various cortical structures. In most structures, VIP cells located in layers I-III, the input layers of the cortex, innervate SOM, PV cells (Krabbe et al. 2018; Pi et al. 2013; Guet-McCreight, Skinner, and Topolnik 2020) and thus provide for a break from ongoing inhibition in excitatory cells in the superficial layer. In the MEC, the majority of the VIP population (89%) is found in the LI-III which forms its primary input domain (Witter et al. 2017). Furthermore, morphologies of VIP cells from LI-III show that these cells are well-positioned to transmit incoming information to cells within their layer and across the different layers of the MEC, thus making them likely candidates to target other interneurons and excitatory cells across the MEC. Our findings also show that a minority of VIP cells may not send projections to the superficial layers. Their specific functional role within the MEC circuit will require further studies. Through our experiments, we show that the VIP<sup>cre</sup>/tdTom mice line are suitable models for future experiments to determine the functions of this cell population in vivo.

## **6 Acknowledgements**

We thank Drs. Marie Oulé, Coralie-Anne Mosser, Jennifer C. Robinson, Alexandra T. Keinath and Robert R. Rozeske for comments on earlier versions of this manuscript. The present study used the services of the Molecular and Cellular Microscopy Platform in the Douglas Hospital Research Center. This work was supported by a McGill University ‘Healthy Brain for Healthy Lives’ CFREF doctoral fellowship to S.B., and funding from the Canadian Institutes for Health Research grants (#367017 and #377074), the National Sciences and Engineering Council (Discovery grant #74105), the Scottish Rite Charitable Foundation, and the Canada Research Chairs Program to M.P.B.

**Author contributions:** All authors helped to conceive and plan this study. S.B. collected and analyzed all data. S.B. and M.P.B. wrote the manuscript.

**Competing interests:** None.

## 7 References

- Ascoli, G. A. (2008). Petilla terminology: Nomenclature of features of GABAergic interneurons of the cerebral cortex. *Nature Reviews ...*, 9(july), 557–568. <https://doi.org/10.1038/nrn2402>.
- Batista-Brito, R., Vinck, M., Ferguson, K. A., Chang, J. T., Laubender, D., Lur, G., ... Cardin, J. A. (2017). Developmental Dysfunction of VIP Interneurons Impairs Cortical Circuits. *Neuron*, 95(4), 884-895.e9. <https://doi.org/10.1016/j.neuron.2017.07.034>
- Bayraktar, T., Welker, E., Freund, T. F., Zilles, K., & Staiger, J. F. (2000). Neurons immunoreactive for vasoactive intestinal polypeptide in the rat primary somatosensory cortex: Morphology and spatial relationship to barrel-related columns. *Journal of Comparative Neurology*, 420(3), 291–304. [https://doi.org/10.1002/\(SICI\)1096-9861\(20000508\)420:3<291::AID-CNE2>3.0.CO;2-H](https://doi.org/10.1002/(SICI)1096-9861(20000508)420:3<291::AID-CNE2>3.0.CO;2-H)
- Boccarda, C. N., Sargolini, F., Thoresen, V. H., Solstad, T., Witter, M. P., Moser, E. I., & Moser, M.-B. (2010). Grid cells in pre- and parasubiculum. *Nature Neuroscience*, 13(8), 987–994. <https://doi.org/10.1038/nn.2602>
- Bonnevie, T., Dunn, B., Fyhn, M., Hafting, T., Derdikman, D., Kubie, J. L., ... Moser, M.-B. (2013). Grid cells require excitatory drive from the hippocampus. *Nature Neuroscience*, 16(3), 309–317. <https://doi.org/10.1038/nn.3311>

- Brun, V. H., Solstad, T., Kjelstrup, K. B., Fyhn, M., Witter, M. P., Moser, E. I., & Moser, M. B. (2008). Progressive increase in grid scale from dorsal to ventral medial entorhinal cortex. *Hippocampus*, 18(12), 1200–1212. <https://doi.org/10.1002/hipo.20504>
- Buetfering, C., Allen, K., & Monyer, H. (2014). Parvalbumin interneurons provide grid cell-driven recurrent inhibition in the medial entorhinal cortex. *Nature Neuroscience*, 17(5), 710–718. <https://doi.org/10.1038/nn.3696>
- Canto, C. B., Wouterlood, F. G., & Witter, M. P. (2008). What does the anatomical organization of the entorhinal cortex tell us? *Neural Plasticity*, 2008. <https://doi.org/10.1155/2008/381243>
- Couey, J. J., Witoelar, A., Zhang, S.-J., Zheng, K., Ye, J., Dunn, B., ... Witter, M. P. (2013). Recurrent inhibitory circuitry as a mechanism for grid formation. *Nature Neuroscience*, 16(3), 318–324. <https://doi.org/10.1038/nn.3310>
- Ferrante, M., Tahvildari, B., Duque, A., Hadzipasic, M., Salkoff, D., Zaghera, E. W., ... McCormick, D. A. (2017). Distinct Functional Groups Emerge from the Intrinsic Properties of Molecularly Identified Entorhinal Interneurons and Principal Cells. *Cerebral Cortex*, 27(6), 3186–3207. <https://doi.org/10.1093/cercor/bhw143>
- Fuchs, E. C., Neitz, A., Pinna, R., Melzer, S., Caputi, A., & Monyer, H. (2016). Local and Distant Input Controlling Excitation in Layer II of the Medial Entorhinal Cortex. *Neuron*, 89(1), 194–208. <https://doi.org/10.1016/j.neuron.2015.11.029>
- Garcia-Junco-Clemente, P., Tring, E., Ringach, D. L., & Trachtenberg, J. T. (2019). State-Dependent Subnetworks of Parvalbumin-Expressing Interneurons in Neocortex. *Cell Reports*, 26(9), 2282–2288.e3. <https://doi.org/10.1016/j.celrep.2019.02.005>

- Garden, D. L. F., Dodson, P. D., O'Donnell, C., White, M. D., & Nolan, M. F. (2008). Tuning of Synaptic Integration in the Medial Entorhinal Cortex to the Organization of Grid Cell Firing Fields. *Neuron*, 60(5), 875–889. <https://doi.org/10.1016/j.neuron.2008.10.044>
- Giocomo, L. M., & Hasselmo, M. E. (2008). Time constants of h current in layer II stellate cells differ along the dorsal to ventral axis of medial entorhinal cortex. *Journal of Neuroscience*, 28(38), 9414–9425. <https://doi.org/10.1523/JNEUROSCI.3196-08.2008>
- Giocomo, L. M., Hussaini, S. a., Zheng, F., Kandel, E. R., Moser, M. B., & Moser, E. I. (2011). Grid cells use HCN1 channels for spatial scaling. *Cell*, 147(5), 1159–1170. <https://doi.org/10.1016/j.cell.2011.08.051>
- Goff, K. M., & Goldberg, E. M. (2019). Vasoactive intestinal peptide-expressing interneurons are impaired in a mouse model of dravet syndrome. *ELife*, 8, 1–28. <https://doi.org/10.7554/eLife.46846>
- Gonchar, Y., Wang, Q., & Burkhalter, A. (2008). Multiple distinct subtypes of GABAergic neurons in mouse visual cortex identified by triple immunostaining. *Frontiers in Neuroanatomy*, 1(MAR). <https://doi.org/10.3389/neuro.05.003.2007>
- Gonzalez-Sulser, A., Parthier, D., Candela, A., McClure, C., Pastoll, H., Garden, D., ... Nolan, M. F. (2014). GABAergic Projections from the Medial Septum Selectively Inhibit Interneurons in the Medial Entorhinal Cortex. *Journal of Neuroscience*, 34(50), 16739–16743. <https://doi.org/10.1523/JNEUROSCI.1612-14.2014>
- Guet-McCreight, A., Skinner, F. K., & Topolnik, L. (2020). Common Principles in Functional Organization of VIP/Calretinin Cell-Driven Disinhibitory Circuits Across Cortical Areas. *Frontiers in Neural Circuits*, 14(June), 1–14. <https://doi.org/10.3389/fncir.2020.00032>

- Hafting, T., Fyhn, M., Molden, S., Moser, M., & Moser, E. I. (2005). Microstructure of a spatial map in the entorhinal cortex. *Nature*, 436(7052), 801–806. <https://doi.org/10.1038/nature03721>
- He, M., Tucciarone, J., Lee, S. H., Nigro, M. J., Kim, Y., Levine, J. M., ... Huang, Z. J. (2016). Strategies and Tools for Combinatorial Targeting of GABAergic Neurons in Mouse Cerebral Cortex. *Neuron*, 91(6), 1228–1243. <https://doi.org/10.1016/j.neuron.2016.08.021>
- Jiang, X., Shen, S., Cadwell, C. R., Berens, P., Sinz, F., Ecker, A. S., ... Tolias, A. S. (2015). Principles of connectivity among morphologically defined cell types in adult neocortex. *Science*, 350(6264), aac9462–aac9462. <https://doi.org/10.1126/science.aac9462>
- Kang, L., & Balasubramanian, V. (2019). A geometric attractor mechanism for self-organization of entorhinal grid modules. *ELife*, 8. <https://doi.org/10.7554/elife.46687>
- Kepecs, A., & Fishell, G. (2014). Interneuron cell types are fit to function. *Nature*, 505(7483), 318–326. <https://doi.org/10.1038/nature12983>
- Krabbe, S., Paradiso, E., D'Aquin, S., Bitterman, Y., Courtin, J., Xu, C., ... Lüthi, A. (2019). Adaptive disinhibitory gating by VIP interneurons permits associative learning. *Nature Neuroscience*, 22(11), 1834–1843. <https://doi.org/10.1038/s41593-019-0508-y>
- Kuchibhotla, K. V., Gill, J. V., Lindsay, G. W., Papadoyannis, E. S., Field, R. E., Sten, T. A. H., ... Froemke, R. C. (2017). Parallel processing by cortical inhibition enables context-dependent behavior. *Nature Neuroscience*, 20(1), 62–71. <https://doi.org/10.1038/nn.4436>

- Lee, S., Kruglikov, I., Huang, Z. J., Fishell, G., & Rudy, B. (2013). A disinhibitory circuit mediates motor integration in the somatosensory cortex. *Nature Neuroscience*, 16(11), 1662–1670. <https://doi.org/10.1038/nn.3544>
- Letzkus, J. J., Wolff, S. B. E., & Lüthi, A. (2015). Disinhibition, a Circuit Mechanism for Associative Learning and Memory. *Neuron*, 88(2), 264–276. <https://doi.org/10.1016/j.neuron.2015.09.024>
- McNaughton, B. L., Battaglia, F. P., Jensen, O., Moser, E. I., & Moser, M.-B. (2006). Path integration and the neural basis of the “cognitive map.” *Nature Reviews Neuroscience*, 7(8), 663–678. <https://doi.org/10.1038/nrn1932>
- Miao, C., Cao, Q., Moser, M., & Moser, E. I. (2017). Parvalbumin and Somatostatin Interneurons Control Different Space-Coding Networks in the Medial Entorhinal Cortex. *Cell*, 171(3), 1–15. <https://doi.org/10.1016/j.cell.2017.08.050>
- Mittelstaedt, M. L., & Mittelstaedt, H. (1980). Homing by path integration in a mammal. *Naturwissenschaften*, 67(11), 566–567. <https://doi.org/10.1007/BF00450672>
- Moser, E. I., Kropff, E., & Moser, M.-B. (2008). Place cells, grid cells, and the brain’s spatial representation system. *Annu. Rev. Neurosci.*, 31, 69–89. <https://doi.org/10.1146/annurev.neuro.31.061307.090723>
- Moser, E. I., Roudi, Y., Witter, M. P., Kentros, C., Bonhoeffer, T., & Moser, M.-B. (2014). Grid cells and cortical representation. *Nature Reviews Neuroscience*, 15(7), 466–481. <https://doi.org/10.1038/nrn3766>

- Ohara, S., Onodera, M., Simonsen, Ø. W., Yoshino, R., Hioki, H., Iijima, T., ... Witter, M. P. (2018). Intrinsic Projections of Layer Vb Neurons to Layers Va, III, and II in the Lateral and Medial Entorhinal Cortex of the Rat. *Cell Reports*, 24(1), 107–116. <https://doi.org/10.1016/j.celrep.2018.06.014>
- Pastoll, H., White, M., & Nolan, M. (2012). Preparation of parasagittal slices for the investigation of dorsal-ventral organization of the rodent medial entorhinal cortex. *Journal of Visualized Experiments : JoVE*, e3802(61), 1–9. <https://doi.org/10.3791/3802>
- Pfeffer, C. K., Xue, M., He, M., Huang, Z. J., & Scanziani, M. (2013). Inhibition of inhibition in visual cortex: The logic of connections between molecularly distinct interneurons. *Nature Neuroscience*, 16(8), 1068–1076. <https://doi.org/10.1038/nn.3446>
- Pi, H.-J., Hangya, B., Kvitsiani, D., Sanders, J. I., Huang, Z. J., & Kepecs, A. (2013). Cortical interneurons that specialize in disinhibitory control. *Nature*, 503(7477), 521–524. <https://doi.org/10.1038/nature12676>
- Prönneke, A., Scheuer, B., Wagener, R. J., Möck, M., Witte, M., & Staiger, J. F. (2015). Characterizing VIP neurons in the barrel cortex of VIPcre/tdTomato mice reveals layer-specific differences. *Cerebral Cortex*, 25(12), 4854–4868. <https://doi.org/10.1093/cercor/bhv202>
- Prönneke, A., Witte, M., Möck, M., & Staiger, J. F. (2020). Neuromodulation Leads to a Burst-Tonic Switch in a Subset of VIP Neurons in Mouse Primary Somatosensory (Barrel) Cortex. *Cerebral Cortex* (New York, N.Y. : 1991), 30(2), 488–504. <https://doi.org/10.1093/cercor/bhz102>

- Ramsden, H. L., Sürmeli, G., McDonagh, S. G., & Nolan, M. F. (2015). Laminar and dorsoventral molecular organization of the medial entorhinal cortex revealed by large-scale anatomical analysis of gene expression. *PLoS Computational Biology*, 11(1), e1004032. <https://doi.org/10.1371/journal.pcbi.1004032>
- Rhomberg, T., Rovira-Esteban, L., Vikór, A., Paradiso, E., Kremser, C., Nagy-Pál, P., ... Hájos, N. (2018). VIP-immunoreactive interneurons within circuits of the mouse basolateral amygdala. *The Journal of Neuroscience*, 38(31), 2063–17. <https://doi.org/10.1523/JNEUROSCI.2063-17.2018>
- Rudy, B. R., Fishell, G., Lee, S., & Leffler-Hjerling, J. (2013). Three Groups of Interneurons Account for Nearly 100% of Neocortical GABAergic Neurons, 71(1), 45–61. <https://doi.org/10.1002/dneu.20853>.Three
- Sargolini, F., Fyhn, M., Hafting, T., McNaughton, B. L., Witter, M. P., Moser, M.-B., & Moser, E. I. (2006). Conjunctive Representation of Position, Direction, and Velocity in Entorhinal Cortex. *Science*, 312(5774), 758–762.
- Solstad, T., Solstad, T., Boccara, C. N., Boccara, C. N., Kropff, E., Kropff, E., ... Moser, E. I. (2008). Representation of geometric borders in the entorhinal cortex. *Science*, 322(December), 1865–1868. <https://doi.org/10.1126/science.1166466>
- Sürmeli, G., Marcu, D. C., McClure, C., Garden, D. L. F., Pastoll, H., & Nolan, M. F. (2015). Molecularly Defined Circuitry Reveals Input-Output Segregation in Deep Layers of the Medial Entorhinal Cortex. *Neuron*, 88(5), 1040–1053. <https://doi.org/10.1016/j.neuron.2015.10.041>

- Swietek, B., Gupta, A., Proddatur, A., & Santhakumar, V. (2016). Immunostaining of biocytin-filled and processed sections for neurochemical markers. *Journal of Visualized Experiments*, 2016(118), 1–9. <https://doi.org/10.3791/54880>
- Tremblay, R., Lee, S., & Rudy, B. (2016). GABAergic Interneurons in the Neocortex: From Cellular Properties to Circuits. *Neuron*, 91(2), 260–292. <https://doi.org/10.1016/j.neuron.2016.06.033>
- Turi, G. F., Li, W. K., Chavlis, S., Pandi, I., O'Hare, J., Priestley, J. B., ... Losonczy, A. (2019). Vasoactive Intestinal Polypeptide-Expressing Interneurons in the Hippocampus Support Goal-Oriented Spatial Learning. *Neuron*, 101(6), 1150-1165.e8. <https://doi.org/10.1016/j.neuron.2019.01.009>
- Tyan, L., Chamberland, S., Magnin, E., Camire, O., Francavilla, R., David, L. S., ... Topolnik, L. (2014). Dendritic Inhibition Provided by Interneuron-Specific Cells Controls the Firing Rate and Timing of the Hippocampal Feedback Inhibitory Circuitry. *Journal of Neuroscience*, 34(13), 4534–4547. <https://doi.org/10.1523/JNEUROSCI.3813-13.2014>
- Winterer, J., Maier, N., Wozny, C., Beed, P., Breustedt, J., Evangelista, R., ... Schmitz, D. (2017). Excitatory Microcircuits within Superficial Layers of the Medial Entorhinal Cortex. *Cell Reports*, 19(6), 1110–1116. <https://doi.org/10.1016/j.celrep.2017.04.041>
- Witter, M. P., Doan, T. P., Jacobsen, B., Nilssen, E. S., & Ohara, S. (2017). Architecture of the Entorhinal Cortex A Review of Entorhinal Anatomy in Rodents with Some Comparative Notes. *Frontiers in Systems Neuroscience*, 11(June), 46. <https://doi.org/10.3389/fnsys.2017.00046>

**figure legends:**

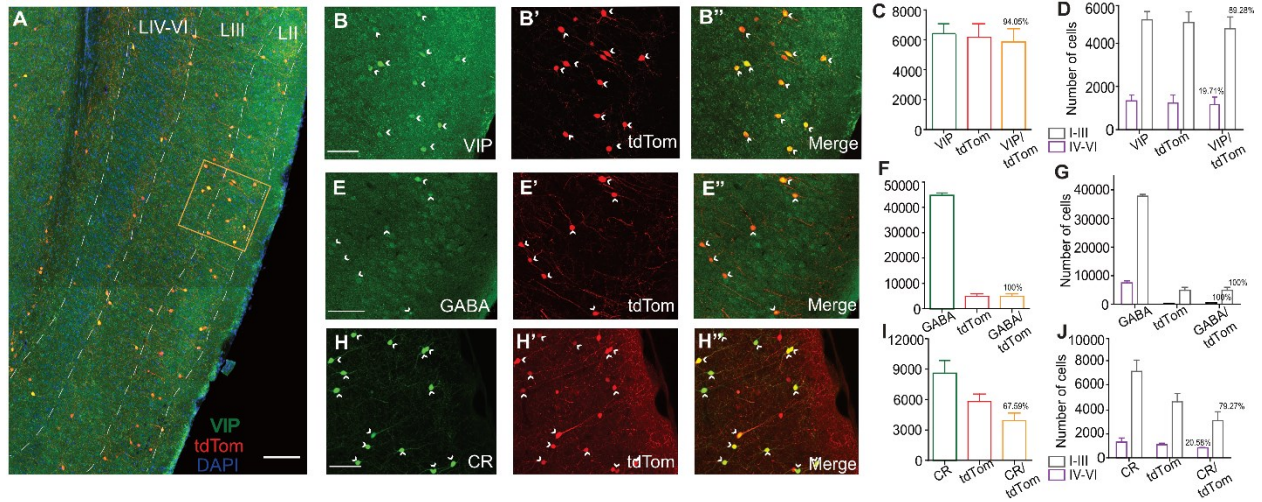


**Figure 1. Specificity of cre-driven fluorescence for VIP in VIPcre/tdTom mice and presence of colocalization with other molecular markers.** (A) Co-expression of VIP (green) and tdTom (red) in a sagittal section of the MEC at low magnification 10x. Layers of the MEC (white dashed lines) marked using DAPI as reference. High magnification of framed area (orange box) is shown in B-B''. (B-H'') 20x maximum projection intensities of a 40- $\mu$ m thick section of superficial MEC treated with IHC using  $\alpha$ VIP AB (B-B''),  $\alpha$ GABA AB (E-E'') and  $\alpha$ CR AB (H-H''). Fluorescence of cre-driven tdTomato expression is shown in red (B'-H') and colocalization of the two channels is shown in (B''-H''). Presence of colocalization is indicated by yellow cell bodies and white arrow heads. Graphs depicting the total number of cells present in the MEC (C, F and I) and distribution of somas in different layers of the MEC (D, G and J) for  $\alpha$ VIP,  $\alpha$ GABA and  $\alpha$ CR respectively are shown here. Percentages displayed for colocalization bar show the number of tdTom positive cell bodies which colocalize with the IHC marker. For IHCs performed for  $\alpha$ VIP and  $\alpha$ CR, n = 3 animals and for IHC performed against  $\alpha$ GABA, n = 2 animals.

Each bar represents a mean and error bars represent SEM. For panels B-H'' scale bars are 250 $\mu$ m.

Scale bar in A is 500 $\mu$ m.

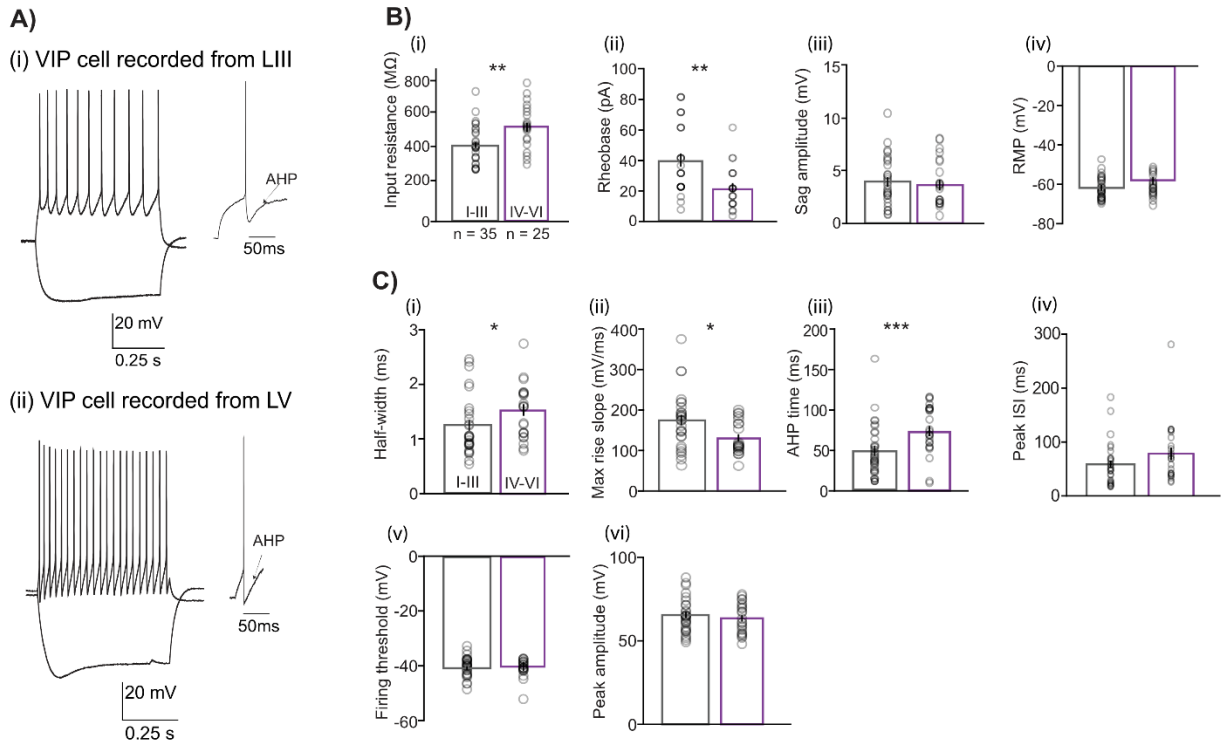


**Figure 2. Comparison of electrophysiological properties between LI-LIII and LIV-LVI VIP cells.** (A) Examples of membrane potential responses to current steps (-80pA for lower trace and +100pA for upper trace) recorded from VIP cells located in the (i) superficial (LIII) and (ii) deep (LV) layers of the MEC. Examples of afterhyperpolarizations (AHP) following action potentials are also shown for the respective cells. (B) Passive and C) Active membrane properties for 60VIP cells separated into layer I-III (n=35) and layers IV-VI (n=25). Except for (iii) sag amplitude where layer I-III (n=33) and layers IV-VI (n=24) and (iv) Peak ISI where layer I-III (n=33) and layers IV-VI (n=22). Each bar represents a mean and error bars represent SEM. Significant differences were found in B (i) input resistance, (ii) rheobase and C(i) half-width, (ii) AHP time and (iii) max rise slope. (\*=  $p < 0.05$ , \*\*=  $p < 0.01$ , \*\*\*=  $p < 0.0001$ )

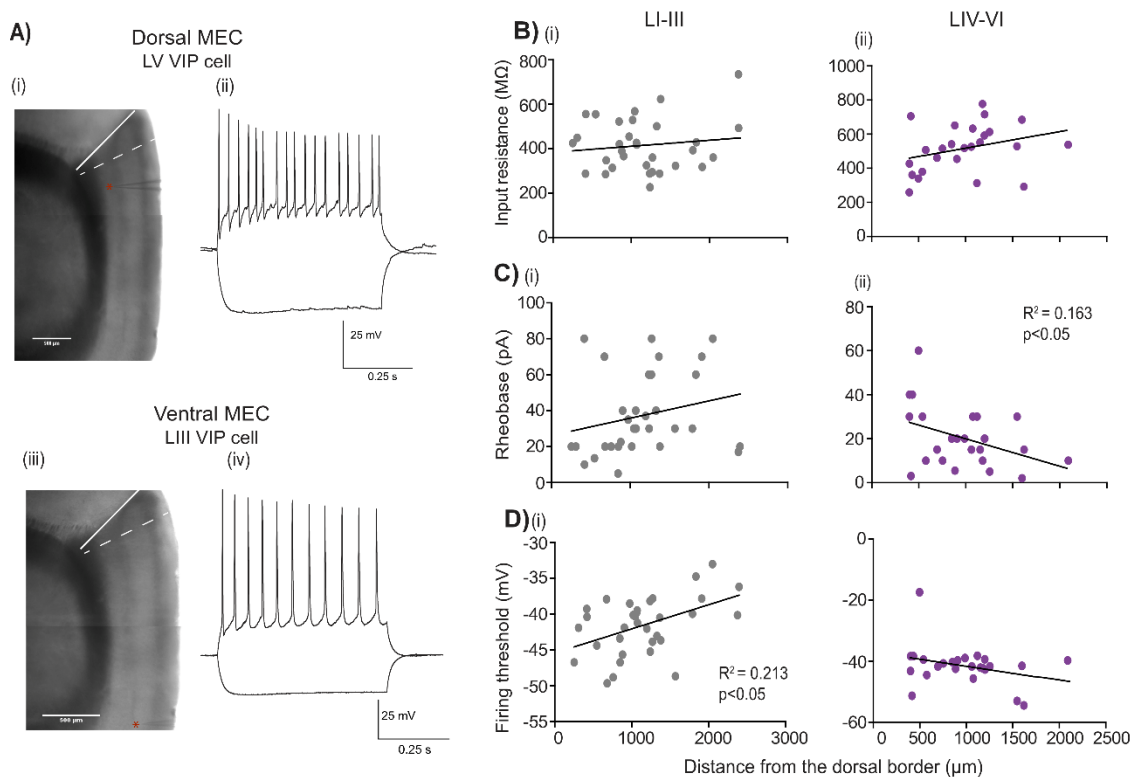


**Figure 3. Passive and Active properties as a function of layer and location along the Dorsal-Ventral axis.** (A (i & iii) Parasagittal brain slice under the experimental microscope (aligned and blended composites of low magnification 4x images). The border between the postrhinal cortex and sensory cortex is indicated by a white solid line, while the dorsal border of the MEC is indicated by a white dashed line. The position of the dorsal cell in A (ii), located 286 $\mu$ m from the dorsal MEC border and the ventral cell shown in A(iv), located 2128 $\mu$ m from the dorsal MEC border, are indicated by a red star near the recording pipette in the respective sections. (A (ii & iv) Examples of membrane potential responses to -80pA (lower traces) and +80pA (upper traces) current step recorded from (ii) LV VIP cell and (iv) LIII VIP cell. (B-D) Passive and active properties plotted as a function of location and layer for individual VIP cells recorded from the superficial layers LI-III: 35 cells (B, C and D (i)) and (B, C, and D (ii)) deep layers LIV-VI: 25 cells. In all panels, black lines indicate linear fits to the data. For cells located in the deep MEC

significance in slope for C(ii) rheobase is observed, and for cells located in the superficial layers significance in slope for D(i) firing threshold is observed.

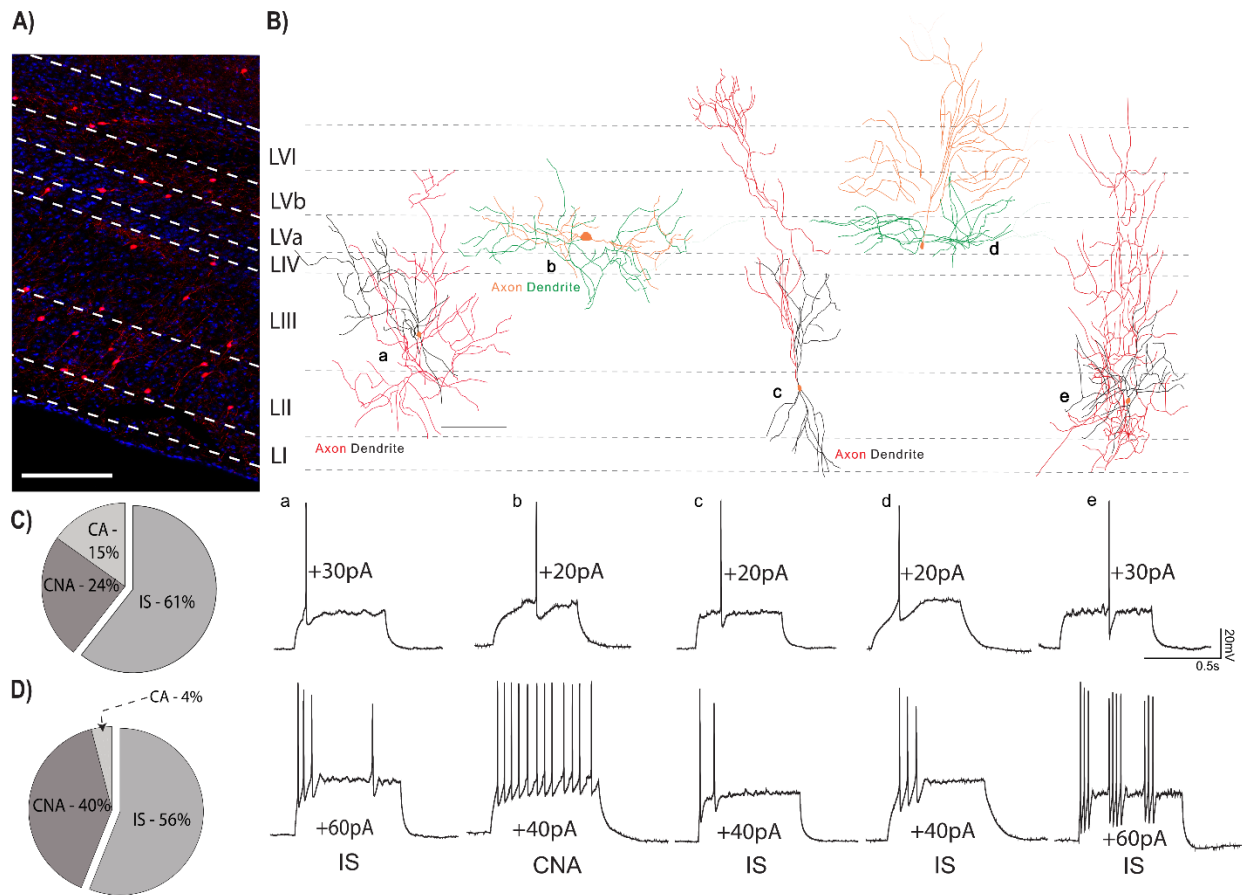


**Figure 4. Variability in firing patterns of VIP cells from layers I-III and IV-VI.**

(A) Distribution of VIP cells (tdTom) in the MEC, the layers have been marked using DAPI as reference. Scale bar is 500µm. (B) The reconstructed morphology of 5 individual VIP cells is shown in a schematic of the MEC. For all cells somas are coloured in orange. For cells recorded in superficial MEC axonal and dendritic processes are coloured in red and black, respectively. For cells recorded from layers IV-VI, axons are in orange while dendrites are coloured green. Below, electrophysiological recordings from the respective cells at rheobase (upper trace) and action potential firing pattern at suprathreshold current (lower traces). Scale bar in B is 100µm. Percentages of various firing pattern observed in the (C) superficial layers of the MEC and (D)

deep layers of the MEC. Abbreviations name the firing pattern after the Petila convention (Ascoli et al.2008; IS, Irregular spiking; CA, Continuous adapting; CNA, continuous non-adapting)

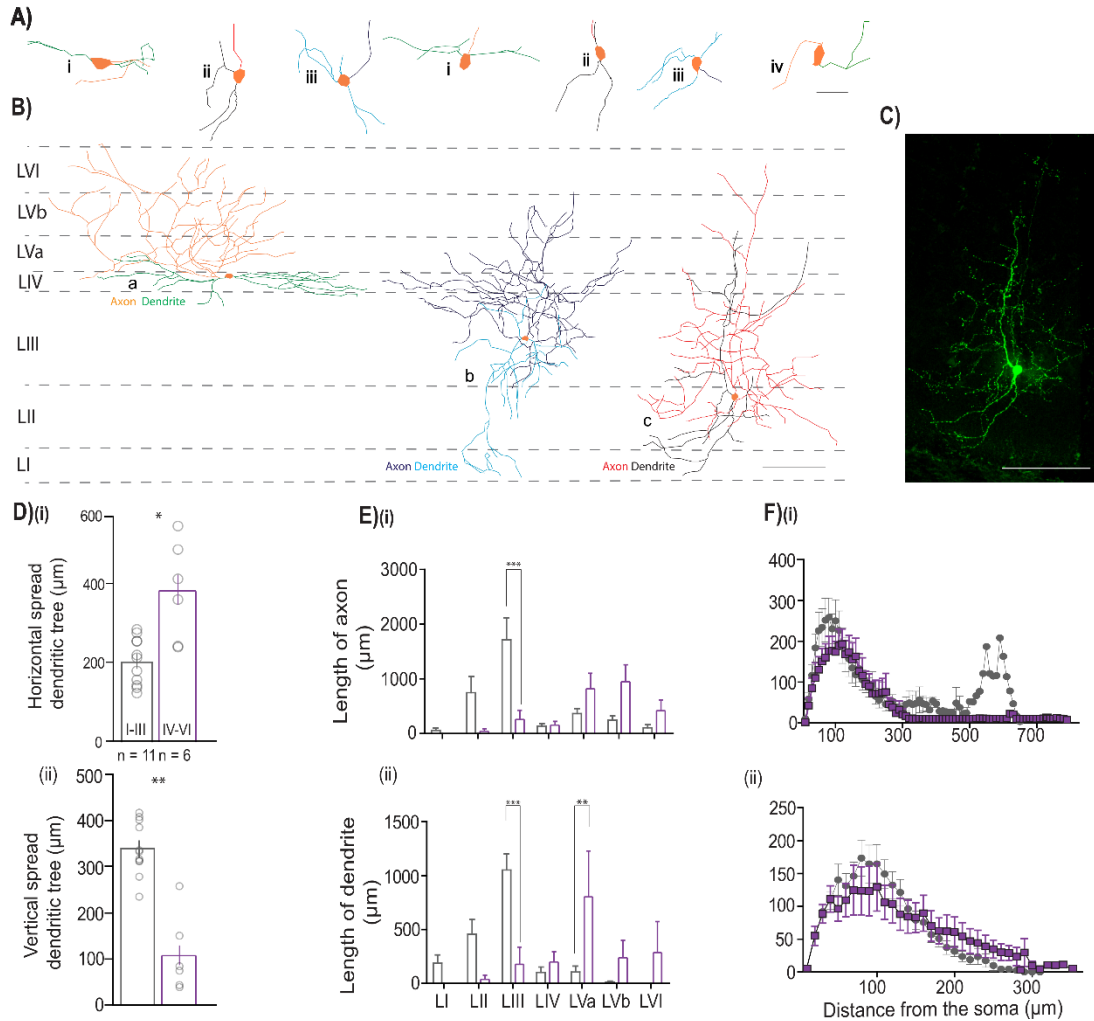
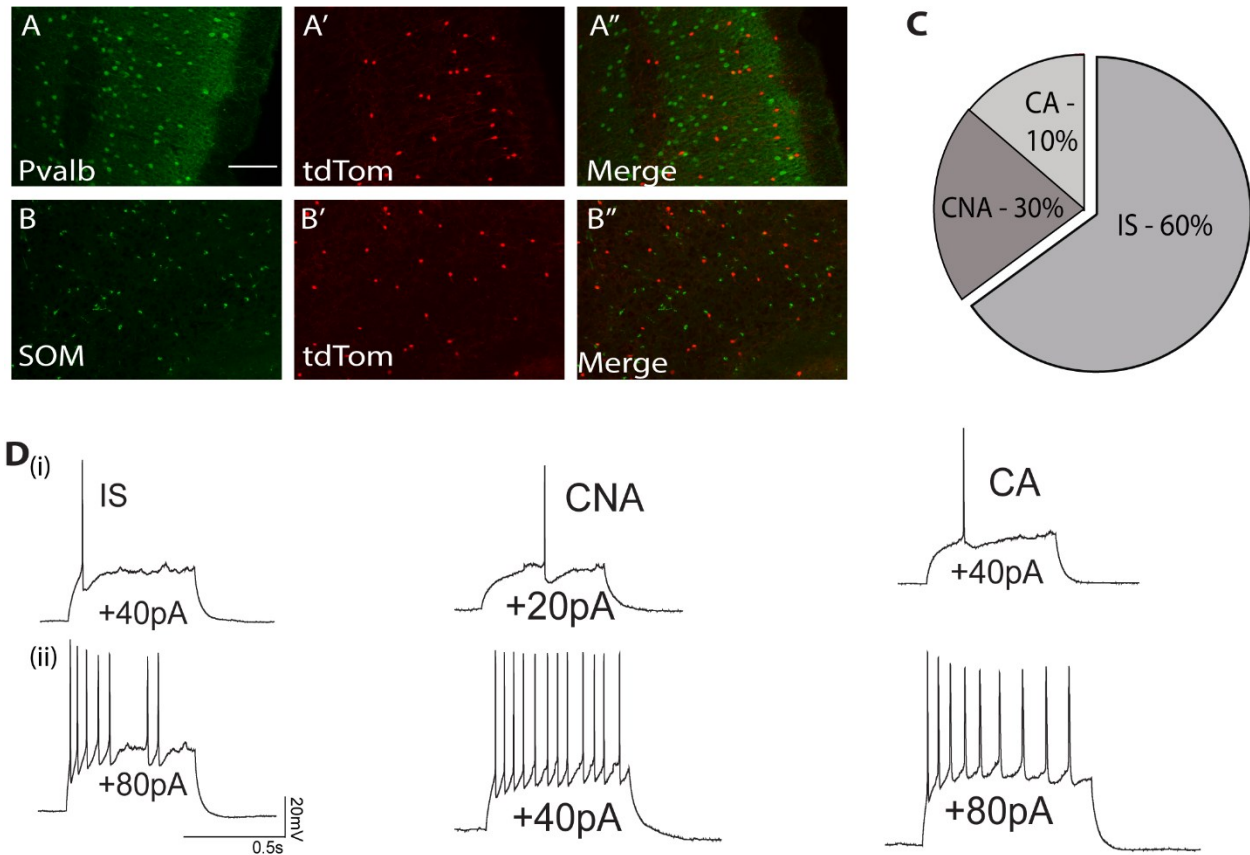


**Figure 5. Morphometric analysis of VIP cells**

(A) Magnified views of the somatodendritic and axonal processes representing the following morphologies: i - horizontal bitufted, ii – vertical bitufted, iii - multipolar and iv - unipolar architectures. Scale bar is  $50\mu\text{m}$ . Please note that in A (ii - right), the axon originates from a primary dendrite. (B) Schematic of the MEC with neuroLucida reconstructions depicting the three predominant morphologies observed in the data; horizontal bitufted in L4 (a; axons in orange,

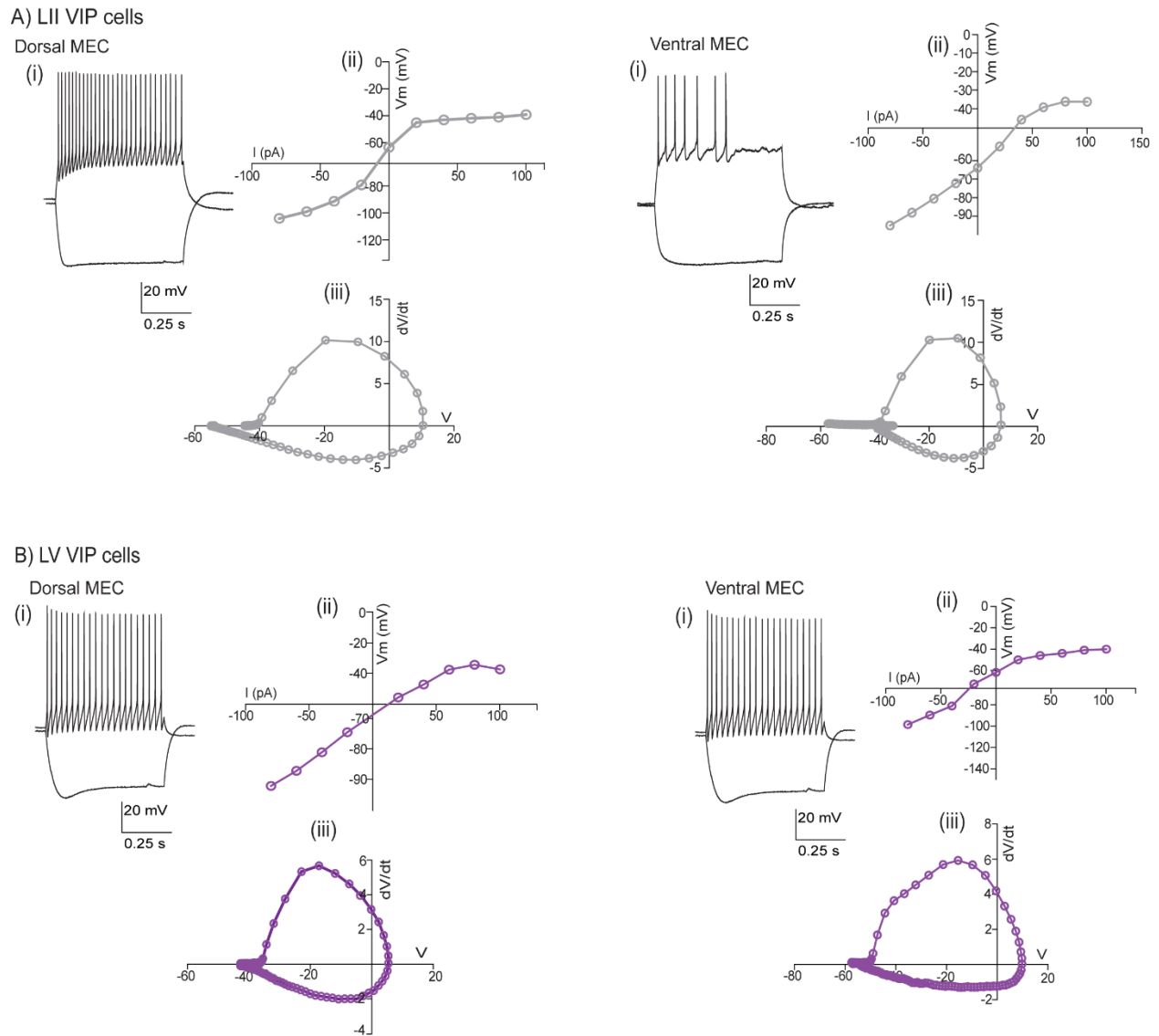
dendrites in green), multipolar VIP neuron in LIII (b; axons in dark blue and dendrites in light blue) and vertical bitufted morphology seen in L2 (c; axons in red, dendrites in blue). Scale bars are 100 $\mu$ m. For all cells, the soma is coloured in orange. (C) Maximum projection intensity of 207 z-stacks of 0.5 $\mu$ m depth taken in 20x magnification of reconstruction seen in (B(c)) of the MEC filled with neurobiotin (GFP). Scale bar is 100 $\mu$ m. (D) Plots depicting different features such as the (i) vertical and (ii) horizontal spread of the dendritic process. Each bar represents a mean and SEM. (E) Graphs assessing the length of processes present in a specific layer for (i) axons and (ii) dendrites. Each bar represents a mean and SEM. (F) Morphological features of (i) dendritic and (ii) axonal arbors obtained from Sholl analysis. Each bar represents a mean and SEM. For all graphs, LI-III = 11 cells, LIV-VI = 6 cells: \*\*\*  $p < 0.001$ , \*\*  $p < 0.01$ , \*  $p < 0.05$

Supplementary figures



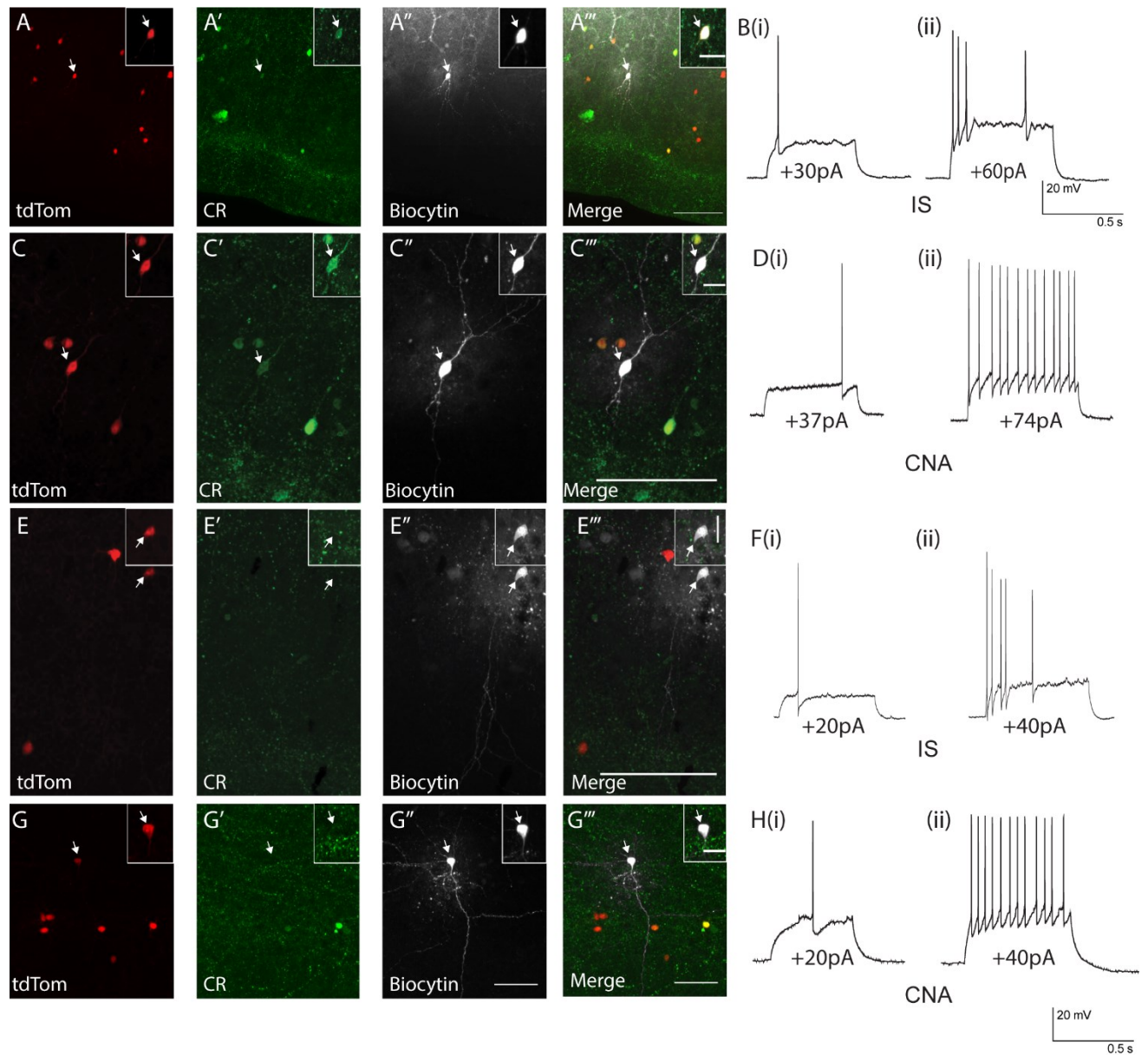
**Supplementary Figure 1**

(A-B'') Maximum projection intensity of a 40- $\mu$ m thick sagittal section of superficial MEC treated with IHC using  $\alpha$ PV AB (A-JA'') and  $\alpha$ Sst AB (B-B''). Scale bar is 250 $\mu$ m. (C) Percentage of action potential firing patterns observed in VIP cells in the MEC. (D) Examples of membrane potential responses to current steps recorded at (i) rheobase and (ii) suprathreshold current. Abbreviations in C and D name the firing pattern after the Petila convention (Ascoli et al.2008; IS, Irregular spiking; CA, Continuous adapting; CNA, continuous non-adapting).



## Supplementary Figure 2

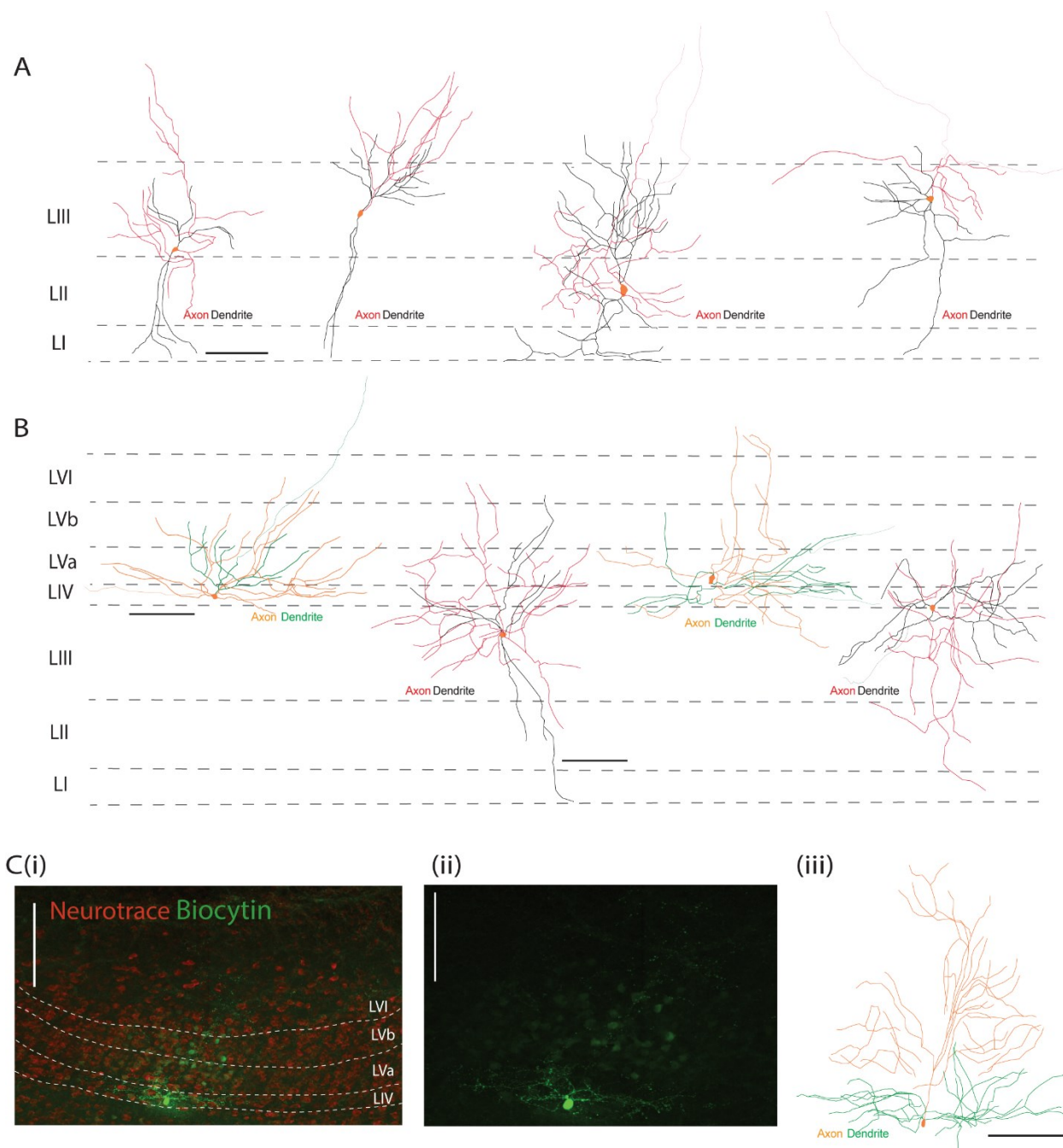
VIP cells located in the A) superficial (LII) and (B) deep (LV) layers of the MEC along the dorsal and ventral axis. In all panels, (i) Examples of membrane potential responses to current steps (-80pA for lower trace and +100pA for upper trace), (ii) Current-voltage response (I-V curve) for each voltage response to varying current step at voltage sag-peak and (iii) Phase plot of first AP to current step double the rheobase current.



### Supplementary Figure 3

Examples of VIP cells that show or lack immunoreactivity for Calretinin (CR). Parasagittal sections of the MEC were processed for immunoreactivity for CR after an *in vitro* recording session. (A-E''') White arrow heads mark the presence of VIP (tdTom), CR (GFP) and Biocytin (gray) in their respective channels, in A''' and E''' colocalization of all three channels indicates presence of CR in the recorded cell.

In panels B and F are shown the electrophysiological recordings from the respective cells at (i) rheobase and action potential firing pattern at (ii) suprathreshold current. In panels E and G the absence of CR marker in the recorded cell is visualized in E' and G'. The morphology of the recorded cell in G is multipolar. In all other panels, the cells display a bitufted morphology. Scale bars in insets are 20 $\mu$ m. Scale bar in G''' is 60 $\mu$ m. In all other panels the scale bar is 100 $\mu$ m. Abbreviations name the firing pattern after the Petila convention (Ascoli et al.2008; IS, Irregular spiking; CA, Continuous adapting; CNA, continuous non-adapting)



### Supplementary Figure 4

(A) The reconstructed morphology of 4 individual VIP cells recorded from the superficial layers is shown in a schematic of the MEC. For all cells the soma are coloured in orange and axonal and dendritic processes are coloured in red and black respectively. Scale bar is 100 $\mu$ m.

(B) The reconstructed morphology of 4 individual VIP cells is shown in a schematic of the MEC. For all cells soma are coloured in orange. For cells recorded in superficial MEC axonal and dendritic processes are coloured in red and black respectively. For cells recorded from layers IV-VI, axons are in orange while dendrites are coloured green. Scale bar is 100 $\mu$ m. (C) Maximum projection intensity of a VIP cell filled with neurobiotin recorded from the deep layers of the MEC.

(C(i)) The layers of the MEC in C(i) are marked with neurotrace as reference. Reconstruction of recorded cell is seen in C(iii). Soma is coloured in orange and axons and dendrites are coloured in orange and green respectively. Scale bar in C (i & ii) is 150 $\mu$ m and scale bar in C(iii) is 100 $\mu$ m.

Table 1

Properties measured	LI-III (n = 35)	LIV-VI (n = 25)	t test
Input resistance (M $\Omega$ )	418 $\pm$ 18.63	511.51 $\pm$ 28.9	p = 0.007
Rheobase (pA)	36.85 $\pm$ 3.64	20.22 $\pm$ 2.66	p = 0.001
Sag amplitude (mV)	4.17 $\pm$ 0.51 (n = 33)	3.55 $\pm$ 0.43 (n = 24)	p = 0.605
Decay tau (ms)	9.93 $\pm$ 2.45	14.17 $\pm$ 3.95	p = 0.264
RMP (mV)	-61.14 $\pm$ 1.12	-41.16 $\pm$ 1.62	p = 0.401
Half-width (ms)	1.25 $\pm$ 0.08	1.6 $\pm$ 0.103	p = 0.008
AHP time (ms)	56.78 $\pm$ 9.51	72.78 $\pm$ 5.21	p = 0.0006
Max rise slope (mV/ms)	174.30 $\pm$ 10.69	126.75 $\pm$ 8.85	p = 0.010
AHP amplitude (mV)	-11.68 $\pm$ 1.12	-11.16 $\pm$ 0.89	p = 0.928
Peak amplitude (mV)	67.28 $\pm$ 1.71	65.71 $\pm$ 2.09	p = 0.594
Half-amplitude (mV)	33.64 $\pm$ 0.85	32.65 $\pm$ 0.98	p = 0.533
Peak ISI (ms)	49.48 $\pm$ 6.26 (n = 33)	45.01 $\pm$ 5.8 (n = 22)	p = 0.870
Steady state ISI (ms)	34.36 $\pm$ 4.29 (n = 32)	29.94 $\pm$ 6.06 (n = 20)	p = 0.318
Spike frequency adaptation %	-9.12 $\pm$ 23.7 (n = 32)	32.09 $\pm$ 8.50 (n = 20)	p = 0.958
Firing threshold	-41.36 $\pm$ 0.65	-41.16 $\pm$ 1.62	p = 0.5739

**Table 1.** Tabulation of all passive and active membrane properties measured for VIP cells located in superficial (LI-LIII) and deep (LIV-LVI) layers in the MEC. p values obtained from t-test.

Table 2

Properties measured	Population average (n = 60)
Input resistance (M $\Omega$ )	457.01 $\pm$ 17.2
Rheobase (pA)	29.92 $\pm$ 2.62
Sag amplitude (mV)	4.05 $\pm$ 0.35 (n = 57)
Decay tau (ms)	11.69 $\pm$ 2.19
RMP (mV)	-60 $\pm$ 1.17
Half-width (ms)	1.40 $\pm$ 0.06
AHP time (ms)	63.45 $\pm$ 6.05
Max rise slope (mV/ms)	154.49 $\pm$ 7.85
AHP amplitude (mV)	-11.76 $\pm$ 0.67
Peak amplitude (mV)	66.62 $\pm$ 1.33
Half-amplitude (mV)	33.22 $\pm$ 0.64
Peak ISI (ms)	52.07 $\pm$ 4.35 (n = 55)
Steady state ISI (ms)	37.59 $\pm$ 3.65 (n = 52)
Spike frequency adaptation %	2.62 $\pm$ 14.45 (n = 52)
Firing threshold (mV)	-41.280 $\pm$ 0.77

**Table 2.** Tabulation of all passive and active membrane properties measured for all VIP cells located across all layers.

## Foreword to Chapter 3

The data presented in Chapter 2 provide comprehensive evidence of the different electrophysiological and morphological properties of VIP cells across various layers of the MEC. The presence of a higher number of vertical bipolar cells in L2 and multipolar cells in L3 suggests that VIP cells in the superficial layers are well-positioned to receive incoming signals before transferring them to their post-synaptic partners across the different layers of the MEC. In this case, understanding the brain regions that send inputs to VIP cells in the superficial layers is key to comprehending how they are positioned and thus influence other cell types within the MEC spatial circuit.

Furthermore, while Chapter 2 provides us with an understanding of various neuroanatomical features of VIP cells in the MEC, it does not shed light on their functional role. To address these gaps, in Chapter 3, we conduct rabies-mediated viral tracing in VIP cells to identify the brain regions that send them monosynaptic input. We further study their function in a novel object location paradigm to ascertain their role in spatial location tasks. Through these experiments, we extend and build upon the previous characterization of VIP cells seen in Chapter 2.

# **Chapter 3: Investigating monosynaptic inputs and behavioural correlates of Vasoactive Intestinal Peptide (VIP) interneurons in the Medial Entorhinal Cortex (MEC).**

Abbreviated title: Input connectivity and behavioural function of VIP cells in the MEC

Saishree Badrinarayanan<sup>1,2,+</sup>, Marie Oulé<sup>1,+</sup>, Rosa – Sundar Maccagno<sup>3</sup>, Michaela Hirsch<sup>3</sup>, Mark P Brandon<sup>1,2,\*</sup>

<sup>+</sup>Authors contributed equally to the study

<sup>1</sup>Department of Psychiatry, Douglas Hospital Research Centre, McGill University, Montreal, QC, Canada.

<sup>2</sup>Integrated Program in Neuroscience, McGill University, Montreal, QC, Canada.

<sup>3</sup>Department of Physiology, McGill University, Montreal, QC, Canada

\* Correspondence: Mark P. Brandon: mark.brandon@mcgill.ca

**Keywords:** VIP interneurons, medial entorhinal cortex, novel object location, immediate early genes, neural circuit, interneurons

## **Abstract**

The Medial entorhinal cortex (MEC) contains discrete cell populations that are important for spatial memory and navigation. While the role of excitatory and some GABAergic cells has been extensively studied, the contribution of Vasoactive Intestinal Peptide (VIP) interneurons remains largely unexplored. To understand if VIP cells integrate incoming information from different brain regions, we used rabies-mediated viral tracing to generate a comprehensive brain-wide map of their presynaptic partners. The connectivity of VIP cells in the MEC reveals that they receive

inputs from the hippocampus CA1, retrosplenial cortex, medial septum, and anterodorsal thalamic nucleus, among other brain regions. To further elucidate the role of VIP cells in spatial memory, we conducted a novel object location paradigm and employed c-Fos and chemogenetic inhibition techniques. Our results revealed active recruitment of VIP cells during the task, and inhibiting VIP cells before the sampling phase led to impaired behavioral performance. These findings provide valuable insights into the role of VIP cells within the spatial-memory circuit of the MEC.

## **1. Introduction**

The Medial entorhinal cortex (MEC) plays a crucial role in encoding spatial information, memory formation of locations, and navigation in animals (Hafting et al. 2005; Sasaki, Leutgeb, and Leutgeb 2015; Moser, Kropff, and Moser 2008). Within the MEC, different types of cells such as Stellate cells (SC) (Tennant et al. 2018; David C. Rowland et al. 2018), Pyramidal cells (PCs) (Zutshi et al. 2018), Parvalbumin (PV) and Somatostatin interneurons (SOM) (Miao et al. 2017) exert significant influence on the micro-circuitry in this structure (Canto, Wouterlood, and Witter 2008). These different cell types work in concert to generate and maintain the various spatially tuned cells, such as grid cells (Hafting et al. 2005), head direction cells, conjunctive-grid cells (Sargolini et al. 2006), aperiodic spatially tuned cells (Diehl et al. 2017) and object vector cells (Høydal et al. 2019) in the MEC. Through the different layers, the MEC forms bi-directional connections with the hippocampus and various other structures. For instance, the MEC send projections to the hippocampus via the perforant path in L2 and the temporoammonic pathway from L3 (Germroth, Schwerdtfeger, and Buhl 1989; Witter et al. 2017). In return the CA1 of the hippocampus exclusively targets the Layer Vb (LVb) of the MEC (Sürmeli et al. 2015; Ohara et al. 2018). The functional relevance of these projections between the two structures have been extensively studied. During spatial navigation and learning, the MEC undergoes structural and

functional plastic changes. The MEC is thought to provide the hippocampal subfields; CA1, DG and CA3 with spatial reference frame from the neural activity of grid cells, boundary cells and head direction cells (Cholvin, Hainmueller, and Bartos 2021; Hafting et al. 2005; Fernández-Ruiz et al. 2017; Knierim, Neunuebel, and Deshmukh 2014). Many studies have further detailed the nature of these inputs and the MEC largely provides self-motion signal (Bush, Barry, and Burgess 2014), and to this end, the MEC is thought to perform path integration, a cognitive function that relies on integrating self-motion cues to update one's location relative to a starting location (Samsonovich and McNaughton 1997; Mittelstaedt and Mittelstaedt 1980). The integration of these self-motion signals takes place across the multiple layers and cell types within the MEC (Witter et al. 2017).

Previous research has extensively explored the role of PV and SOM interneurons (Buetfering, Allen, and Monyer 2014; Fuchs et al. 2016; Miao et al. 2017), as well as the excitatory cells SC (Tennant et al. 2018; Winterer et al. 2017) and PC (Zutshi et al. 2018), in modulating MEC activity, underscoring the importance of maintaining an excitatory/inhibitory (E/I) balance in the microcircuit to maintain neural stability.

Recent studies in other cortical structures emphasize the significance of E/I balance in regulating neural activity and plasticity during learning within brain circuits (Krabbe et al. 2019; Karnani et al. 2016; Pi et al. 2013). The Vasoactive Intestinal Peptide (VIP) interneuron is an emerging candidate in this context as they play a key role in controlling neural activity within these microcircuits via disinhibition (Pfeffer 2014; Pi et al. 2013). These cells target inhibitory cells (preferably SOM) and some excitatory cells in various brain regions such as the basolateral amygdala (BLA) (Rhomberg et al. 2018; Krabbe et al. 2019), the hippocampus CA1 (Tyan et al. 2014; Turi et al. 2019), the primary motor cortex (Garcia-Junco-Clemente et al. 2017) and the

somatosensory cortex (Wall et al. 2016; S. Lee et al. 2013). They also receive diverse inputs from various brain regions and thus can have a profound impact on shaping neural activity (Topolnik and Tamboli 2022; Letzkus, Wolff, and Lüthi 2015). Thus, making them key candidates in shaping local neural activity within a structure. Despite extensive investigations into PV, SOM, SC, and PC cells in the MEC, there remains a significant gap in understanding the role of VIP cells in the MEC's spatial circuit and their connectivity with other regions projecting to the MEC.

In this study, we aim to bridge this knowledge gap by unraveling the VIP circuitry using rabies-mediated viral tracing, which revealed the monosynaptic inputs driving their activity in the MEC. Surprisingly, we uncovered intricate connections from diverse regions, including the CA1 region of the hippocampus, the retrosplenial cortex (RSC), the medial septum (MS), and the anterodorsal thalamic nucleus (ADN). Additionally, we employed a novel object location paradigm and utilized c-Fos and chemogenetic inhibition techniques to further probe the role of VIP cells in spatial memory. Our results demonstrate that VIP cells are actively recruited during the task, and inhibiting VIP cells before the sampling phase led to impaired behavioral performance. This detailed analysis represents an important step towards understanding the role of interneurons within the microcircuits of the MEC. Our findings also provide intriguing avenues for further investigation into the *in vivo* role of the VIP cells in the spatial – memory circuit, paving the way for exciting future research.

## **2 Materials and Methods**

### *2.1 Animals*

This study was carried out in accordance with the recommendations of the Canadian Council on Animal Care and the McGill University Animal Care Committee. The protocol was approved by the McGill University Animal Care Committee. Animals were housed in a temperature-

controlled room with a 12/12 h light/dark cycle and food and water ad libitum. For this study, we crossed homozygous *Vip-ires-cre* (*VIPtm1(cre)Zjh*, The Jackson Laboratory, Bar Harbor USA) mice with homozygous *Ai9 lox-stop-lox-tdTomato cre-reporter* strain mice (RRID: IMSR JAX:007905) to generate *VIP-tdTom* mice in which *tdTom* (RFP) is exclusively expressed in cells that have *cre* recombinase. *Tom* fluorescence was used to identify *VIP* cells (Badrinarayanan et al. 2021; Prönneke et al. 2015).

## *2.2 Stereotaxic surgeries for viral transfection:*

For viral transfection, *VIP-cre* mice between the age of 5-8 weeks of age were anesthetized via inhalation of a combination of oxygen and 5% Isoflurane before being transferred to the stereotaxic frame (David Kopf Instruments), where anesthesia was maintained via inhalation of oxygen and 0.5-2.5% Isoflurane for the duration of the surgery. Body temperature was maintained with a heating pad and eyes were hydrated with gel (Optixcare). Carprofen (10 ml/kg) and saline (0.5 ml) were administered subcutaneously at the beginning of each surgery. All injections were administered via glass pipettes connected to a Nanoject II (Drummond Scientific) injector at a flow rate of 23 nl/sec. For each craniotomy, 2 injection sites from bregma along the medial lateral axis were used. For the first site, the injection pipette was lowered 3.65mm from the bregma and for the 2<sup>nd</sup> site it was lowered at 3.45mm from bregma. For both injection sites, the pipette was moved 0.280mm anterior to transverse sinus to target the MEC. The depth of the injection site was determined from the extent at which the micropipette bent once it hit the dura lining surface of the brain. Approximate depths for 5-week-old mice were: 1<sup>st</sup> injection: -2.240, 2<sup>nd</sup> injection site: -3.00. For each injection site, the pipette was retracted 200µm after the first bend and the virus was injected at 3 different depth along the dorsal-ventral at 300µm intervals along extent of the MEC, such that the last injection site usually corresponded to -1.450 to -1.750 along the DV axis. After

each injection, the micropipette was left undisturbed for 3-4 minutes to allow for the infusion of the virus before injecting into the next site. A total of 400µl of virus was injected in each animal.

### *2.2.1 Injection timeline for rabies mediated viral tracing:*

For tracing monosynaptic inputs to VIP cells, (n = 5) we used VIP-ires-cre mice. These animals were unilaterally injected with a 1:1 combination of AAV.fDIO.mRuby.TVA and AAV.fDIO.oPBG (Gift from Prof.Byungkook Lim, UCSD, (Knowland et al. 2017) or AAV2/8-hSyn-FLEX-TVA-P2A-eGFP-2A-oG (ULaval Vector Core). After allowing for 4 weeks of expression, animals were anesthetized as previously described and EnvA.RV-G.eGFP or RABV-DeltaG-EnvA-mCherry was injected using scar on skull as a guide for location. One-week post injection, animals were sacrificed for detection of inputs and starter cells.

### *2.2.2 Injection timeline for chemogenetic viral expression:*

For chemogenetic experiments, (n = 15) VIP-cre mice were injected bilaterally or unilaterally with the cre-mediated Designer Receptor Exclusively Activated by Designer Drugs (DREADDs) viral construct AAV8.hsyn.DIO.hm4di.mcherry using the injection strategy as described above. The original titre of this virus, sourced from Addgene, was 4.3e12 GC-ml and was diluted in sterile PBS (1 parts virus to 2 parts PBS) before surgical microinjection. All injections were administered via glass pipettes connected to a Nanoject II (Drummond Scientific) using the same coordinates as described above. After waiting for 4 weeks of expression, the mice were handled and habituated before testing them in the novel object location paradigm as described below.

## *2.3 Habituation and handling for behavior experiment:*

### *2.3.1 For c-Fos experiments:*

One week prior to testing in the novel object location paradigm, VIPtdtom (n = 14) mice were handled daily for 3-5 minutes.

### *2.3.2 For the chemogenetic experiments:*

Animals were subjected to behavioral testing after 5 weeks post-surgery. After the animals could recover from surgeries (2 weeks), they were then handled for 3 weeks. This involved: For the first week, animals were handled for 3-5 minutes. For the second week, they were restrained by the scruff and for the last week, the animals were administered I.P injections with saline.

## *2.4 Memory testing using novel object location paradigm*

To test spatial memory, we adapted a novel object location paradigm from (van Goethem, van Hagen, and Prickaerts 2018). Briefly, mice were placed in an opaque circular chamber measuring (40cm) surrounded by black walls equipped with salient high contrast distal visual cues (black and white stripe, circle, or star). The positions of the distal cues remained consistent throughout experiments. The chamber was cleaned prior to testing and between sessions using a disinfectant like peroxiguard and the bedding was evenly redistributed to mask the smell. Over the first 4 days the animals were habituated to the testing box. For the first 2 days of habituation, the mice spent 10 min in the circular chamber without the presence of objects. On days 3-4 of habituation the mice were introduced to two 10 min sessions with objects. During habituation, a session consisted of a 10 min exploration phase. On day 5, the first day of testing, animals spent 15 min during a ‘sample phase’ and tested in the arena 90 mins after sampling. This ‘test’ phase lasted for 6 mins. For each phase, the mouse was placed into the test box, and allowed to explore. Between phases the mouse was removed from the test box and placed in their home cage while the floor and walls

of the box and objects were cleaned with a disinfectant and the box prepared for the next phase. At the end of a testing session the mouse was placed back into its home cage, and the test box and objects cleaned and prepared for the next mouse.

The phases of the object location task were structured in the following way:

Habituation phase Day 1-2: the box contained no objects. Habituation phase Day 3-4: the box contained 2 different objects. Day 5, Sampling phase: the box contained two copies of the same object (these objects were different from the ones used in the habituation phase), placed in the same line facing each other, Test phase: one object was moved to a novel location, either (12 cm from the original location: dissimilar location, or 3 cm from the original location: extra-similar location, in either vertical direction) (Fig 4A). To ensure that changes in behavior were not a result of preference for a certain object or side of the arena, the location of the objects were counterbalanced between different groups across different days (If animals were tested in a dissimilar version of the task, then in the counterbalanced version they were tested in the extra-similar version of the task). For both tasks, the time spent exploring each object in the sample and test phases were measured.

#### *2.4.1 For the c-Fos experiment:*

VIPtdTom animals of either sex were used for c-Fos experiments (N = 9 animals, male, and n = 5 animals, female). For the c-Fos experiments, some animals were also tested in the control version of the task. In this version, the animals underwent the same steps as previously described. However, during the test phase on the 5th day of the behavior protocol, the objects weren't moved and remained in the same location as during the sampling phase. After the test, the animals were placed in their home cage, and after 90 minutes, they were perfused, and their brains were serially sectioned for c-Fos staining.

#### *2.4.2 For the chemogenetic experiments:*

VIP-cre mice injected with AAV8.hsyn.DIO.hm4di.mcherry in the MEC were administered with either JHU drug diluted with saline (Bonaventura et al. 2019) or saline 30 mins prior to sampling phase. VIP-cre animals (n = 5) (matched for the age and sex as experimental group) were also used to test the effect of JHU on the mice. For this, the VIP-cre animals with no viral injections were injected with just JHU drug 30 min prior to sampling phase. To test the same animals in the counterbalanced version of the task, animals were reintroduced to the arena 2 weeks after the last test phase. Mice were then perfused after testing and the brains were serially sectioned to confirm viral expression and specificity of the injection location.

Discrimination ratios for both groups were quantified as:

As mice are known to exhibit a preference for exploring objects that have been moved to a new location (Ennaceur and Delacour 1988; van Goethem, van Hagen, and Prickaerts 2018), we measured their ability to discriminate between the moved and non-moved objects using a discrimination ratio:  $(\text{The time taken to explore the moved object} - \text{the time taken to the unmoved object}) / \text{total exploration time (s)}$  (Total time taken to explore both objects).

#### *2.5 Immunohistochemistry*

Mice were deeply anesthetized and intracardially perfused with 4% paraformaldehyde in PBS. Brains were dissected, post-fixed by immersion in the same fixative. Fixed brains were snap-frozen in dry ice-chilled isopentane before being cut into 35- $\mu\text{m}$ -thick sections using a cryostat (Leica Microsystems). Every 4<sup>th</sup> section was collected for IHC.

### *2.5.1 Rabies circuit mapping:*

For circuit mapping experiments, whole brains from injected animals were sliced in the coronal (n = 2) and sagittal plane (n = 3) to retrieve whole brain sections. Post slicing, the sections were rinsed in 1X PBS (3x 5 min) and blocked with 1X PBS containing 0.45% fish gelatin and 0.25% Triton-X (3x 15 min each). Sections were then incubated with primary antibodies for 48hrs at 4°C on a rotating shaker. The following primary antibodies were used to amplify GFP, RFP and stain for choline-acetyltransferase (ChAt) respectively: 1:1000 Rb- $\alpha$ -GFP A10262 (ThermoFisher Scientific), 1:10,000 Chk- $\alpha$ -RFP CA600-901-379 (VWR Rockland) and 1:200 Gt- $\alpha$ -ChAt AB144P (Millipore Sigma). Alexa Fluor dyes conjugated to either 488, 555 and 568 were used for secondary antibodies at 1:1000 dilutions. The sections were mounted onto glass slides (Fisherbrand Superfrost Plus Microscope Slides), and cover slipped using DAPI mounting medium.

### *2.5.2 c-Fos immunostaining:*

To stain for c-Fos, whole brains from animals were sliced in the sagittal plane. Post slicing, the sections were rinsed in 1X PBS (3x 10 min) and then incubated in 1X PBS containing 0.3% Triton-X with a 1:1000 dilution of Rb-  $\alpha$ -c-Fos AB222699 (abcam) at room temperature for 24hrs. This was then followed by a rinsing step in 1X PBS and then incubated in a secondary antibody (Alexa Fluor dye conjugated to 488) for 2 hrs at RT, followed by a final series of washes in 1X PBS (3x 10min). The sections were mounted onto glass slides (Fisherbrand Superfrost Plus Microscope Slides), and cover slipped using DAPI mounting medium.

### *2.6 Tracing of input regions for rabies circuit tracing experiments:*

For visualization, analysis and quantification purposes, the sections from the rabies experiment were imaged with a VS-120 Olympus slide scanner under epifluorescence in DAPI, FITC, and

TRITC channels using an optical filter set from Semrock (Part Number: DA/FI/TR 4X4M-C-000), an Orca r2 Hamamatsu monochrome camera, and an Olympus  $\times 10$  objective (Molecular and Cellular Microscopy Platform—Douglas Research Center, Montreal, Canada). Virtual Slide Images (.vsi) files acquired from the slide scanner were opened in FIJI using the BIOP VSI Reader (EPFL, Lausanne, Switzerland) and exported as individual TIFF files for further analysis in FIJI (Image J version 2.1.0) and QuPath (Software version 0.4.3.1).

*Mouse brain atlas and regional analysis:*

Next, to detect the input cells (either GFP+ or RFP+) within the MEC and in other brain regions, we used ABBA – Aligning Big Brain Atlas (Fiji Plugin) an open source software developed by EPFL, Lausanne (<https://biop.github.io/ijp-imagetoatlas/>) to register and align the Allen Atlas using both affine and spline transformation on our sagittal and coronal sections. We then imported the output from ABBA and performed manual counting in the region of interests (ROI) outlined using the Allen Atlas in QuPath. We calculated the convergence index defined as the total number of inputs targeting a single VIP cells (Total number of inputs for an ROI/Total number of starter cells) and the fraction of inputs defined as the percentage of inputs a brain region sends to VIP cells in the MEC (Total number of inputs for an ROI/Total number of presynaptic inputs in the entire brain) for each animal.

*Identification of brain regions:*

The brain regions, as defined by the Allen brain Atlas were identified as PERI – Perirhinal area AuD – Auditory cortex, Dorsal, V2L – Secondary Visual Cortex, V1 – Primary visual cortex, V2MM/V2ML – Secondary visual cortex, medial, RSP/A30 – Retrosplenial cortex, PIR 2 – Piriform cortex, BLA – Basolateral amygdala, BMA – Basomedial amygdaloid complex, CLA – Claustrum, MS – Medial Septum, HDB – Horizontal limb of the diagonal band, RM –

Retromammillary nucleus, LPLR – Lateral Posterior thalamic nuclei, LDVL – Lateral dorsal thalamic nuclei, ADN – Anterodorsal thalamic nuclei, IAD – Interantero dorsal thalamic nuclei, VA – Ventral anterodorsal thalamic nuclei, Rt – Reticular nucleus.

### *2.7 Image acquisition and Data analysis for c-Fos quantification*

Quantification of VIP, c-Fos and VIPc-Fos +ve cells/co-localization was performed using the optical fractionator method in StereoInvestigator software with a Zeiss ApoTome structured illumination device on a widefield microscope. Contours were drawn to delineate the superficial (L1-III) and deep layers (LIV-VI) of the MEC using DAPI as reference. Using live counting, an experimenter who was blind to the experimental conditions counted all markers according to optical dissector inclusion-exclusion criteria at each cell's widest point. Separate markers were used to count the number of Tom (VIP), c-Fos (GFP) and co-localized or double labeled cells (yellow).

### *2.8 Data analysis and statistics*

Statistical analyses were performed with GraphPad Prism 8. We ran unpaired Student t tests (Mann Whitney U), one-way analysis of variance (ANOVA) or two-way ANOVAs, with Tukey or Bonferroni multiple comparison corrections. Data are presented as mean  $\pm$  SEM with individual data points. Differences were considered significant when  $p < 0.05$ . Additionally, column statistics against a theoretical mean of 0 was performed on the behavioural analysis, if  $\alpha = 0.05$ , the animal was considered to have learnt during the paradigm.

## 3 Results

### 3.1 Monosynaptic tracing of inputs to VIP cells in the MEC

#### 3.1.1 Confirmation of starter cells in the MEC

To identify long-range input regions that are specific to VIP cells in the MEC, we utilized the monosynaptic rabies virus (RV) tracing system (Callaway and Luo 2015; Knowland et al. 2017). Animals (n = 5) were first injected with the rabies pseudotyped virus AAV-fDIO-TVA-mCherry or AAV-fDIO-TVA-eGFP using coordinates listed above. After waiting for 4 weeks of expression, the animals were injected with EnvA.RV-G.eGFP or EnvA.RV-mCherry (depending on the TVA virus used). After one week, the animals were perfused, and the brains were retrieved for whole brain sectioning (Fig 1 A). Out of the 5 animals, 2 animals were excluded as their injection targets were not specific to the MEC. The sections for the 3 animals were taken for further analysis.

It has been shown that helper virus could have potential leak expression of TVA and subsequent rabies expression in the absence of Cre (Callaway and Luo 2015), therefore we conducted control experiments by injecting the helper virus (AAV2/8-hSyn-FLEX-TVA-P2A-eGFP-2A-oG, ULaval) in VIPtdTom mice (n = 2) to look at the specificity of the virus to tdTom cells, which have been previously shown to be specific for VIP cells in the MEC and other cortical structures (Badrinarayanan et al. 2021; Prönneke et al. 2015). We examined the fraction of GFP+ cells (Fig 1 B(iii)) that colocalized with tdTomato (Fig 1 B(ii)). We found that 97% of the GFP+ cells colocalized with tdTom (Fig 1 B(iv)), thus confirming the specificity of the helper virus to Cre+ cells.

The next step was to identify and quantify the total number of starter cells in the MEC. To do this, we counted the number of cells that colocalized with the fluorescent markers for TVA and RV (Fig 1 C), depending on the virus injected. We found that our injection strategy was not specific

for the superficial layers of the MEC and instead targeted all layers of the MEC (Fig 1 D(i)), superficial layers (LI-III) had more starter cells present compared to deep layers (LIV-VI) ( $p = 0.05$ ,  $35 \pm 0.57$  vs  $8.33 \pm 2.028$   $n=3$  for both groups, one-tailed, Mann-Whitney U Test). As VIP interneurons are not homogeneously distributed across the MEC layers, and since our injection strategy targeted both deep and superficial layers, we decided to combine the total number of starter cells across the different layers to quantify the inputs received by VIP cells in the MEC.

Since the total number of input cells could be dependent on the number of starter cells that were labeled from the injection strategy, we also calculated a ratio of the total starter cells to the input cells in the entire brain for each animal, similar to (C. Lee et al. 2023). We found that the ratio was very similar for animals that were sliced in the sagittal plane (animal 1, 1:67; animal 2, 1:70) and for the animal sliced in the coronal plane the ratio was 1:57. Despite the difference in the ratios between the two slicing planes, we noted that the input regions were similar across all 3 animals.

### *3.1.2 Entorhinal and Hippocampal inputs to VIP cells in the MEC*

Previous studies have shown that cells within the MEC are highly interconnected with the exception of sparse connections between excitatory cells (Canto, Wouterlood, and Witter 2008; Zutshi et al. 2018; Winterer et al. 2017; Fuchs et al. 2016). In line with this, we found that VIP cells in the MEC receive input from all layers of the MEC (Fig 2 A, Fig 3 A). We didn't quantify the molecular or electrophysiological nature of these inputs and therefore, they could be excitatory or inhibitory connections.

Reciprocal projections between the hippocampus and the MEC has been extensively studied in the past (Naber, Lopes Da Silva, and Witter 2001; Sürmeli et al. 2015; Witter et al. 2017; Bonnevie et al. 2013; D. C. Rowland et al. 2013). Dorsal proximal CA1 and distal subiculum send

projections to neurons in both LVA and LVb of the MEC with a preference for LVb, while ventral proximal CA1 and distal subiculum send projections to LVA and LVb, with a preference for LVA (Ohara et al. 2023). While these studies targeted all cell types in layers LVA and LVb, with a focus on excitatory cells, the neural identity of other targets for these hippocampal and subiculum projections in these layers has not been investigated in detail. In our data we noted that VIP cells receive extensive input from dorsal and ventral CA1 of the hippocampus and the distal subiculum (Fig 2B, Fig 3B (i, ii and iii)). Since our injection strategy targeted all layers of the MEC, it is possible that some of our starter cells in LVb and LVA are also recipients of the projections from the hippocampus and subiculum.

### *3.1.3 VIP cells in MEC receive a wide variety of inputs from various cortical, sub-cortical and thalamic regions*

Studies using anterograde and retrograde tracers like fast blue, fluorogold and rabies mediated tracing have found that extensive projections from various brain regions target both excitatory and inhibitory cells in different layers of the MEC. For instance, the superficial layers of the MEC receives inputs from the orbitofrontal cortex (Witter et al. 2017), medial septum (Gonzalez-Sulser et al. 2014; Schlesiger et al. 2021a; Desikan et al. 2018), postrhinal cortex (Koganezawa et al. 2015) and the pre and para-subiculum (Caballero-Bleda and Witter 1994). The latter also targets the deep layers of the MEC. Cortical areas such as the retrosplenial cortex (RSC) (Czajkowski et al. 2013), medial prefrontal cortex (mPFC), anterior cingulate cortex (ACC), and the medial secondary visual cortex (V2M) and secondary visual cortex lateral (V2L) project to L5 but their specific targets are not known. The MEC also receives projections from the claustrum and basolateral amygdala (BLA) (Canto, Wouterlood, and Witter 2008; Witter et al. 2017; Dolorfo and Amaral 1998; Schlesiger et al. 2021a).

Consistent with previous literature, we observed inputs from various regions including the perirhinal cortex, the RSC, BLA and claustrum (Fig 2C). We also noted extensive projections from the medial septum (Fig 2C, Fig 3B (i and ii)), and the anterodorsal thalamic nucleus (ADN) (Fig 2C, Fig 3C (i and ii)). The inputs from the latter were surprising, although previous reports have noted very sparse projections from the ADN to the MEC (Van Groen and Wyss 1995).

We find that the majority of the input originated from within the MEC (41.6%) followed by CA1(pyramidal layer) of the hippocampus (25.6%), the subiculum (11.3%). With respect to extra hippocampal regions, the following regions send the majority of the input: the RSC (5.7%), the ADN (4.7%) and MS/HDB (2.3%) (Supplementary Fig 1). Thus, VIP cells in the MEC receive inputs from regions known to be ‘spatial processing centers’ of the brain (Canto, Wouterlood, and Witter 2008; Witter et al. 2017).

### *3.2 VIP cells show c-Fos activation in a novel object location task*

To test if VIP cells are involved in spatial processing, we performed the novel object location tasks (Ennaceur and Delacour 1988) in VIPtdTom mice. Previous studies have shown that the MEC is involved in the paradigm and preferentially processes spatial change in this version of the task (Rodo, Sargolini, and Save 2017; Tennant et al. 2018). To see if VIP cells are activated during this task, we took advantage of immediate early genes (IEG) and used the activity dependent marker c-Fos (Kinnavane et al. 2017; Dragunow 1996) to identify cells that were activated during the test phase of the task.

Once the animals were habituated to the paradigm, we conducted tests on day 5. Only animals that met the criterion of spending at least 20 seconds in the sampling phase (with each object receiving at least 10 seconds of exploration) were included in our analysis. Our findings demonstrated that animals could discriminate between an object that had been moved to a dissimilar location

(representing the classic novel object location task variation) and an extra similar condition (serving as a negative control, as previous studies have shown that animals are unable to discriminate in an extra-similar version of this task, (van Goethem, van Hagen, and Prickaerts 2018)) (Fig 4 B(i)) ( $p = 0.0007$ ,  $0.313 \pm 0.041$   $n = 8$  vs  $-0.0375 \pm 0.019$   $n = 6$ ,  $U = 0$ , Mann-Whitney test, two-tailed). To ensure that our results were not driven by difference in exploration time as both male and female mice were used for the experiment, we compared their exploration time during the sampling phase and found that there was no significant difference between the male and female exploration time (Fig 4 B(ii)) ( $p = 0.437$ ,  $34.24 \pm 8.64.9s$   $n = 9$  vs  $31.37 \pm 9.39.1s$   $n = 5$ ,  $U = 16$ , Mann-Whitney test, two-tailed).

Next, we asked if VIP cells are activated during the novel object location task. We found some VIP cells expressed c-Fos during the test phase (Fig 4C(iii)). We further quantified the number of c-Fos expressing cells in the MEC in a layer-independent (Fig 4D(i)) and dependent manner (Fig 4E(i)). We performed the same quantifications for VIP cells that co-localized with c-Fos (VIPc-Fos+ve) (Fig 4D(ii) and Fig E(ii)). Interestingly we saw no significant difference in c-Fos counts across the MEC for the different conditions (One way ANOVA followed by Bonferroni's multiple comparisons test) while VIPc-Fos counts across the different conditions showed some differences, with counts in the extra similar condition being significantly different from the control group ( $p = 0.0089$ ,  $12.76 \pm 1.682$   $n = 4$  vs  $28.83 \pm 2.92$   $n = 3$ , One way ANOVA followed by Bonferroni's multiple comparisons test). We next looked at the distribution of c-Fos and VIPc-Fos cells across the different layers of the MEC. Like the results observed for the layer independent analysis, we found that VIPc-Fos cells in the superficial layers were more active in the extra-similar condition compared to behavior control (Fig 4 E (ii)).

### *3.3 Inhibition of VIP cells prior to sampling results in behavioural deficits in a novel object location task.*

If VIP cells are indeed active during the test phase of the novel object location paradigm, would their inactivation lead to behavioural deficits? To test this, we selectively inhibited VIP cells by expressing the DREADDs (Urban and Roth 2015) virus AAV-DIO-hSyn-hM4Di-mCherry in the MEC of VIPcre mice (Fig 5A and B). We used the ligand JHU that binds to the DREADDs receptors (Bonaventura et al. 2019) to inhibit the activity of VIP cells prior to sampling phase. As the MEC also receives extensive projections from the contralateral hemisphere (Caputi et al. 2022) we initially employed a bilateral and unilateral strategy to target the MEC. Since we didn't see any difference between either injection strategy (Supplementary Fig 2 B and C), we continued with a unilateral approach to express DREADDs in VIPs.

We found the inhibition of VIP cells prior to sampling for the dissimilar condition results in significant reduction in the discrimination ratio in the experimental group compared to saline control ( $*p < 0.05$ ,  $0.039 \pm 0.0437$   $n = 8$  vs  $0.252 \pm 0.0193$   $n = 4$ , One-way ANOVA followed by Tukey's multiple comparison test) and JHU no DREADDs group ( $**p < 0.05$ ,  $0.039 \pm 0.0437$   $n = 8$  vs  $0.268 \pm 0.079$   $n = 6$ , One-way ANOVA followed by Tukey's multiple comparison test) (Fig 5C(i)). We did not see this deficit in the experimental group for animals that sampled the extra-similar version of the paradigm (Fig 5C(ii)). To ensure that our results were not driven by difference in exploration time between the experimental and control groups, we compared the exploration time for all experimental groups against all control groups during the sampling phase ( $p = 0.56$ ,  $36.45 \pm 2.9$   $n = 15$  vs  $35.31 \pm 4$   $n = 14$ ,  $U = 91$ , Mann Whitney Test)(Supplementary Fig2 D(i)) and test phase ( $p = 0.71$ ,  $14.67 \pm 1.54$   $n = 15$  vs  $13.9 \pm 1.3$   $n = 14$ ,  $U = 96$ , Mann Whitney Test) (Supplementary Fig2 D(ii)) and found no significant difference between them.

## 4 Discussion

Defining how subgroups of neurons are interconnected is critical to understand how cortical networks function. In this study we characterized monosynaptic inputs that could directly drive VIP cells in the MEC. Through rabies mediated viral tracing we found that VIP cells receive inputs from several cortical, sub-cortical and thalamic regions including CA1 of the hippocampus, the RSC, the MS and the ADN. These inputs indicate that VIP cells could indirectly control the transmission of memory and navigation related information both to and from the MEC to the hippocampus. To further understand this, we tested the role of MEC VIP neurons in supporting spatial memory using the novel object location paradigm. Using a combination of behavior, immunohistological detection of the c-Fos protein, and DREADDs inactivation of VIP cells, our results indicate that VIP cells are activated and necessary for performance on this task. These findings add to the growing body of work on interneurons in the MEC and their function in the spatial navigation system.

Many studies have focused on understanding the circuit dynamics within the MEC and how different cell types are connected to each other. While most of these studies have concentrated on PV (Buetfering, Allen, and Monyer 2014; Miao et al. 2017), SOM (Kecskés et al. 2020; Miao et al. 2017), SC, and pyramidal cells (Zutshi et al. 2018; Fuchs et al. 2016), very little is known about the connectivity and function of other interneuron classes (Desikan et al. 2018). In this study, we utilized the monosynaptic rabies virus (RV) tracing system to identify long-range input regions specific to VIP cells in the MEC. By targeting all layers of the MEC, our results revealed that VIP cells receive the majority of their inputs from different layers of the MEC, suggesting a high degree of interconnectivity within this region. While the nature of these inputs can be both excitatory and inhibitory, the authors in (Fuchs et al. 2016) found that 5HT3R cells in the MEC contact each other

and receive extensive projections from all excitatory cell types. As VIP interneurons are a subclass of 5HT3R and express the calcium binding protein Calretinin (Kepecs and Fishell 2014) it is highly likely that through our experiments we have traced the inputs to a subset of the 5HT3R+/VIP+ population.

Furthermore, we observe a high degree of connectivity between VIP cells in the MEC and the hippocampus CA1 (pyramidal layer), the subiculum and the RSC (Fig 2, Supplementary Fig 1). As a majority of the input arising from CA1 are from the pyramidal layer, we can assume that this input is excitatory in nature (Sürmeli et al. 2015). We noted a few cells in the CA1 pyramidal layer and a few cell bodies in the CA2 region, an input previously reported in (D. C. Rowland et al. 2013). Given that the CA1 inputs are known to target the deep layers of the MEC (Witter et al. 2017; Sürmeli et al. 2015; van Wijngaarden, Babl, and Ito 2020), it appears that along with electrophysiological and morphological differences previously reported in VIP cells (Badrinarayanan et al. 2021; Ferrante et al. 2017), there might be a topographical organization to the inputs received by VIP cells in the deep vs the superficial layers. This topographical organization of inputs could also extend along the dorsal-ventral axis of the MEC, as we noticed that inputs from ventral CA1 were more prominent for the animal in which the injection strategy also targeted the ventral MEC (for presence of ventral CA1 input see Fig 1 A(i), For only dorsal CA1 see Fig 3 A(i)). More data to support this observation is required.

As previously mentioned, the MEC is a highly interconnected region that receives a plethora of input from various brain regions known for their role in spatial navigation and memory (Witter et al. 2017). Our data suggest that VIP cells are a likely candidate to receive these diverse inputs to modulate local activity within the MEC. We found that the inputs received by VIP cells are considerably similar to the inputs the general population of the MEC receives (Canto, Wouterlood,

and Witter 2008; Witter et al. 2017). However, our data showing projections from the ADN and that it subsequently makes up close to 4.7% of the total inputs (Supplementary Fig 1 B) was surprisingly high. In (Van Groen and Wyss 1995), the authors noted that ADN input to the MEC was sparse and localized to the deep layers and caudal extent of the entorhinal cortex. Our data suggests that this sparse projection might be specific to VIP cells in the MEC. However, using the RV system to trace the inputs to PV and SOM interneurons in the MEC will be needed to support this claim. For instance, in other studies that have conducted monosynaptic retrograde tracing in different interneuron populations they have noted that all three interneuron populations (PV, SOM and VIP) receive inputs in similar proportion but have found that VIP interneurons receive a significantly higher proportion from distant cortical structures, for example: in the somatosensory cortex, VIP cells receive more thalamic inputs (Wall et al. 2016), while in the primary motor cortex (MOp) they receive more inputs from the orbitofrontal cortex (C. Lee et al. 2023). Interestingly (Wall et al. 2016) also report that VIPs cells have a higher starter cell to input cell ratio.

Another interesting finding from our study were the inputs from the MS. Previous reports have noted that specific MS GABAergic cell types contact different interneuron sub-populations within the MEC (Gonzalez-Sulser et al. 2014; Schlesiger et al. 2021a). Along with this, there is a plethora of studies supporting the role of acetylcholine as a key modulator of hippocampal and entorhinal function (both MEC and LEC) (Okada, Hashimoto, and Kobayashi 2022; Desikan et al. 2018). Furthermore, (Desikan et al. 2018) show that septal cholinergic projections co-release GABA but exclusively depolarize 5HT3aR interneurons in LI-II of the MEC via nAChR (nicotinic acetylcholine receptor). Previous studies have also shown that most 5HT3aR interneurons in LI and LII in the cortex were repeatedly shown to inhibit preferentially, if not exclusively, GABAergic interneurons (Jiang et al. 2015; Christophe et al. 2002). Our preliminary results reveal

that some of the MS projecting cells are cholinergic cells (Supplementary Fig 1C) and thus, VIP cells in the superficial layers could be activated by these axons.

#### *4.1 VIP interneurons are in a unique position in the MEC to receive and transmit input from various spatial processing centers in the brain*

The diversity of these inputs to VIP cells highlights a potential role for their importance in the circuit dynamics within the MEC. Previous studies have shown that the local circuits within the different layers are required to maintain an E/I balance in the MEC. For instance, inhibition of different classes of cells (Miao et al. 2017; Zutshi et al. 2018; Schlesiger et al. 2021a) have noted that in most manipulations, the HD code and border code remains unaltered in the circuitry. In fact, in (Brandon et al. 2011), the authors noted that MS inactivation disrupts spatial periodicity of grid and conjunctive grid cells, but the latter maintain their directional tuning. As a majority of conjunctive grid cells are found in the deep layers of the MEC (Sargolini et al. 2006; Boccara et al. 2010) and that VIP cells in the MEC receive robust signal from the regions with known head direction tuning like the subiculum, RSC and ADN, we envisage a scenario where head direction signal modulates the activity of deep VIP cells, which could transfer the input (via disinhibition) or modulate the ongoing activity (via inhibition) of other L5b cells that also receive CA1, subiculum and RSC input. As L5b has recurrent connections with L2 SC cells, this can help create a feedback loop of pure spatial input (via grid cells in L2) and conjunctive representation (via L5 cells) of the animal's environment (Sürmeli et al. 2015; Gerlei et al. 2021).

#### *4.2 VIP interneurons in the MEC are involved in a novel object location paradigm*

Finally, we investigated the potential involvement of VIP cells in spatial processing at the behavioral level. We performed a novel object location task that takes advantage of the animal's spontaneous tendency to explore relocated or moved objects and examined the activation of VIP

cells using the IEG c-Fos as a marker of activity. In our results we found higher incidence of VIPc-Fos+ve cells in the extra similar condition (Fig 4D(ii) and E(ii)), where the animal shows no discrimination skill (Fig 4 B(i)). We hypothesize a few reasons for this observation, 1) The activity in the MEC detects the spatial change, yet the output from the MEC is inhibited by competing circuits that are also involved in this task. For instance, in (Allegra et al. 2020) the authors find that cells within the DG, which are also a recipient of MEC input via reelin cells in L2 (Witter et al. 2017), show robust activity in the presence of similar visual cues, however neuronal discrimination in CA1 is required for behavioural performance. In line with this, it is possible that the VIPc-Fos+ve activity is higher compared to control for the extra similar paradigm. Interestingly, previous lesion and inactivation studies have noted the importance of the MEC in detecting spatial change in this version of the task. Studies inactivating the MEC and stellate cells in the L2 show that MEC has a profound effect on the animal's ability to detect the novel location of the object in the dissimilar version of the task (Van Cauter et al. 2013; Tennant et al. 2018). Consistent with these findings, we find that inactivation of VIP cells prior to the sampling phase leads to a behavioural deficit, while the same manipulation for the extra-similar condition shows no difference to control (Fig 5C). Interestingly, in a different version of the novel object location task, the authors of (Rodo, Sargolini, and Save 2017) find that rats with lesions to the MEC are able to process spatial information as well as SHAM rats when the complexity of the task is low (similar and extra similar). This supports the possibility that VIP cells in the MEC might detect spatial changes regardless of the scale of change, yet, behaviourally the readout of this input is dependent on downstream structures and other circuits recruited during this paradigm.

Given the nature of inputs received by VIP cells, it is also interesting to note that lesions to the ADN (Aggleton and Nelson 2015; Perry and Mitchell 2019), and cholinergic input from MS

(Okada, Hashimoto, and Kobayashi 2022) are required for an animal to successfully discriminate in a novel object location paradigm, when the object has been moved to a dissimilar location.

While our results suggest that the MEC and VIP cells are involved in spatial tasks like novel object location, further investigations with a larger sample size in the c-Fos study are required to fully understand the involvement of VIP cells in detecting spatial change. Additionally, conducting more experiments to uncover the output connectivity of VIP cells, either through in vitro studies (Krabbe et al. 2019) or anterograde tracing experiments (Ohara et al. 2022) will enhance our understanding of this cell type within the MEC circuits. Furthermore, by confirming the specificity of the reported inputs in other interneuron populations within the MEC and exploring the connections between various input areas and VIP cells in awake behaving animals, we can gain valuable insights into their specific roles and contributions within the MEC circuitry.

## 5 References

- Aggleton, John P., and Andrew J.D. Nelson. 2015. “Why Do Lesions in the Rodent Anterior Thalamic Nuclei Cause Such Severe Spatial Deficits?” *Neuroscience and Biobehavioral Reviews* 54: 131–44. <https://doi.org/10.1016/j.neubiorev.2014.08.013>.
- Allegra, Manuela, Lorenzo Posani, Ruy Gómez-Ocádiz, and Christoph Schmidt-Hieber. 2020. “Differential Relation between Neuronal and Behavioral Discrimination during Hippocampal Memory Encoding.” *Neuron* 108 (6): 1103-1112.e6. <https://doi.org/10.1016/j.neuron.2020.09.032>.
- Badrinarayanan, Saishree, Frédéric Manseau, Sylvain Williams, and Mark P. Brandon. 2021. “A Characterization of the Electrophysiological and Morphological Properties of Vasoactive

- Intestinal Peptide (VIP) Interneurons in the Medial Entorhinal Cortex (MEC).” *Frontiers in Neural Circuits* 15 (July): 653116. <https://doi.org/10.3389/fncir.2021.653116>.
- Boccarda, Charlotte N., Francesca Sargolini, Veslemøy Hult Thoresen, Trygve Solstad, Menno P. Witter, Edvard I. Moser, and May-Britt Moser. 2010. “Grid Cells in Pre- and Parasubiculum.” *Nature Neuroscience* 13 (8): 987–94. <https://doi.org/10.1038/nn.2602>.
- Bonaventura, Jordi, Mark A.G. Eldridge, Feng Hu, Juan L. Gomez, Marta Sanchez-Soto, Ara M. Abramyan, Sherry Lam, et al. 2019. “High-Potency Ligands for DREADD Imaging and Activation in Rodents and Monkeys.” *Nature Communications* 10 (1). <https://doi.org/10.1038/s41467-019-12236-z>.
- Bonnevie, Tora, Benjamin Dunn, Marianne Fyhn, Torkel Hafting, Dori Derdikman, John L. Kubie, Yasser Roudi, Edvard I. Moser, and May-Britt Moser. 2013. “Grid Cells Require Excitatory Drive from the Hippocampus.” *Nature Neuroscience* 16 (3): 309–17. <https://doi.org/10.1038/nn.3311>.
- Brandon, Mark P., Andrew R. Bogaard, Christopher P. Libby, Michael A. Connerney, Kishan Gupta, and Michael E. Hasselmo. 2011. “Reduction of Theta Rhythm Dissociates Grid Cell Spatial Periodicity from Directional Tuning.” *Science* 332 (6029): 595–99. <https://doi.org/10.1126/science.1201652>.
- Buetfering, Christina, Kevin Allen, and Hannah Monyer. 2014. “Parvalbumin Interneurons Provide Grid Cell-Driven Recurrent Inhibition in the Medial Entorhinal Cortex.” *Nature Neuroscience* 17 (5): 710–18. <https://doi.org/10.1038/nn.3696>.

- Bush, Daniel, Caswell Barry, and Neil Burgess. 2014. "What Do Grid Cells Contribute to Place Cell Firing?" *Trends in Neurosciences* 37 (3): 136–45. <https://doi.org/10.1016/j.tins.2013.12.003>.
- Caballero-Bleda, Maria, and Menno P. Witter. 1994. "Projections from the Presubiculum and the Parasubiculum to Morphologically Characterized Entorhinal-Hippocampal Projection Neurons in the Rat." *Experimental Brain Research* 101 (1): 93–108. <https://doi.org/10.1007/BF00243220>.
- Callaway, E. M., and L. Luo. 2015. "Monosynaptic Circuit Tracing with Glycoprotein-Deleted Rabies Viruses." *Journal of Neuroscience* 35 (24): 8979–85. <https://doi.org/10.1523/JNEUROSCI.0409-15.2015>.
- Canto, Cathrin B., Floris G. Wouterlood, and Menno P. Witter. 2008. "What Does the Anatomical Organization of the Entorhinal Cortex Tell Us?" *Neural Plasticity* 2008. <https://doi.org/10.1155/2008/381243>.
- Caputi, Antonio, Xinghua Liu, Elke C. Fuchs, Yu Chao Liu, and Hannah Monyer. 2022. "Medial Entorhinal Cortex Commissural Input Regulates the Activity of Spatially and Object-Tuned Cells Contributing to Episodic Memory." *Neuron* 110 (20): 3389-3405.e7. <https://doi.org/10.1016/j.neuron.2022.08.013>.
- Cauter, Tiffany Van, Jeremy Camon, Alice Alvernhe, Coralie Elduayen, Francesca Sargolini, and Etienne Save. 2013. "Distinct Roles of Medial and Lateral Entorhinal Cortex in Spatial Cognition." *Cerebral Cortex* 23 (2): 451–59. <https://doi.org/10.1093/cercor/bhs033>.

- Cholvin, Thibault, Thomas Hainmueller, and Marlene Bartos. 2021. "The Hippocampus Converts Dynamic Entorhinal Inputs into Stable Spatial Maps." *Neuron* 109 (19): 3135-3148.e7. <https://doi.org/10.1016/j.neuron.2021.09.019>.
- Christophe, Elodie, Aline Roebuck, Jochen F. Staiger, Daniel J. Lavery, Serge Charpak, and Etienne Audinat. 2002. "Two Types of Nicotinic Receptors Mediate an Excitation of Neocortical Layer I Interneurons." *Journal of Neurophysiology* 88 (3): 1318-27. <https://doi.org/10.1152/jn.2002.88.3.1318>.
- Czajkowski, Rafał, Jørgen Sugar, Sheng Jia Zhang, Jonathan J. Couey, Jing Ye, and Menno P. Witter. 2013. "Superficially Projecting Principal Neurons in Layer V of Medial Entorhinal Cortex in the Rat Receive Excitatory Retrosplenial Input." *Journal of Neuroscience* 33 (40): 15779-92. <https://doi.org/10.1523/JNEUROSCI.2646-13.2013>.
- Desikan, Srinidhi, David E. Koser, Angela Neitz, and Hannah Monyer. 2018. "Target Selectivity of Septal Cholinergic Neurons in the Medial and Lateral Entorhinal Cortex." *Proceedings of the National Academy of Sciences* 115 (11): E2644-52. <https://doi.org/10.1073/pnas.1716531115>.
- Diehl, Geoffrey W, Olivia J Hon, Stefan Leutgeb, Jill K Leutgeb, San Diego, La Jolla, San Diego, and La Jolla. 2017. "Grid and Non-Grid Cells in Medial Entorhinal Cortex Represent Spatial Location and Environmental Features with Complementary Coding Schemes." *Neuron* 94 (1): 83-92. <https://doi.org/10.1016/j.neuron.2017.03.004>.Grid.
- Dolorfo, Cynthia L., and David G. Amaral. 1998. "Entorhinal Cortex of the Rat: Organization of Intrinsic Connections." *Journal of Comparative Neurology* 398 (1): 49-82. [https://doi.org/10.1002/\(SICI\)1096-9861\(19980817\)398:1<49::AID-CNE4>3.0.CO;2-9](https://doi.org/10.1002/(SICI)1096-9861(19980817)398:1<49::AID-CNE4>3.0.CO;2-9).

- Dragunow, M. 1996. "A Role for Immediate-Early Transcription Factors in Learning and Memory." *Behavior Genetics* 26 (3): 293–99. <https://doi.org/10.1007/BF02359385>.
- Ennaceur, A., and J. Delacour. 1988. "A New One-Trial Test for Neurobiological Studies of Memory in Rats. 1: Behavioral Data." *Behavioural Brain Research* 31 (1): 47–59. [https://doi.org/10.1016/0166-4328\(88\)90157-X](https://doi.org/10.1016/0166-4328(88)90157-X).
- Fernández-Ruiz, Antonio, Azahara Oliva, Gergő A. Nagy, Andrew P. Maurer, Antal Berényi, and György Buzsáki. 2017. "Entorhinal-CA3 Dual-Input Control of Spike Timing in the Hippocampus by Theta-Gamma Coupling." *Neuron* 93 (5): 1213-1226.e5. <https://doi.org/10.1016/j.neuron.2017.02.017>.
- Ferrante, Michele, Babak Tahvildari, Alvaro Duque, Muhamed Hadzipasic, David Salkoff, Edward William Zagher, Michael E. Hasselmo, and David A. McCormick. 2017. "Distinct Functional Groups Emerge from the Intrinsic Properties of Molecularly Identified Entorhinal Interneurons and Principal Cells." *Cerebral Cortex* 27 (6): 3186–3207. <https://doi.org/10.1093/cercor/bhw143>.
- Fuchs, Elke C., Angela Neitz, Roberta Pinna, Sarah Melzer, Antonio Caputi, and Hannah Monyer. 2016. "Local and Distant Input Controlling Excitation in Layer II of the Medial Entorhinal Cortex." *Neuron* 89 (1): 194–208. <https://doi.org/10.1016/j.neuron.2015.11.029>.
- Garcia-Junco-Clemente, Pablo, Taruna Ikrar, Elaine Tring, Xiangmin Xu, Dario L Ringach, and Joshua T Trachtenberg. 2017. "An Inhibitory Pull–Push Circuit in Frontal Cortex." *Nature Neuroscience* 20 (3): 389–92. <https://doi.org/10.1038/nn.4483>.

- Gerlei, Klára Z., Christina M. Brown, Gülşen Sürmeli, and Matthew F. Nolan. 2021. “Deep Entorhinal Cortex: From Circuit Organization to Spatial Cognition and Memory.” *Trends in Neurosciences* 44 (11): 876–87. <https://doi.org/10.1016/j.tins.2021.08.003>.
- Germroth, P., W. K. Schwerdtfeger, and E. H. Buhl. 1989. “Morphology of Identified Entorhinal Neurons Projecting to the Hippocampus. A Light Microscopical Study Combining Retrograde Tracing and Intracellular Injection.” *Neuroscience* 30 (3): 683–91. [https://doi.org/10.1016/0306-4522\(89\)90161-9](https://doi.org/10.1016/0306-4522(89)90161-9).
- Goethem, Nick P. van, Britt T.J. van Hagen, and Jos Prickaerts. 2018. “Assessing Spatial Pattern Separation in Rodents Using the Object Pattern Separation Task.” *Nature Protocols* 13 (8): 1763–92. <https://doi.org/10.1038/s41596-018-0013-x>.
- Gonzalez-Sulser, A., D. Parthier, A. Candela, C. McClure, H. Pastoll, D. Garden, G. Sürmeli, and M. F. Nolan. 2014. “GABAergic Projections from the Medial Septum Selectively Inhibit Interneurons in the Medial Entorhinal Cortex.” *Journal of Neuroscience* 34 (50): 16739–43. <https://doi.org/10.1523/JNEUROSCI.1612-14.2014>.
- Groen, Thomas Van, and J. Michael Wyss. 1995. “Projections from the Anterodorsal and Anteroveniral Nucleus of the Thalamus to the Limbic Cortex in the Rat.” *Journal of Comparative Neurology* 358 (4): 584–604. <https://doi.org/10.1002/cne.903580411>.
- Hafting, T., M. Fyhn, S. Molden, M. Moser, and E. I. Moser. 2005. “Microstructure of a Spatial Map in the Entorhinal Cortex.” *Nature* 436 (7052): 801–6. <https://doi.org/10.1038/nature03721>.

- Høydal, Øyvind Arne, Emilie Ranheim Skytøen, Sebastian Ola Andersson, May Britt Moser, and Edvard I. Moser. 2019. "Object-Vector Coding in the Medial Entorhinal Cortex." *Nature* 568 (7752): 400–404. <https://doi.org/10.1038/s41586-019-1077-7>.
- Jiang, X., S. Shen, C. R. Cadwell, P. Berens, F. Sinz, A. S. Ecker, S. Patel, and A. S. Tolias. 2015. "Principles of Connectivity among Morphologically Defined Cell Types in Adult Neocortex." *Science* 350 (6264): aac9462–aac9462. <https://doi.org/10.1126/science.aac9462>.
- Karnani, M. M., J. Jackson, I. Ayzenshtat, A. Hamzehei Sichani, K. Manoocheri, S. Kim, and R. Yuste. 2016. "Opening Holes in the Blanket of Inhibition: Localized Lateral Disinhibition by VIP Interneurons." *Journal of Neuroscience* 36 (12): 3471–80. <https://doi.org/10.1523/JNEUROSCI.3646-15.2016>.
- Kecskés, Miklós, Nóra Henn-Mike, Ágnes Agócs-Laboda, Szilárd Szócs, Zoltán Petykó, and Csaba Varga. 2020. "Somatostatin Expressing GABAergic Interneurons in the Medial Entorhinal Cortex Preferentially Inhibit Layer III-V Pyramidal Cells." *Communications Biology* 3 (1): 1–13. <https://doi.org/10.1038/s42003-020-01496-x>.
- Kepecs, Adam, and Gordon Fishell. 2014. "Interneuron Cell Types Are Fit to Function." *Nature* 505 (7483): 318–26. <https://doi.org/10.1038/nature12983>.
- Kinnavane, Lisa, Eman Amin, Cristian M. Olarte-Sánchez, and John P. Aggleton. 2017. "Medial Temporal Pathways for Contextual Learning: Network c- Fos Mapping in Rats with or without Perirhinal Cortex Lesions." *Brain and Neuroscience Advances* 1: 239821281769416. <https://doi.org/10.1177/2398212817694167>.

- Knierim, James J, Joshua P Neunuebel, and Sachin S Deshmukh. 2014. “Functional Correlates of the Lateral and Medial Entorhinal Cortex.” *Phil Trans R Soc B*.
- Knowland, Daniel, Varoth Lilascharoen, Christopher Pham Pacia, Sora Shin, Eric Hou Jen Wang, and Byung Kook Lim. 2017. “Distinct Ventral Pallidal Neural Populations Mediate Separate Symptoms of Depression.” *Cell* 170 (2): 284-297.e18. <https://doi.org/10.1016/j.cell.2017.06.015>.
- Koganezawa, N., R. Gisetstad, E. Husby, T. P. Doan, and M. P. Witter. 2015. “Excitatory Postrhinal Projections to Principal Cells in the Medial Entorhinal Cortex.” *Journal of Neuroscience* 35 (48): 15860–74. <https://doi.org/10.1523/JNEUROSCI.0653-15.2015>.
- Krabbe, Sabine, Enrica Paradiso, Simon D’Aquin, Yael Bitterman, Julien Courtin, Chun Xu, Keisuke Yonehara, et al. 2019. “Adaptive Disinhibitory Gating by VIP Interneurons Permits Associative Learning.” *Nature Neuroscience* 22 (11): 1834–43. <https://doi.org/10.1038/s41593-019-0508-y>.
- Lee, Candice, Sandrine L. Côté, Nima Raman, Hritvic Chaudhary, Bryan C. Mercado, and Simon X. Chen. 2023. “Whole-Brain Mapping of Long-Range Inputs to the VIP-Expressing Inhibitory Neurons in the Primary Motor Cortex.” *Frontiers in Neural Circuits* 17 (May): 1093066. <https://doi.org/10.3389/fncir.2023.1093066>.
- Lee, Soohyun, Illya Kruglikov, Z Josh Huang, Gord Fishell, and Bernardo Rudy. 2013. “A Disinhibitory Circuit Mediates Motor Integration in the Somatosensory Cortex.” *Nature Neuroscience* 16 (11): 1662–70. <https://doi.org/10.1038/nn.3544>.

- Letzkus, Johannes J., Steffen B.E. Wolff, and Andreas Lüthi. 2015. “Disinhibition, a Circuit Mechanism for Associative Learning and Memory.” *Neuron* 88 (2): 264–76. <https://doi.org/10.1016/j.neuron.2015.09.024>.
- Miao, Chenglin, Qichen Cao, May-britt Moser, and Edvard I Moser. 2017. “Parvalbumin and Somatostatin Interneurons Control Different Space-Coding Networks in the Medial Entorhinal Cortex.” *Cell* 171 (3): 1–15. <https://doi.org/10.1016/j.cell.2017.08.050>.
- Mittelstaedt, M. L., and H. Mittelstaedt. 1980. “Homing by Path Integration in a Mammal.” *Naturwissenschaften* 67 (11): 566–67. <https://doi.org/10.1007/BF00450672>.
- Moser, Edvard I, Emilio Kropff, and May-Britt Moser. 2008. “Place Cells, Grid Cells, and the Brain’s Spatial Representation System.” *Annu. Rev. Neurosci.* 31: 69–89. <https://doi.org/10.1146/annurev.neuro.31.061307.090723>.
- Naber, Pieterke A., Fernando H. Lopes Da Silva, and Menno P. Witter. 2001. “Reciprocal Connections between the Entorhinal Cortex and Hippocampal Fields CA1 and the Subiculum Are in Register with the Projections from CA1 to the Subiculum.” *Hippocampus* 11 (2): 99–104. <https://doi.org/10.1002/hipo.1028>.
- Ohara, Shinya, Mariko Onodera, Øyvind W. Simonsen, Rintaro Yoshino, Hiroyuki Hioki, Toshio Iijima, Ken Ichiro Tsutsui, and Menno P. Witter. 2018. “Intrinsic Projections of Layer Vb Neurons to Layers Va, III, and II in the Lateral and Medial Entorhinal Cortex of the Rat.” *Cell Reports* 24 (1): 107–16. <https://doi.org/10.1016/j.celrep.2018.06.014>.
- Ohara, Shinya, Märt Rannap, Ken-ichiro Tsutsui, Andreas Draguhn, Alexei V. Egorov, and Menno P. Witter. 2022. “Hippocampal-Medial Entorhinal Circuit Is Differently Organized along the Dorsoventral Axis in Rodents.” *BioRxiv*, 2022.05.30.493979.

- Ohara, Shinya, Märt Rannap, Ken Ichiro Tsutsui, Andreas Draguhn, Alexei V. Egorov, and Menno P. Witter. 2023. "Hippocampal-Medial Entorhinal Circuit Is Differently Organized along the Dorsoventral Axis in Rodents." *Cell Reports* 42 (1). <https://doi.org/10.1016/j.celrep.2023.112001>.
- Okada, Kana, Kouichi Hashimoto, and Kazuto Kobayashi. 2022. "Cholinergic Regulation of Object Recognition Memory." *Frontiers in Behavioral Neuroscience* 16 (September): 1–10. <https://doi.org/10.3389/fnbeh.2022.996089>.
- Perry, Brook A.L., and Anna S. Mitchell. 2019. "Considering the Evidence for Anterior and Laterodorsal Thalamic Nuclei as Higher Order Relays to Cortex." *Frontiers in Molecular Neuroscience* 12 (July): 1–8. <https://doi.org/10.3389/fnmol.2019.00167>.
- Pfeffer, Carsten K. 2014. "Inhibitory Neurons: Vip Cells Hit the Brake on Inhibition." *Current Biology* 24 (1): R18–20. <https://doi.org/10.1016/j.cub.2013.11.001>.
- Pi, Hyun-Jae, Balázs Hangya, Duda Kvitsiani, Joshua I. Sanders, Z. Josh Huang, and Adam Kepecs. 2013. "Cortical Interneurons That Specialize in Disinhibitory Control." *Nature* 503 (7477): 521–24. <https://doi.org/10.1038/nature12676>.
- Prönneke, Alvar, Bianca Scheuer, Robin J. Wagener, Martin Möck, Mirko Witte, and Jochen F. Staiger. 2015. "Characterizing VIP Neurons in the Barrel Cortex of VIP<sup>cre</sup>/TdTomato Mice Reveals Layer-Specific Differences." *Cerebral Cortex* 25 (12): 4854–68. <https://doi.org/10.1093/cercor/bhv202>.
- Rhomberg, Thomas, Laura Rovira-Esteban, Attila Vikór, Enrica Paradiso, Christian Kremser, Petra Nagy-Pál, Orsolya I Papp, et al. 2018. "VIP-Immunoreactive Interneurons within

- Circuits of the Mouse Basolateral Amygdala.” *The Journal of Neuroscience* 38 (31): 2063–17. <https://doi.org/10.1523/JNEUROSCI.2063-17.2018>.
- Rodo, Christophe, Francesca Sargolini, and Etienne Save. 2017. “Processing of Spatial and Non-Spatial Information in Rats with Lesions of the Medial and Lateral Entorhinal Cortex: Environmental Complexity Matters.” *Behavioural Brain Research* 320: 200–209. <https://doi.org/10.1016/j.bbr.2016.12.009>.
- Rowland, D. C., A. P. Weible, I. R. Wickersham, H. Wu, M. Mayford, M. P. Witter, and C. G. Kentros. 2013. “Transgenically Targeted Rabies Virus Demonstrates a Major Monosynaptic Projection from Hippocampal Area CA2 to Medial Entorhinal Layer II Neurons.” *Journal of Neuroscience* 33 (37): 14889–98. <https://doi.org/10.1523/JNEUROSCI.1046-13.2013>.
- Rowland, David C., Horst A. Obenaus, Emilie R. Skytøen, Qiangwei Zhang, Cliff G. Kentros, Edvard I. Moser, and May Britt Moser. 2018. “Functional Properties of Stellate Cells in Medial Entorhinal Cortex Layer II.” *eLife* 7: 1–17. <https://doi.org/10.7554/eLife.36664>.
- Samsonovich, a, and B L McNaughton. 1997. “Path Integration and Cognitive Mapping in a Continuous Attractor Neural Network Model.” *The Journal of Neuroscience: The Official Journal of the Society for Neuroscience* 17 (15): 5900–5920.
- Sargolini, Francesca, Marianne Fyhn, Torkel Hafting, Bruce L McNaughton, Menno P Witter, May-Britt Moser, and Edvard I Moser. 2006. “Conjunctive Representation of Position, Direction, and Velocity in Entorhinal Cortex.” *Science* 312 (5774): 758–62.

- Sasaki, Takuya, Stefan Leutgeb, and Jill K. Leutgeb. 2015. "Spatial and Memory Circuits in the Medial Entorhinal Cortex." *Current Opinion in Neurobiology* 32: 16–23. <https://doi.org/10.1016/j.conb.2014.10.008>.
- Schlesiger, Magdalene Isabell, Tobias Ruff, Duncan Archibald Allan MacLaren, Isabel Barriuso-Ortega, Khalid Magomedovich Saidov, Ting Yun Yen, and Hannah Monyer. 2021. "Two Septal-Entorhinal GABAergic Projections Differentially Control Coding Properties of Spatially Tuned Neurons in the Medial Entorhinal Cortex." *Cell Reports* 34 (9): 108801. <https://doi.org/10.1016/j.celrep.2021.108801>.
- Sürmeli, Gülşen, Daniel Cosmin Marcu, Christina McClure, Derek L F Garden, Hugh Pastoll, and Matthew F. Nolan. 2015. "Molecularly Defined Circuitry Reveals Input-Output Segregation in Deep Layers of the Medial Entorhinal Cortex." *Neuron* 88 (5): 1040–53. <https://doi.org/10.1016/j.neuron.2015.10.041>.
- Tennant, Sarah A, Lukas Fischer, Derek L F Garden, Klara Zsofia Gerliei, Cristina Martinez-Gonzalez, Christina McClure, Emma R Wood, and Matthew F Nolan. 2018. "Stellate Cells in the Medial Entorhinal Cortex Are Required for Spatial Learning," 1313–24. <https://doi.org/10.1016/j.celrep.2018.01.005>.
- Topolnik, Lisa, and Suhel Tamboli. 2022. "The Role of Inhibitory Circuits in Hippocampal Memory Processing." *Nature Reviews Neuroscience* 23 (8): 476–92. <https://doi.org/10.1038/s41583-022-00599-0>.
- Turi, Gergely Farkas, Wen Ke Li, Spyridon Chavlis, Ioanna Pandi, Justin O'Hare, James Benjamin Priestley, Andres Daniel Grosmark, et al. 2019. "Vasoactive Intestinal Polypeptide-

- Expressing Interneurons in the Hippocampus Support Goal-Oriented Spatial Learning.”  
Neuron 101 (6): 1150-1165.e8. <https://doi.org/10.1016/j.neuron.2019.01.009>.
- Tyan, L., S. Chamberland, E. Magnin, O. Camire, R. Francavilla, L. S. David, K. Deisseroth, and L. Topolnik. 2014. “Dendritic Inhibition Provided by Interneuron-Specific Cells Controls the Firing Rate and Timing of the Hippocampal Feedback Inhibitory Circuitry.” *Journal of Neuroscience* 34 (13): 4534–47. <https://doi.org/10.1523/JNEUROSCI.3813-13.2014>.
- Urban, Daniel J., and Bryan L. Roth. 2015. “DREADDs (Designer Receptors Exclusively Activated by Designer Drugs): Chemogenetic Tools with Therapeutic Utility.” *Annual Review of Pharmacology and Toxicology* 55 (1): 399–417. <https://doi.org/10.1146/annurev-pharmtox-010814-124803>.
- Wall, Nicholas R., Mauricio de la Parra, Jordan M. Sorokin, Hiroki Taniguchi, Z. Josh Huang, and Edward M. Callaway. 2016. “Brain-Wide Maps of Synaptic Input to Cortical Interneurons.” *Journal of Neuroscience* 36 (14): 4000–4009. <https://doi.org/10.1523/JNEUROSCI.3967-15.2016>.
- Wijngaarden, Joeri B.G. van, Susanne S. Babl, and Hiroshi T. Ito. 2020. “Entorhinal-Retrosplenial Circuits for Allocentric-Egocentric Transformation of Boundary Coding.” *ELife* 9: 1–25. <https://doi.org/10.7554/eLife.59816>.
- Winterer, Jochen, Nikolaus Maier, Christian Wozny, Prateep Beed, Jörg Breustedt, Roberta Evangelista, Yangfan Peng, Tiziano D’Albis, Richard Kempter, and Dietmar Schmitz. 2017. “Excitatory Microcircuits within Superficial Layers of the Medial Entorhinal Cortex.” *Cell Reports* 19 (6): 1110–16. <https://doi.org/10.1016/j.celrep.2017.04.041>.

Witter, Menno P., Thanh P. Doan, Bente Jacobsen, Eirik S. Nilssen, and Shinya Ohara. 2017.

“Architecture of the Entorhinal Cortex A Review of Entorhinal Anatomy in Rodents with Some Comparative Notes.” *Frontiers in Systems Neuroscience* 11 (June): 46. <https://doi.org/10.3389/fnsys.2017.00046>.

Zutshi, Ipshita, Maylin L Fu, Varoth Lilascharoen, Jill K Leutgeb, Byung Kook Lim, and Stefan

Leutgeb. 2018. “Recurrent Circuits within Medial Entorhinal Cortex Superficial Layers Support Grid Cell Firing.” *Nature Communications* 9 (1). <https://doi.org/10.1038/s41467-018-06104-5>.

## 6 Figures and Figure legends

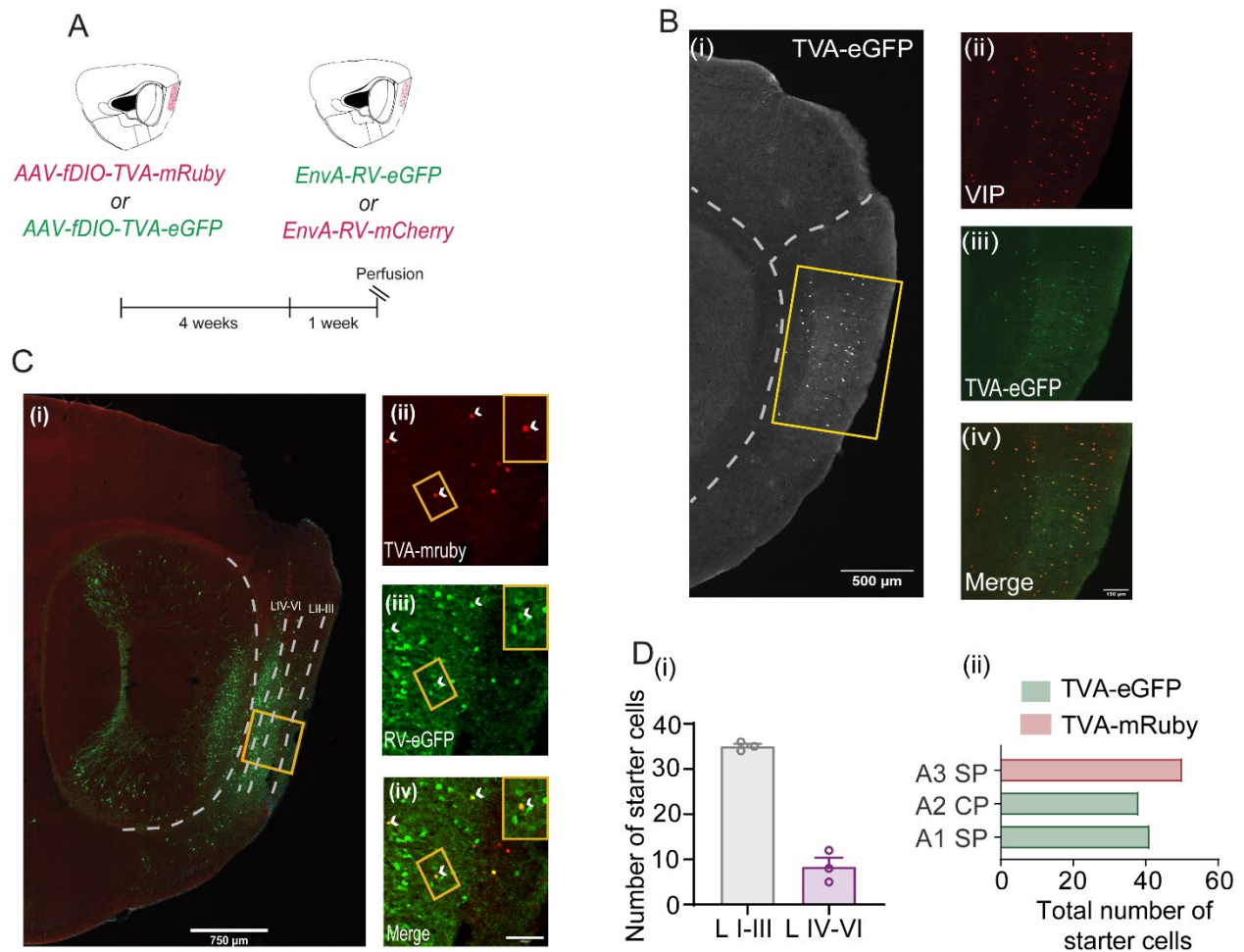


**Figure 1. Rabies viral strategy and confirmation of starter cells**

A) Strategy for helper virus and rabies virus injection in VIP-cre mice (n= 3). The helper virus (Either TVA-mRuby or TVA-eGFP) was injected first and then 4 weeks later, the rabies virus (RV-eGFP or RV-mCherry) was injected. The animals were perfused a week later for whole brain sectioning. B) Confirmation of TVA specificity in a VIPtdTom mouse. TVA-eGFP was injected in a VIPtdTom animal. Colocalization of (ii) VIP and (iii) TVA-eGFP was quantified by counting all (iv) co-labelled cells.

C) Image of injection site and starter cells. Layers of the MEC are marked by dashed lines. A magnified view of the starter and input cells within the MEC are denoted by yellow boxes and white arrows. Transfection of VIP cells by (ii) TVA receptors and (iii) EnvA protein. colocalization of the two channels is seen in (iv) the starter cell. D) Quantification of starter cells in the MEC. The number of starter cells across the different layers of the MEC (i), while (ii) shows the total number of starter cells for all 3 animals, with both viral strategies. CP - coronal plane, SP-sagittal plane.

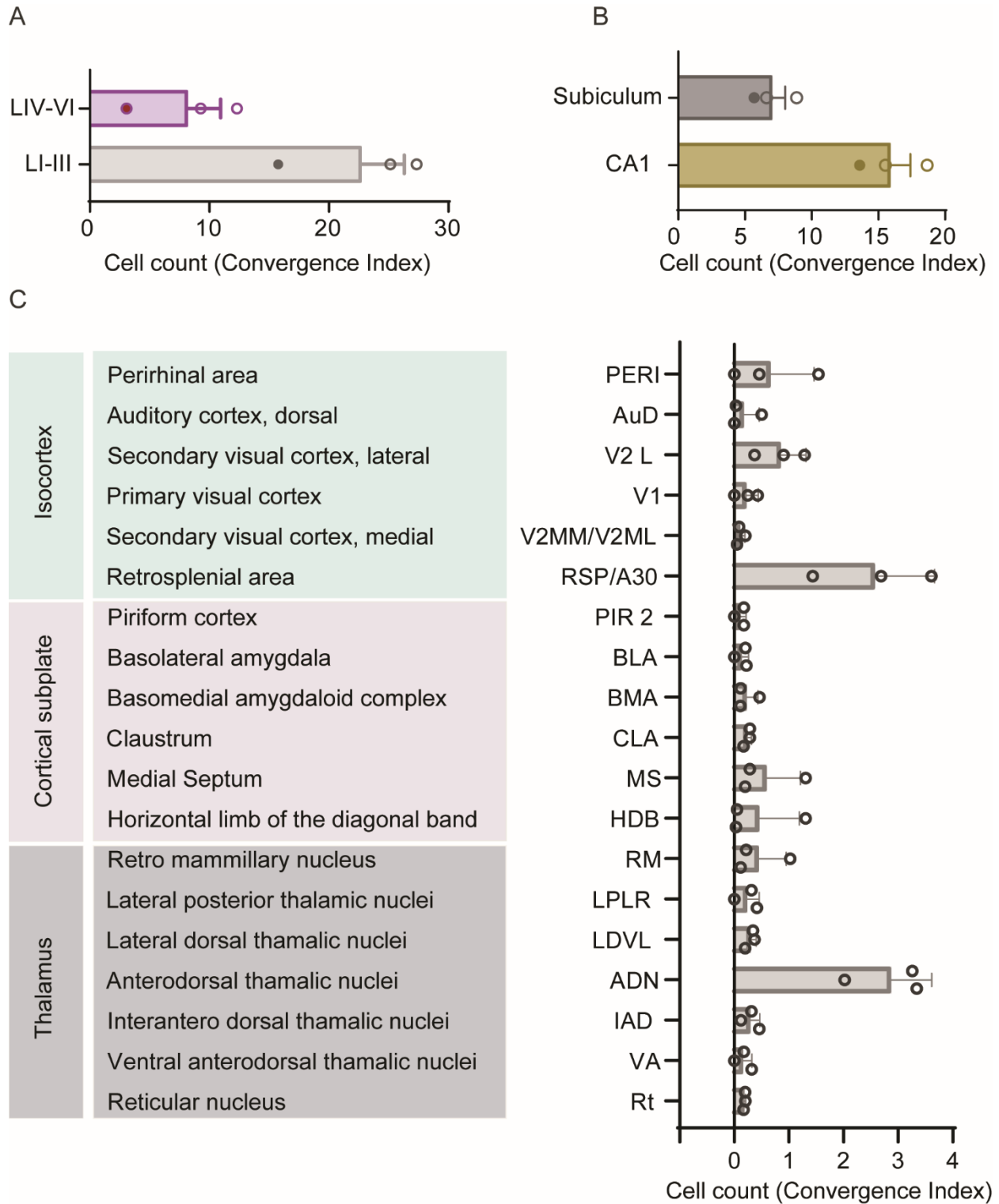
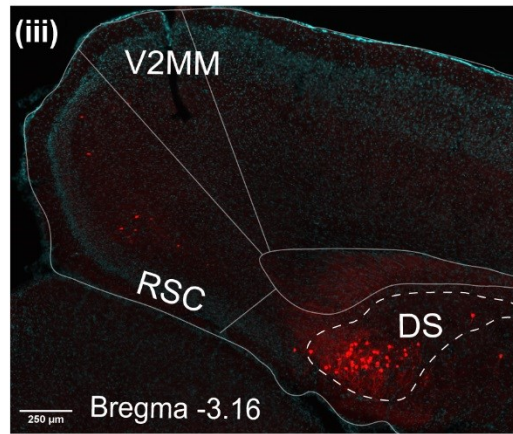
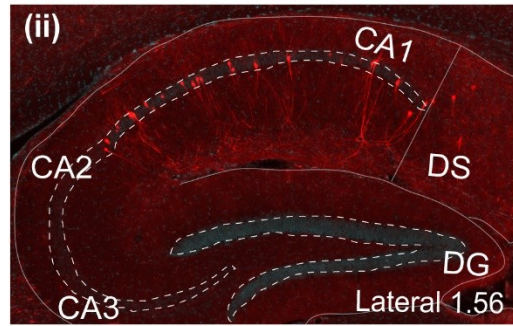
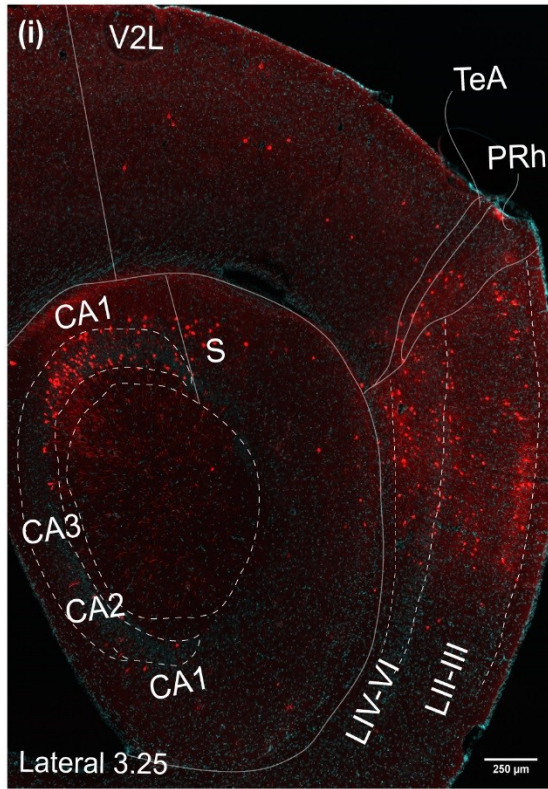


**Figure 2. Generating and quantifying brain wide inputs to VIP cells in the MEC**

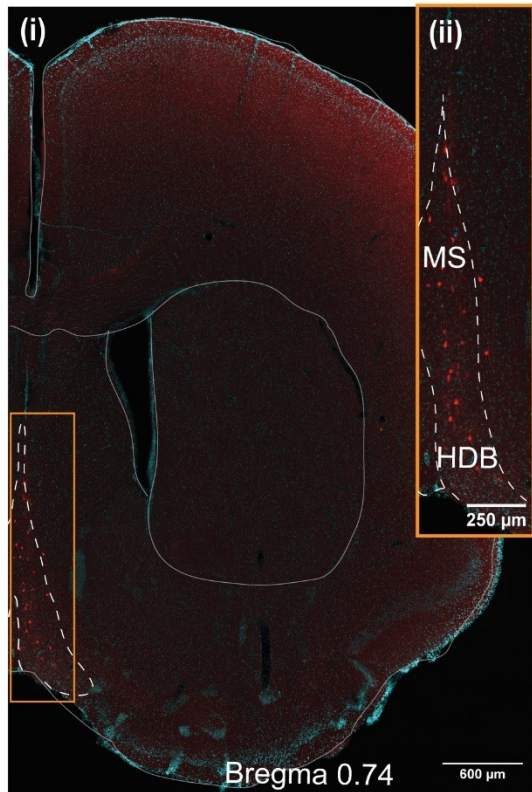
A) Input cell quantification within the different layers of the MEC. B) Input cell quantification for cells projecting from the CA1 and subiculum C) Input cell quantification for different brain regions located in the isocortex, cortical subplate and the thalamus, as defined by the Allen Brain Atlas. The convergence index for all graphs was calculated as a ratio of the number of inputs from a given brain region over the number of starter cells quantified in an animal.  $N = 3$  for all panels.

For the total fraction of inputs from different brain regions see Supplementary Fig 1.

A



B



C

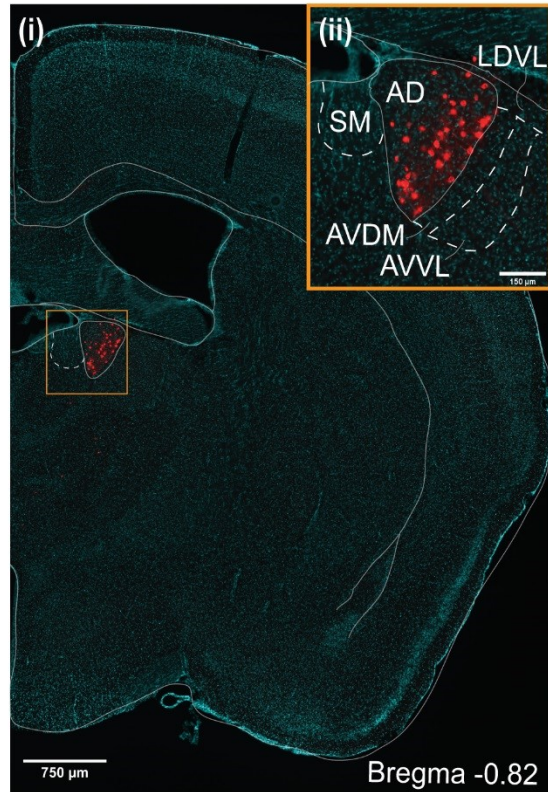


**Figure 3. Local and long-range connectivity from distinct regions of the brain to VIP cells in the MEC**

A) Representative image of monosynaptic input from (i) different layers of the MEC, secondary visual cortex, perihinal cortex (ii) CA1(pyramidal layer) of the hippocampus and (iii) Dorsal subiculum and Retrosplenial cortex B) Monosynaptic input from the (i) Medial septum and (ii) Anterior dorsal thalamic nucleus. In each figure, insets represent high magnification of the region.

In all panels, DAPI is in Cyan and RV is in RFP channel. For anatomical abbreviations, see methods or Figure 2.

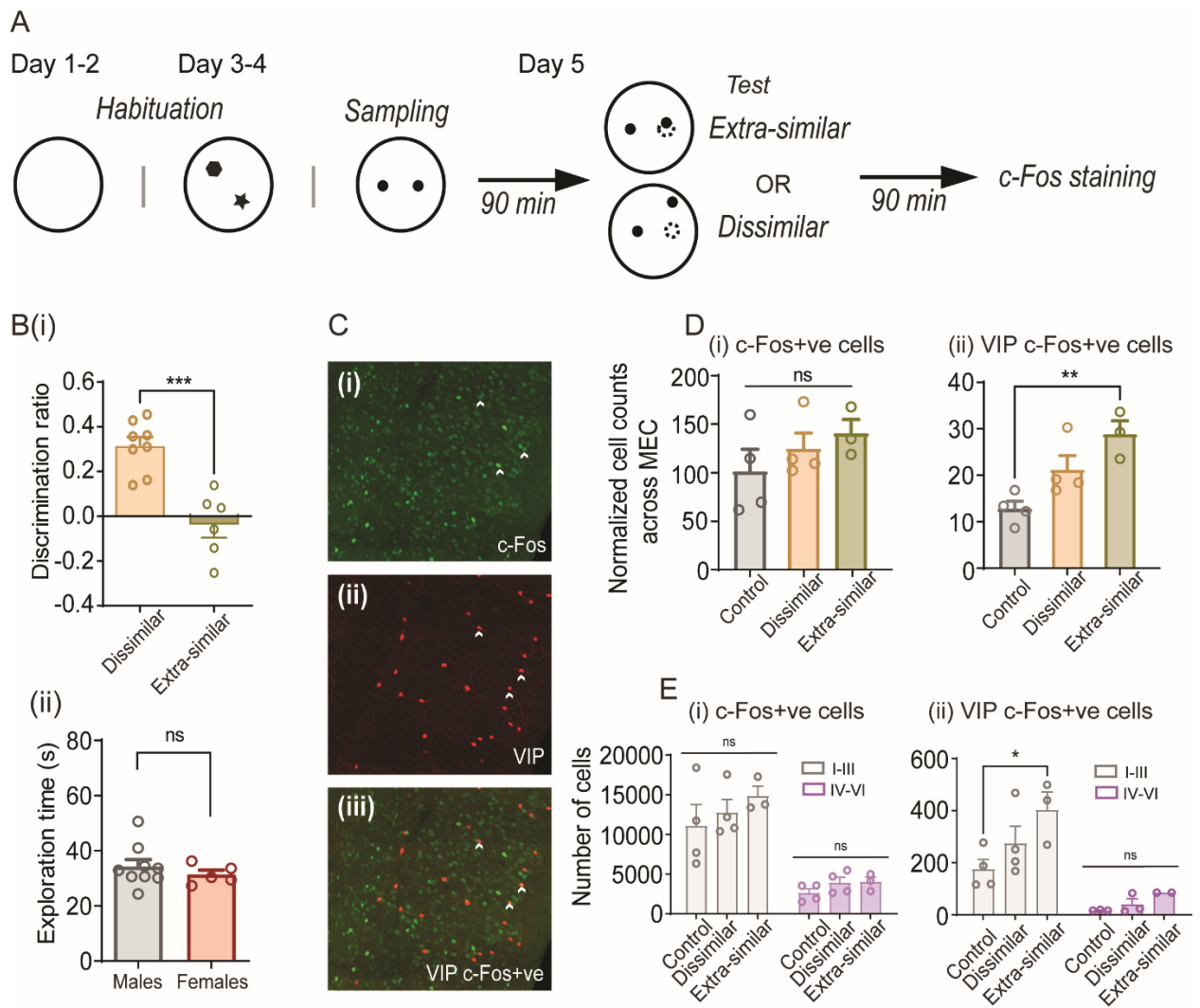


#### **Figure 4. Detecting cFos expression in VIP cells**

A) Schematic of the novel object location paradigm that was used to test spatial memory in mice.

B) In panel (i) Discrimination ratios for the dissimilar (n = 8 animals) and extra-similar paradigm (n = 6 animals) show a significant difference, ( $p = 0.0007$ ,  $0.313 \pm 0.041$  n = 8 vs  $-0.0375 \pm 0.019$  n = 6,  $U = 0$ , Mann-Whitney test, two tailed) (ii) Exploration time during sampling phase for male and female mice shows no significant differences. n = 9 male mice and n = 5 female mice ( $p = 0.437$ ,  $34.24 \pm 8.64.9s$  n=9 vs  $31.37 \pm 9.39.1s$  n=5,  $U = 16$ , Mann-Whitney test, two tailed) C) Immunohistochemistry was performed for (i) c-Fos (GFP), (ii)VIP (tdTom). Panel (iii) shows colocalization of tdTom cells positive for c-Fos D) Distribution of (i) c-Fos and (ii) c-Fos positive VIP cells across the whole MEC (Control group n = 4 animals, dissimilar paradigm n = 3 animals, extrasimilar paradigm n = 3 animals) E. Quantification of (i) c-Fos positive cells and (ii) c-Fos positive VIP cells in the superficial (I-III) vs deep layers of the MEC (IV-VI).

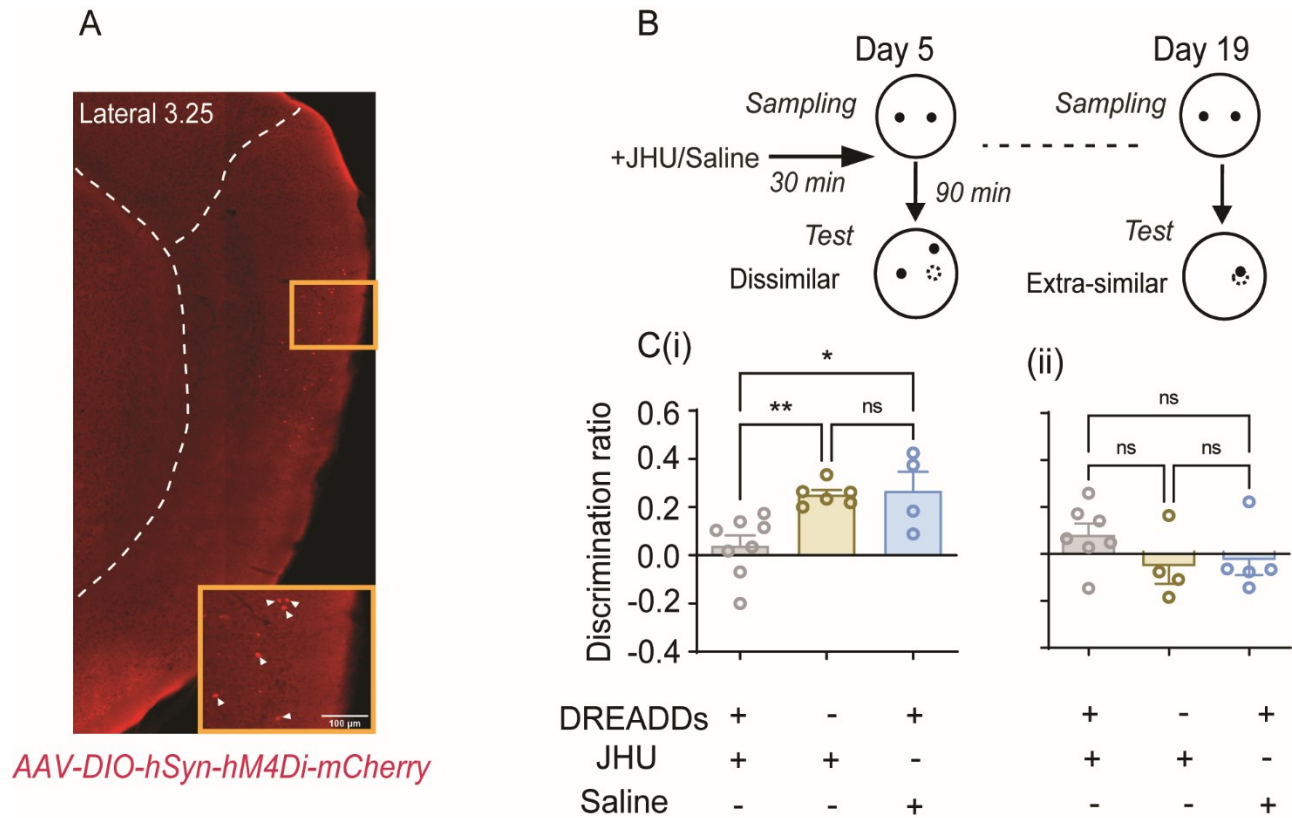
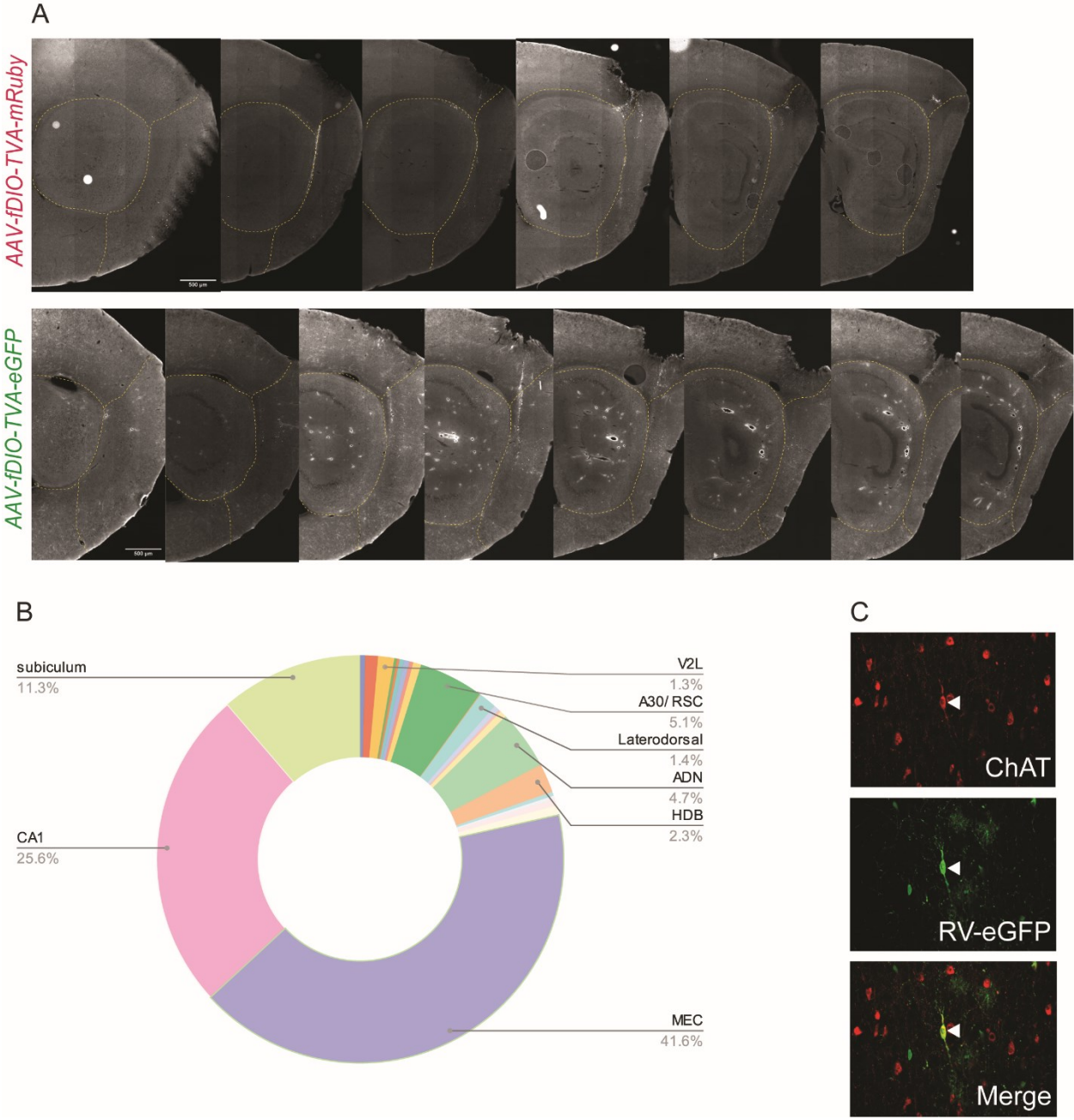


**Figure 5 Inhibition of VIP cells causes a behavioural deficit during a novel object location task**

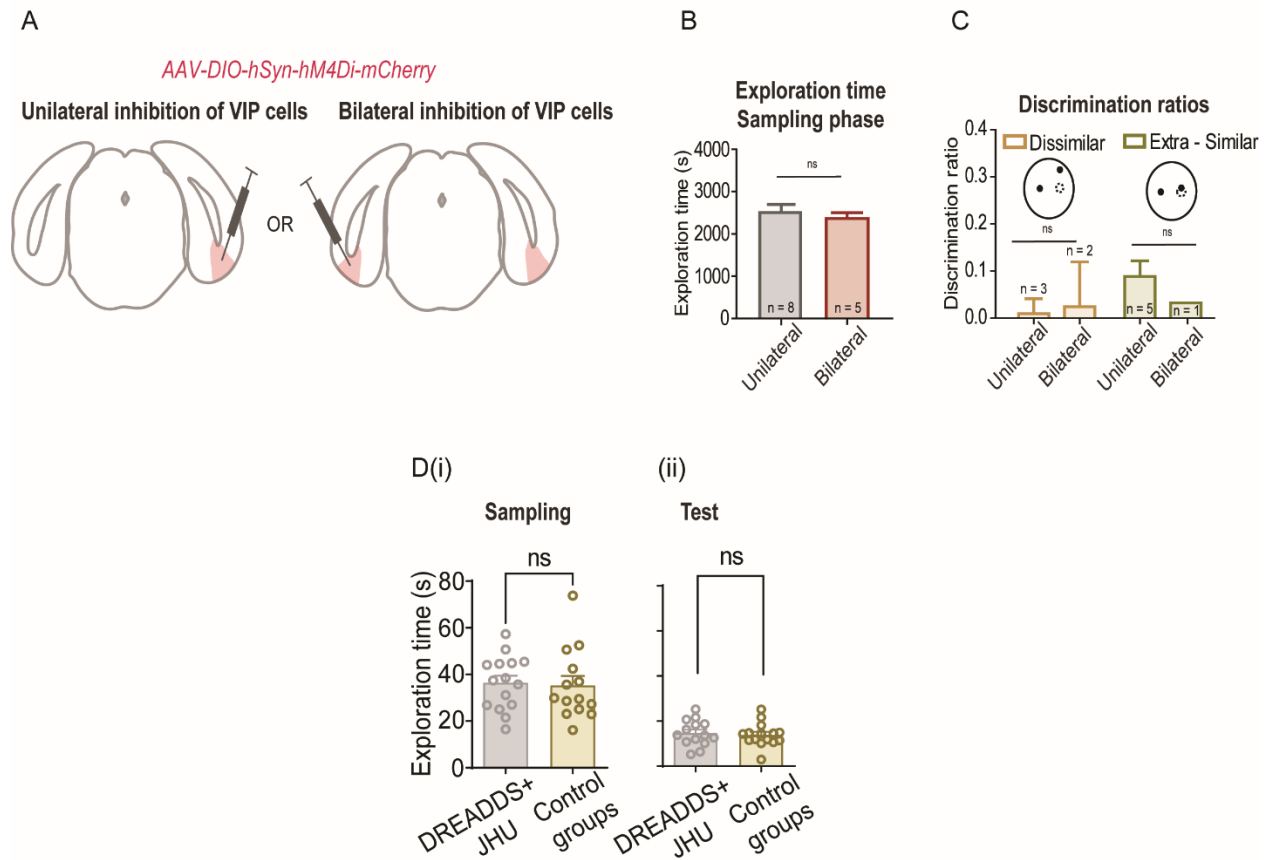
A) Sagittal section of the MEC from a VIP-Cre mouse injected with AAV-DIO-hSyn-hM4Di-mCherry. Inset shows magnified view of the injection site and white arrows point to cell bodies transfected by virus. B) Extended version of the novel object location task as seen in Fig 4A. In the adapted version, animals were re-introduced to the arena 2 weeks after the last test phase to test the same animals in the counterbalanced version of the task. C) Discrimination ratios for animals (i) in the dissimilar task shows significant differences in the discrimination ratio in the experimental group compared to saline control ( $*p < 0.05$ ,  $0.039 \pm 0.0437$   $n = 8$  vs  $0.252 \pm 0.0193$   $n = 4$ , One way ANOVA followed by Tukey's multiple comparison test) and JHU no DREADDs group ( $**p < 0.05$ ,  $0.039 \pm 0.0437$   $n = 8$  vs  $0.268 \pm 0.079$   $n = 6$ , One way ANOVA followed by

Tukey's multiple comparison test) (n = 8 animals). While in the (ii) extra similar paradigm we do not see any significant differences in the discrimination ratios.



Supplementary figure 1

A) Sagittal sections of animals injected with (i) AAV.fDIO.mRuby.TVA and (ii) AAV2/8-hSyn-FLEX-TVA-P2A-eGFP-2A-oG, starter cells within the sections are seen in white. B) Fraction of inputs for each brain area. This is calculated as the percentage of presynaptic cells per ROI (as defined by the Allen Brain Atlas) over the sum of total inputs from the entire brain. C) IHC staining for ChAT shows that some RV-eGFP cells colocalize with this marker.



## Supplementary figure 2

A) Schematic showing the bilateral and unilateral strategies used to target the MEC for inhibition of VIP cells. B) Comparing the exploration time from the sampling phase of animals injected with the bilateral or unilateral strategy showed no significant differences. C) Comparing the

discrimination ratios for dissimilar and extrasimilar conditions showed no significant differences between either group. D) Exploration time for (i) sampling phase and (ii) test phase showed no significant differences between control and experimental groups.

## Chapter 4. Discussion

### 4.1 Connecting the dots: Characterization, Inputs and Spatial Functions of VIP cells in the MEC

The findings presented in this thesis contribute to our understanding of VIP interneurons in the MEC and shed light on their heterogeneity, input connectivity, and functional implications during the novel object location task.

In the first paper we focus on the characterization of VIP cells in terms of their distribution, morphology, and electrophysiological properties within the MEC. First, we validated the efficiency of a VIP cre-driver mouse line as a suitable model system for studying the VIP population in the MEC. Our results confirmed and extend on previous studies of VIP interneurons (Ferrante et al. 2017). We found that VIP neurons in the MEC represent a heterogeneous population of GABAergic cells, similar to reports from other brain regions such as the hippocampus (Topolnik and Tamboli 2022; Tyan et al. 2014), barrel cortex (S. Lee et al. 2013; Prönneke et al. 2015), and the basolateral amygdala (Rhombert et al., 2018; Krabbe et al., 2019). This heterogeneity was confirmed through molecular characterization, the identification of different firing patterns and morphologies using *in vitro* electrophysiology. Second, in terms of firing patterns, our data show that VIP cells with irregular spiking (IS) are the most prominent type. The morphological and electrophysiological analysis revealed differences between superficial and deep VIP cells. These results indicate distinct input and output domains for these cells within the MEC circuitry. We also observed a gradient in both active and passive membrane properties along the dorsoventral extent of the MEC.

In the second paper we delve into the inputs, connectivity, and functional implications of VIP interneurons in the MEC, particularly in the context of spatial memory. Using rabies-mediated viral tracing, we identified the monosynaptic inputs that drive VIP cells in the MEC. Our data revealed connections from various cortical, subcortical, and thalamic regions, including the CA1 region of the hippocampus, the retrosplenial cortex (RSC), the medial septum (MS), and the anterodorsal thalamic nucleus (ADN). The projection between the ADN and VIP cells in the MEC is a remarkable one as previous reports have stated that the projections from ADN are sparse (Van Groen and Wyss 1995). Collectively, these inputs suggest that VIP cells in the MEC play a role in modulating the transmission of spatial navigation and memory-related information between the MEC and the hippocampus. Additionally, we employed a novel object location paradigm to investigate the functional implications of VIP cells in spatial memory. Using c-Fos and DREADDs mediated inhibition, our results indicate that VIP cells are recruited during the task, and inhibition of VIP cells prior to sampling led to impaired behavioral performance, suggesting their involvement in spatial memory processes.

The integration of the findings from both papers reveals intriguing insights into the role of VIP interneurons within the MEC circuitry and further extends our understanding of the micro-circuitry of the MEC and its importance for spatial functions.

#### **4.2 Potential circuit-level mechanisms for VIP mediated inhibition/disinhibition:**

Based on our experiments and previous research, we have explored potential mechanisms through which VIP cells may mediate their inhibitory/disinhibitory activity in the MEC. VIP cells are generally known to exert disinhibitory effects in cortical and subcortical structures, and we have observed that inhibiting VIP cells prior to sampling in a novel object location task affects the animal's ability to detect new object layouts. These findings are consistent with studies that

demonstrate a similar effect when the SCs are inactivated (Tennant et al., 2018). Moreover, these SCs have been shown to be crucial for mice to learn to estimate location and perform motor-based path integration in a virtual reality task. Interestingly, inhibiting the long-range disinhibitory projections from the MS to PV cells, which results in increased PV cell activation in the MEC does not result in deficits in the animal's ability to discriminate between stationary and moved objects in the novel object location task (Schlesiger et al., 2021). This manipulation was done on long-range projecting cells, so it is possible that not all PV cells in the MEC were activated. However, it does appear that the MS PV  $\rightarrow$  PV MEC is not a primary route for the modulation of SC cells in the MEC. Based on these observations, we propose that VIP cells in the MEC predominantly exhibit disinhibitory functions, selectively inhibiting the interneuron population that targets PCs and SCs. Based on this hypothesis, we predict that modulating the activity of VIP cells (in this case inhibiting local VIP interneurons in the MEC) leads to increased interneuron activity, thereby reducing the output of excitatory cells and causing behavioral deficits in detecting spatial changes in the dissimilar version of the task. Furthermore, we believe that this manipulation of VIP's activity can allow for the modulation of SC recruitment, potentially finely tuning the communication between SC and DG, which is known to play a crucial role in the NOL task and spatial memory in general (Figure 1 A and B). Although it is possible that some VIP cells provide direct inhibitory connections onto excitatory cells (Figure 1 C) (Krabbe et al. 2019; Tyan et al. 2014). However, the presence of an increased IS (Irregular Spiking) firing pattern and the predominance of CR/VIP in our dataset support the notion of a predominantly disinhibitory circuit mediated through VIP cells.

Based on our observations from the behavioral studies, we have noticed a higher recruitment of VIP cells in conditions when the animal is exposed to similar conditions. We additionally propose

that the level of VIP activation plays a significant role in shaping the ability of SCs to create a distinct representation of a novel yet similar experience. Specifically, strong VIP activity, driven by similar upstream inputs from ADN/MS/RSC (Chao et al. 2022), could hinder SCs' capacity to generate a new map, preventing the SCs from forming a distinct representation of the test phase in comparison to the sampling phase. Due to this, the downstream structures that receive SC input, such as the DG (Canto, Wouterlood, and Witter 2008; Klink and Alonso 1997) don't have a new neural readout. Hence, we observe increased c-Fos activation but no difference in the behavior of the animal in the similar condition vs novel conditions of the paradigm.

In line with this, we believe that during novel conditions, VIP cells may receive partially different inputs from their pre-synaptic partners, enabling precise modulation of SC activity and the emergence of a distinct representation during the test phase compared to the sampling phase. Supporting this hypothesis, previous studies have shown the involvement of thalamic nuclei (Winter, Clark, and Taube 2015), dorsal hippocampus (Bonnievie et al. 2013), and the medial septum (Brandon et al. 2011) in the modulation of the activity of grid cells and in spatial tasks such as the novel object location (Chao et al. 2022; Sziklas 1999; Tennant et al. 2018).

### **4.3 Critical considerations:**

Although the above experiments have provided valuable insights, there are still a few technical and theoretical factors that need to be considered.

#### *4.3.1 Characterization of VIP cells across the different layers of the MEC:*

Our results confirm that VIP interneurons are a specific sub-class of GABAergic cells that do not overlap with PV or SOM, however, previous studies have noted that VIP cells can co-express other molecular markers such as CCK, CR or 5HT3aR (Rudy et al. 2013; Kepecs and Fishell

2014). In our data, we find that 67.5% of VIP cells are positive for CR, however we did not test the presence of the other molecular markers mentioned. It is to be noted that little is known about VIP cells that co-express CCK as they represent a very small percentage of neurons in the cortex (Ascoli et al. 2008), while VIP cells that co-express CR are thought to be disinhibitory in their mode of action (Turi et al. 2019; Gulyás, Hájos, and Freund 1996)

Interestingly, a sub-class of VIP cells can also express ChAT at the presynaptic terminal (Prönneke et al. 2020; Bayraktar et al. 2000; Dudai et al. 2021). While these studies do not find a difference in the electrophysiological properties between ChAT +ve/ChAT -ve VIP cells, we did not attempt to characterize or identify the presence of this population in our *in vitro* study.

Reconstruction of cells after an *in vitro* recording session can help us ascertain if the morphology and electrophysiological features of the cell are correlated. However, it isn't the most suitable method to determine if the cells are long-range projecting. In our study, biocytin-filled cells revealed that VIP cells have different morphologies, however, it is possible that based on the orientation of the brain slice, some features of the dendritic and axonal arbors were cut and thus the full extent of the dendrite and axonal arborization were not captured using this method.

#### 4.3.2 *Monosynaptic retrograde tracing of inputs to VIP cells:*

In various cortical structures, rabies-mediated viral tracing has been used to uncover inputs that can drive different cell populations. Through these studies, we have gained insight that PV, SOM and VIP interneurons within a cortical/sub-cortical structure receive inputs from the same regions (depending on which structure the starter cells were transfected). However, the quantity of these inputs varies between the different interneuron populations (C. Lee et al. 2023; Wickersham et al. 2007; Beier et al. 2015; Wall et al. 2016). In the present study, we only traced inputs to VIP

cells thus making it difficult to conclude if the projections we observed are specific to this population in the MEC.

In addition to this, it appears that there can be a topographic organization to how the inputs in the MEC are received (CA1 and subiculum inputs selectively target the deep layers of the MEC) (Sürmeli et al. 2015; Canto, Wouterlood, and Witter 2008). Since we utilized an injection strategy to target the VIP cells in the MEC and transfected cells across all layers, it is difficult to ascertain if VIP cells in the deep layers receive different inputs compared to the VIP cells in the superficial layers of the MEC. Furthermore, the presence of a projection does not reveal its functional significance. Hence the importance of the projections from the various structures to VIP cells in the MEC needs to be further explored. We suggest potential ways to do this in section 4.4

#### *4.3.3 Using c-Fos as an activity marker:*

In our study, we used c-Fos to assess if VIP cells are involved in a spatial task such as the novel object location paradigm. In our experiment, we perfused our animals 90mins after the test phase (not sampling) and find that VIP cells are recruited during this task. However, as c-Fos expression can be a delayed marker for neuronal activity, it is possible we could have a mixed population of VIP cells, for instance, some cells could have been activated towards the end of the sampling phase, while others could have been active during the test phase in the same animal. Another factor to consider is that c-Fos labeling represents the activation state of a population of neurons. It is possible that within a labeled population, only a subset of neurons may be actively engaged in an aspect of the task (object identification vs location-specific coding), while others may be less involved or completely irrelevant. Therefore, c-Fos labeling should be interpreted as a proxy for neuronal activation at the population level rather than reflecting the activity of every

individual neuron, as it does not provide evidence for what is being encoded by the cell at that time point. (Kinnavane et al. 2017; Miyashita et al. 2009; Dragunow 1996).

The use of c-Fos and other activity markers like *Arc* and *Zif* has been widely employed in neuroscience research to study neuronal activation patterns, especially in the context of learning and memory. Some studies have noted that *Arc* is more sensitive towards learning and memory (Kovács 2008). While this could be used as an alternative method to determine the recruitment of VIP cells in the novel object location task, it is also important to note that immediate early genes and activity-dependent markers do not provide direct information about the specific physiological processes occurring within activated neurons. Therefore, it is important to integrate these findings with other complementary approaches such as *in vivo* recordings to obtain a more comprehensive understanding of neuronal activity (Kovács 2008)

#### 4.3.4 Inhibition of VIP cells using DREADDs virus:

With the generation of modified designer G-protein coupled receptors (GPCR) that are exclusively activated by designer drugs (DREADDs) (Urban and Roth 2015), it has been possible to successfully inhibit circuits in freely behaving animals. Its success can be credited to its minimal basal activity and high selectivity for the ligand. The muscarinic receptor hM4Di remains inactive in the absence of the ligand and is insensitive to acetylcholine, but mediates an inhibitory effect in neural cells when expressed (Saloman et al. 2016; Roth 2016) and its ligand is injected. Interestingly the kinetics for hM4Di-mediated inhibition is still relatively unclear. While some studies suggest that this receptor suppresses neuronal action potential firing via GIRK-mediated membrane hyperpolarization (Armbruster et al. 2007), some studies have also shown that alternative processes such as blockage of pre-synaptic release might be responsible for the inhibition caused by activation of hM4Di receptor (Roth 2016; Wiegert et al. 2017). Most

importantly, the effectiveness of DREADD-mediated inhibition depends on the pharmacokinetics of the ligand (Stachniak, Ghosh, and Sternson 2014; Wiegert et al. 2017; Iyer et al. 2016; Bonaventura et al. 2019). This can be a 'bottleneck' for this technique as the ligands like JHU and CNO has the capacity to bind to endogenous GPCRs present in the tissue. Hence, controls in which the hM4Di receptor is not expressed but the ligand is administered must be performed to account for the effect of this on normal cells. We conducted these experimental controls in our experiments (Group: JHU no DREADDs) and found that the ligand had no effect on the behaviour of the mice.

While DREADDs can provide for effective and sustained inhibition of cells for up to many hours after the administration of the ligand (Miao et al. 2017; Bonaventura et al. 2019), it doesn't provide for the immediate effect that optogenetics can offer when the opsins are illuminated (Kitamura et al. 2015). Given that our c-Fos results showed that VIP cells are active during the task but couldn't provide a time point resolution, we decided to inhibit the cells prior to sampling based on previous studies where it was shown that VIP cells are important during the learning phase of a task (Letzkus, Wolff, and Lüthi 2015; Topolnik and Tamboli 2022). *In vivo* studies have shown that maximal inhibition occurs 30min after JHU administration (Bonaventura et al. 2019) but this doesn't discount the effect of residual inhibition in mice during the test phase of the task. Combining electrophysiological recordings with the administration of JHU can provide valuable insights into the temporal dynamics of sustained inhibition induced by the ligand. However, it is crucial to acknowledge the inherent variability across different techniques used to modulate neural activity in awake behaving animals. Such variations should be considered in terms of their potential to achieve temporal, spatial, and selective inhibition, particularly within the timescale of the specific behavioral paradigm under investigation.

#### 4.4 Future Directions:

While this thesis offers novel insights into the involvement of VIP interneurons in the MEC circuitry, it also raises unanswered questions regarding the role of these cells within the spatial system of the MEC. Follow-up studies have the potential to address these inquiries and can leverage the current findings as a foundation for further investigation. For instance, based on our patch experiment data, it would be intriguing to identify the post-synaptic targets of VIP cells and ascertain whether superficial VIP cells engage with different cell types compared to deep layer VIP cells. One potential approach to explore this *in vitro* is by expressing channelrhodopsin with GFP reporter in VIP cells; similar to (Krabbe et al. 2019; Pi et al. 2013) and utilizing a Dlx reporter with a RFP reporter virus to transfect the entire interneuron population in the MEC (Dimidschstein et al. 2016) in the same animal. The hDlx virus can be employed to identify and record from interneurons while simultaneously activating VIP cells within the same tissue slice. By examining the presence or absence of inhibitory post-synaptic potentials, we could uncover the connectivity patterns of VIP cells with interneurons and excitatory cell populations in the MEC (For preliminary results refer to Figure 2).

Previous studies have noted that the inhibition of PV cells disrupted the hexagonal spatial selectivity observed in grid cells, particularly in layer II of the MEC. On the other hand, silencing SOM cells did not affect grid cells or speed cells but instead led to a reduction in the spatial selectivity of cells with irregular firing patterns. The activity of border cells and head direction cells remained unaffected by either intervention (Miao et al. 2017; Buetfering, Allen, and Monyer 2014). It would be interesting to uncover the effect of VIP cells inhibition in a similar experiment and compare them to existing findings. Given that VIP cells receive inputs from ADN, the subiculum and the RSC, we predict that disruption in VIP cell activity will affect the tuning of HD

cells and other spatially tuned cells in the MEC. These findings can then be compared to existing studies involving other interneurons.

Additionally, studies have shown the presence of object vector coding in the MEC (Høydal et al. 2019) and the importance of contralateral MEC projections for these cells (Caputi et al. 2022). As VIP cells also receive input from the perirhinal cortex and secondary visual cortex, regions known to code for object identity (Agster, Kara L. and Burwell 2009), although (Fiorilli et al. 2023) show secondary visual cortex to be specific for object identity, and the perirhinal cortex for coding of reward outcome. Nevertheless, it would be interesting to conduct *in vivo* electrophysiological recordings or large scale two photon recordings (Zong et al. 2022) in the MEC, while an animal performs the NOL task. Manipulation of VIP cells via DREADDs or optogenetics (Depending on the technique used) around objects in the sampling phase can further help us understand the functional significance of these various projections from different structures to VIP cells in the MEC.

Another hypothetical experiment could examine the interaction of VIP cells in the MEC with the MS. The MS acts as a generator for theta oscillations, which are prominent during active exploration and coordinate the activity of different cell types in the MEC, including principal cells, interneurons, and grid cells, contributing to the formation and updating of spatial representations (Pastoll, Ramsden, and Nolan 2012; Brandon et al. 2011). In the hippocampus, VIP cells were shown to be active during theta off cycles and during quiet wakefulness (Francavilla et al. 2018). From our results, we find that VIP cells receive cholinergic input from the MS and therefore believe that this projection may play a vital role when the animal is actively exploring the arena during the sampling phase of the dissimilar phase of the novel location task.

By further investigating the connections between various input areas and VIP cells, we can enhance our understanding of their contributions within the MEC circuitry in awake behaving animals. In this study, our behavioral task focuses on examining the involvement of these cells in spatial tasks and shows that VIP cells are essential for discriminating spatial memories. However, this task is not suited to test the animal's ability to learn and recall contextual information or study encoding vs retrieval (such as fear conditioning (Krabbe et al. 2019)) or tests the animal's ability to utilize only self-location cues and inputs for navigation (like path integration (Rowland et al. 2018; McNaughton et al. 2006)). Therefore, it would be valuable to explore the role of VIP cells in paradigms that specifically evaluate their function in these scenarios. Given that VIP cells and the MEC receive diverse inputs from regions like the BLA, RSC, and the ADN - areas involved in the tasks - investigating their role in such contexts would provide valuable insights.

## **Conclusion and Summary**

In conclusion, this study of VIP interneurons in the MEC offers a promising avenue of research to uncover the mechanisms underlying cortical circuit dynamics and cognitive processes. Furthermore, investigating the functional implications of VIP cells beyond spatial memory, including their involvement in other cognitive processes, can enhance our understanding of their role in cortical function. As demonstrated in this thesis, VIP interneurons may play a critical role in maintaining the balance between excitation and inhibition within the MEC, facilitating the coordination of activity across multiple brain regions and contributing to the overall functioning of the MEC.

## Figures and Figure Legends

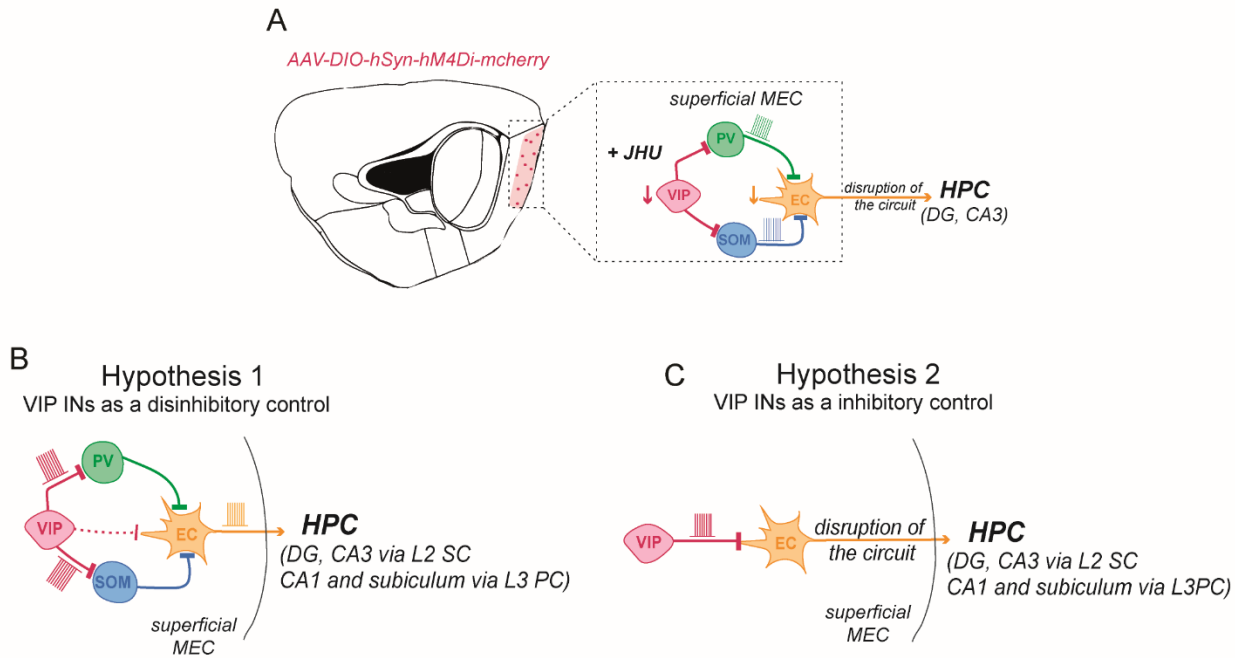


### Figure 1 Potential circuit level-mechanisms mediating disinhibition/inhibition via VIP cells

In Panel A) is a schematic of the MEC with transfection of the inhibitory DREADDs virus.

According to the results, inhibiting VIP cells before sampling leads to a reduction in the activity of excitatory cells (EC) in the MEC.

In Panels B and C are hypothetical ways in which VIP cells could mediate their activity. B) In hypothesis 1, VIP cells exert an inhibitory effect on the interneurons with a minor inhibitory projection onto the excitatory cells. In C) VIP cells directly inhibit the activity of the excitatory cells in the MEC.

Excitatory cells include layer 2 stellate cells and layer 3 pyramidal cells.

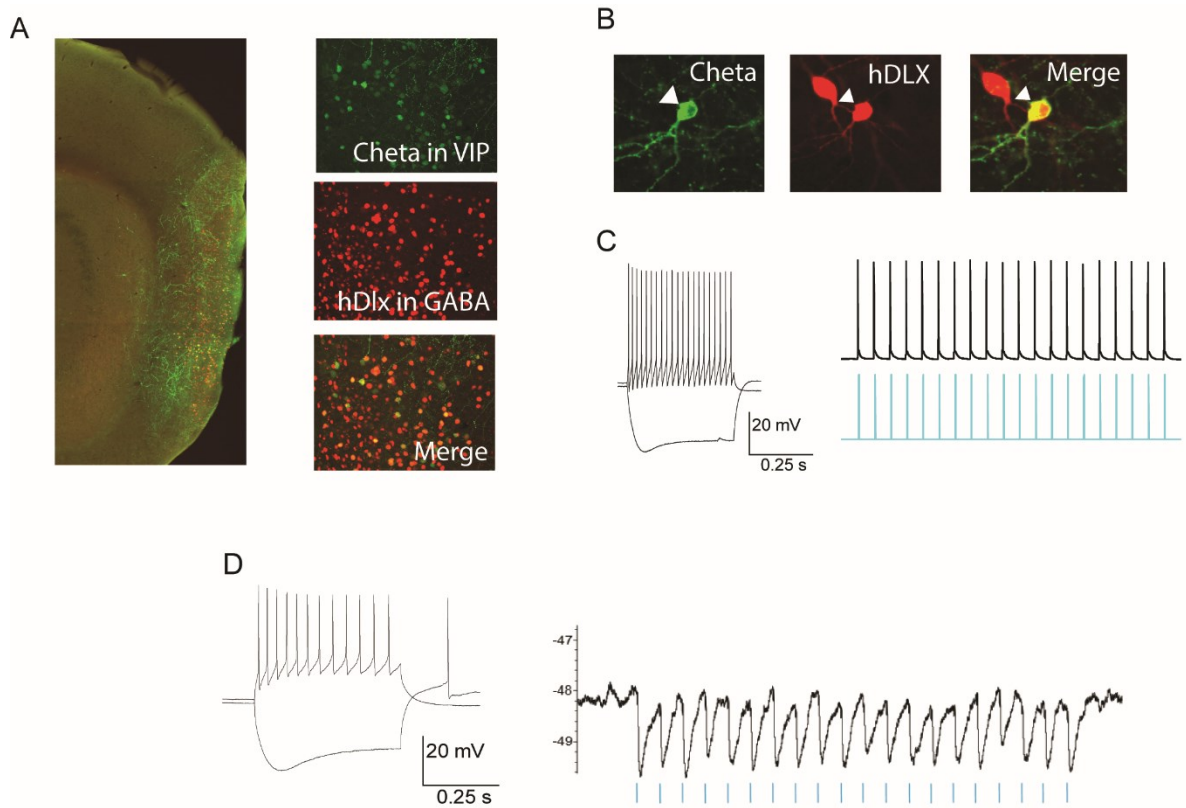


## Figure 2 Identifying post-synaptic targets of VIP cells in the MEC

In Panel A) a representative section of the MEC is shown, where a combination of AAV-Ef1a-DIO ChETA-EYFP and pAAV-hDlx-GiDREADD-dTomato viruses is exclusively injected to target interneurons. The interneurons are identified by the red fluorescent protein (RFP) signal.

In Panel B) we specifically stimulate VIP cells using a stimulation frequency of 5Hz with a 500ms interval between each pulse, for a total duration of 4 seconds, aiming to induce action potentials as demonstrated in Panel (C).

In Panel D) under the same stimulation conditions, we observe inhibitory post-synaptic potentials in a putative interneuron. It is important to note that the sample size for this panel is n=1.

## References

- Agster, Kara L. and Burwell, ebecca D. 2009. "Cortical Efferents of the Perirhinal, Postrhinal, and Entorhinal Cortices of the Rat." *Hippocampus*, no. 19: 1159–86. <https://doi.org/10.1002/hipo.20578>.
- Alonso, A, and R Klink. 1993. "Differential Electroresponsiveness of Stellate and Pyramidal-like Cells of Medial Entorhinal Cortex Layer II." *Journal of Neurophysiology* 70 (1): 128–43.
- Armbruster, B. N., X. Li, M. H. Pausch, S. Herlitze, and B. L. Roth. 2007. "Evolving the Lock to Fit the Key to Create a Family of G Protein-Coupled Receptors Potently Activated by an Inert Ligand." *Proceedings of the National Academy of Sciences* 104 (12): 5163–68. <https://doi.org/10.1073/pnas.0700293104>.
- Aronov, Dmitriy, Rhino Nevers, and David W. Tank. 2017. "Mapping of a Non-Spatial Dimension by the Hippocampal–Entorhinal Circuit." *Nature* 543 (7647): 719–22. <https://doi.org/10.1038/nature21692>.
- Ascoli, GA, L Alonso-Nanclares, SA Anderson, G Barrionuevo, R Benavides-Piccione, A Burkhalter, G Buzsaki, et al. 2008. "Petilla Terminology: Nomenclature of Features OfGABAergic Interneurons of the Cerebral Cortex." *Nat Rev Neurosci.* 9: 557–568.
- Barry, C., and N. Burgess. 2014. "Neural Mechanisms of Self-Location." *Current Biology* 24 (8): R330–39. <https://doi.org/10.1016/j.cub.2014.02.049>.
- Batista-Brito, Renata, Martin Vinck, Katie A. Ferguson, Jeremy T. Chang, David Laubender, Gyorgy Lur, James M. Mossner, et al. 2017. "Developmental Dysfunction of VIP Interneurons Impairs Cortical Circuits." *Neuron* 95 (4): 884-895.e9.

<https://doi.org/10.1016/j.neuron.2017.07.034>.

Bayraktar, Tan, Egbert Welker, Tamas F. Freund, Karl Zilles, and Jochen F. Staiger. 2000.

“Neurons Immunoreactive for Vasoactive Intestinal Polypeptide in the Rat Primary Somatosensory Cortex: Morphology and Spatial Relationship to Barrel- Related Columns.” *Journal of Comparative Neurology* 420 (3): 291–304. [https://doi.org/10.1002/\(SICI\)1096-9861\(20000508\)420:3<291::AID-CNE2>3.0.CO;2-H](https://doi.org/10.1002/(SICI)1096-9861(20000508)420:3<291::AID-CNE2>3.0.CO;2-H).

Beier, Kevin T., Elizabeth E. Steinberg, Katherine E. Deloach, Stanley Xie, Kazunari Miyamichi,

Lindsay Schwarz, Xiaojing J. Gao, Eric J. Kremer, Robert C. Malenka, and Liqun Luo. 2015. “Circuit Architecture of VTA Dopamine Neurons Revealed by Systematic Input-Output Mapping.” *Cell* 162 (3): 622–34. <https://doi.org/10.1016/j.cell.2015.07.015>.

Boccaro, Charlotte N., Francesca Sargolini, Veslemøy Hult Thoresen, Trygve Solstad, Menno P.

Witter, Edvard I. Moser, and May-Britt Moser. 2010. “Grid Cells in Pre- and Parasubiculum.” *Nature Neuroscience* 13 (8): 987–94. <https://doi.org/10.1038/nn.2602>.

Bonaventura, Jordi, Mark A.G. Eldridge, Feng Hu, Juan L. Gomez, Marta Sanchez-Soto, Ara M.

Abramyan, Sherry Lam, et al. 2019. “High-Potency Ligands for DREADD Imaging and Activation in Rodents and Monkeys.” *Nature Communications* 10 (1). <https://doi.org/10.1038/s41467-019-12236-z>.

Bonnevie, Tora, Benjamin Dunn, Marianne Fyhn, Torkel Hafting, Dori Derdikman, John L. Kubie,

Yasser Roudi, Edvard I. Moser, and May-Britt Moser. 2013. “Grid Cells Require Excitatory Drive from the Hippocampus.” *Nature Neuroscience* 16 (3): 309–17. <https://doi.org/10.1038/nn.3311>.

Brandon, Mark P., Andrew R. Bogaard, Christopher P. Libby, Michael A. Connerney, Kishan

- Gupta, and Michael E. Hasselmo. 2011. "Reduction of Theta Rhythm Dissociates Grid Cell Spatial Periodicity from Directional Tuning." *Science* 332 (6029): 595–99. <https://doi.org/10.1126/science.1201652>.
- Brun, Vegard Heimly, Trygve Solstad, Kirsten Brun Kjelstrup, Marianne Fyhn, Menno P. Witter, Edvard I. Moser, and May Britt Moser. 2008. "Progressive Increase in Grid Scale from Dorsal to Ventral Medial Entorhinal Cortex." *Hippocampus* 18 (12): 1200–1212. <https://doi.org/10.1002/hipo.20504>.
- Buetfering, Christina, Kevin Allen, and Hannah Monyer. 2014. "Parvalbumin Interneurons Provide Grid Cell-Driven Recurrent Inhibition in the Medial Entorhinal Cortex." *Nature Neuroscience* 17 (5): 710–18. <https://doi.org/10.1038/nn.3696>.
- Butler, William N., Kiah Hardcastle, and Lisa M. Giocomo. 2019. "Remembered Reward Locations Restructure Entorhinal Spatial Maps." *Science* 363 (6434): 1447–52. <https://doi.org/10.1126/science.aav5297>.
- Canto, Cathrin B., Floris G. Wouterlood, and Menno P. Witter. 2008. "What Does the Anatomical Organization of the Entorhinal Cortex Tell Us?" *Neural Plasticity* 2008. <https://doi.org/10.1155/2008/381243>.
- Caputi, Antonio, Xinghua Liu, Elke C. Fuchs, Yu Chao Liu, and Hannah Monyer. 2022. "Medial Entorhinal Cortex Commissural Input Regulates the Activity of Spatially and Object-Tuned Cells Contributing to Episodic Memory." *Neuron* 110 (20): 3389–3405.e7. <https://doi.org/10.1016/j.neuron.2022.08.013>.
- Chao, Owen Y., Susanne Nikolaus, Yi Mei Yang, and Joseph P. Huston. 2022. "Neuronal Circuitry for Recognition Memory of Object and Place in Rodent Models." *Neuroscience and*

Couey, Jonathan J, Aree Witoelar, Sheng-Jia Zhang, Kang Zheng, Jing Ye, Benjamin Dunn, Rafal Czajkowski, et al. 2013. "Recurrent Inhibitory Circuitry as a Mechanism for Grid Formation." *Nature Neuroscience* 16 (3): 318–24. <https://doi.org/10.1038/nn.3310>.

Deng, Wei, James B Aimone, and Fred H Gage. 2010. "New Neurons and New Memories: How Does Adult Hippocampal Neurogenesis Affect Learning and Memory?" *Nature Reviews Neuroscience* 11 (5): 339–50. <https://doi.org/10.1038/nrn2822>.

Diehl, Geoffrey W, Olivia J Hon, Stefan Leutgeb, Jill K Leutgeb, San Diego, La Jolla, San Diego, and La Jolla. 2017. "Grid and Non-Grid Cells in Medial Entorhinal Cortex Represent Spatial Location and Environmental Features with Complementary Coding Schemes." *Neuron* 94 (1): 83–92. <https://doi.org/10.1016/j.neuron.2017.03.004>.Grid.

Dimidschstein, Jordane, Qian Chen, Robin Tremblay, Stephanie L. Rogers, Giuseppe Antonio Saldi, Lihua Guo, Qing Xu, et al. 2016. "A Viral Strategy for Targeting and Manipulating Interneurons across Vertebrate Species." *Nature Neuroscience* 19 (12): 1743–49. <https://doi.org/10.1038/nn.4430>.

Dragunow, M. 1996. "A Role for Immediate-Early Transcription Factors in Learning and Memory." *Behavior Genetics* 26 (3): 293–99. <https://doi.org/10.1007/BF02359385>.

Dudai, Amir, Nadav Yayon, Hermona Soreq, and Michael London. 2021. "Cortical VIP+/ChAT+ Interneurons: From Genetics to Function." *Journal of Neurochemistry* 158 (6): 1320–33. <https://doi.org/10.1111/jnc.15263>.

- Ferrante, Michele, Babak Tahvildari, Alvaro Duque, Muhamed Hadzipasic, David Salkoff, Edward William Zagher, Michael E. Hasselmo, and David A. McCormick. 2017. “Distinct Functional Groups Emerge from the Intrinsic Properties of Molecularly Identified Entorhinal Interneurons and Principal Cells.” *Cerebral Cortex* 27 (6): 3186–3207. <https://doi.org/10.1093/cercor/bhw143>.
- Fiorilli, J, P Marchesi, T Ruikes, R Buckton, M Duque Quintero, and J Bjaalie. 2023. “Neural Correlates of Object Identity and Reward Outcome in the Corticohippocampal Hierarchy : Double Dissociation between Perirhinal and Secondary Visual Cortex.”
- Francavilla, Ruggiero, Vincent Villette, Xiao Luo, Simon Chamberland, Einer Muñoz-Pino, Olivier Camiré, Kristina Wagner, Viktor Kis, Peter Somogyi, and Lisa Topolnik. 2018. “Connectivity and Network State-Dependent Recruitment of Long-Range VIP-GABAergic Neurons in the Mouse Hippocampus.” *Nature Communications* 9 (1): 1–17. <https://doi.org/10.1038/s41467-018-07162-5>.
- Fu, Yu, Jason M. Tucciarone, J. Sebastian Espinosa, Nengyin Sheng, Daniel P. Darcy, Roger A. Nicoll, Z. Josh Huang, and Michael P. Stryker. 2014. “A Cortical Circuit for Gain Control by Behavioral State.” *Cell* 156 (6): 1139–52. <https://doi.org/10.1016/j.cell.2014.01.050>.
- Fuchs, Elke C., Angela Neitz, Roberta Pinna, Sarah Melzer, Antonio Caputi, and Hannah Monyer. 2016. “Local and Distant Input Controlling Excitation in Layer II of the Medial Entorhinal Cortex.” *Neuron* 89 (1): 194–208. <https://doi.org/10.1016/j.neuron.2015.11.029>.
- Gerlei, Klára Z., Christina M. Brown, Gülşen Sürmeli, and Matthew F. Nolan. 2021. “Deep Entorhinal Cortex: From Circuit Organization to Spatial Cognition and Memory.” *Trends in Neurosciences* 44 (11): 876–87. <https://doi.org/10.1016/j.tins.2021.08.003>.

- Geva-Sagiv, Maya, Liora Las, Yossi Yovel, and Nachum Ulanovsky. 2015. "Spatial Cognition in Bats and Rats: From Sensory Acquisition to Multiscale Maps and Navigation." *Nature Reviews Neuroscience* 16 (2): 94–108. <https://doi.org/10.1038/nrn3888>.
- Giocomo, Lisa M., Syed a. Hussaini, Fan Zheng, Eric R. Kandel, May Britt Moser, and Edvard I. Moser. 2011. "Grid Cells Use HCN1 Channels for Spatial Scaling." *Cell* 147 (5): 1159–70. <https://doi.org/10.1016/j.cell.2011.08.051>.
- Gonzalez-Sulser, A., D. Parthier, A. Candela, C. McClure, H. Pastoll, D. Garden, G. Surmeli, and M. F. Nolan. 2014. "GABAergic Projections from the Medial Septum Selectively Inhibit Interneurons in the Medial Entorhinal Cortex." *Journal of Neuroscience* 34 (50): 16739–43. <https://doi.org/10.1523/JNEUROSCI.1612-14.2014>.
- Groen, Thomas Van, and J. Michael Wyss. 1995. "Projections from the Anterodorsal and Anteroveniral Nucleus of the Thalamus to the Limbic Cortex in the Rat." *Journal of Comparative Neurology* 358 (4): 584–604. <https://doi.org/10.1002/cne.903580411>.
- Gulyás, a I, N Hájos, and T F Freund. 1996. "Interneurons Containing Calretinin Are Specialized to Control Other Interneurons in the Rat Hippocampus." *The Journal of Neuroscience : The Official Journal of the Society for Neuroscience* 16 (10): 3397–3411. <https://doi.org/10.1523/JNEUROSCI.16-10-03397.1996>.
- Hafting, T., M. Fyhn, S. Molden, M. Moser, and E. I. Moser. 2005. "Microstructure of a Spatial Map in the Entorhinal Cortex." *Nature* 436 (7052): 801–6. <https://doi.org/10.1038/nature03721>.
- Høydal, Øyvind Arne, Emilie Ranheim Skytøen, Sebastian Ola Andersson, May Britt Moser, and Edvard I. Moser. 2019. "Object-Vector Coding in the Medial Entorhinal Cortex." *Nature* 568

(7752): 400–404. <https://doi.org/10.1038/s41586-019-1077-7>.

Hull, Clark Leonard. 1943. “Principles of Behavior: An Introduction to Behavior Theory.”

Iyer, Shrivats M., Sam Vesuna, Charu Ramakrishnan, Karen Huynh, Stephanie Young, Andre Berndt, Soo Yeun Lee, Christopher J. Gorini, Karl Deisseroth, and Scott L. Delp. 2016. “Optogenetic and Chemogenetic Strategies for Sustained Inhibition of Pain.” *Scientific Reports* 6 (August): 1–10. <https://doi.org/10.1038/srep30570>.

Jacobs, Joshua, Michael J. Kahana, Arne D. Ekstrom, Matthew V. Mollison, and Itzhak Fried. 2010. “A Sense of Direction in Human Entorhinal Cortex.” *Proceedings of the National Academy of Sciences* 107 (14): 6487–92. <https://doi.org/10.1073/pnas.0911213107>.

Kang, Louis, and Vijay Balasubramanian. 2019. “A Geometric Attractor Mechanism for Self-Organization of Entorhinal Grid Modules.” *ELife* 8. <https://doi.org/10.7554/elife.46687>.

Kanter, Benjamin R., Christine M. Lykken, Daniel Avesar, Aldis Weible, Jasmine Dickinson, Benjamin Dunn, Nils Z. Borgesius, Yasser Roudi, and Clifford G. Kentros. 2017. “A Novel Mechanism for the Grid-to-Place Cell Transformation Revealed by Transgenic Depolarization of Medial Entorhinal Cortex Layer II.” *Neuron* 93 (6): 1480-1492.e6. <https://doi.org/10.1016/j.neuron.2017.03.001>.

Karnani, M. M., J. Jackson, I. Ayzenshtat, A. Hamzehei Sichani, K. Manoocheri, S. Kim, and R. Yuste. 2016. “Opening Holes in the Blanket of Inhibition: Localized Lateral Disinhibition by VIP Interneurons.” *Journal of Neuroscience* 36 (12): 3471–80. <https://doi.org/10.1523/JNEUROSCI.3646-15.2016>.

Kepecs, Adam, and Gordon Fishell. 2014. “Interneuron Cell Types Are Fit to Function.” *Nature*

505 (7483): 318–26. <https://doi.org/10.1038/nature12983>.

Kinnavane, Lisa, Eman Amin, Cristian M. Olarte-Sánchez, and John P. Aggleton. 2017. “Medial Temporal Pathways for Contextual Learning: Network c- *Fos* Mapping in Rats with or without Perirhinal Cortex Lesions.” *Brain and Neuroscience Advances* 1: 239821281769416. <https://doi.org/10.1177/2398212817694167>.

Kitamura, Takashi, Chen Sun, Jared Martin, Lacey J. Kitch, Mark J. Schnitzer, and Susumu Tonegawa. 2015. “Entorhinal Cortical Ocean Cells Encode Specific Contexts and Drive Context-Specific Fear Memory.” *Neuron* 87 (6): 1317–31. <https://doi.org/10.1016/j.neuron.2015.08.036>.

Klink, R, and a Alonso. 1997. “Morphological Characteristics of Layer II Projection Neurons in the Rat Medial Entorhinal Cortex.” *Hippocampus* 7 (5): 571–83. [https://doi.org/10.1002/\(SICI\)1098-1063\(1997\)7:5<571::AID-HIPO12>3.0.CO;2-Y](https://doi.org/10.1002/(SICI)1098-1063(1997)7:5<571::AID-HIPO12>3.0.CO;2-Y).

Kovács, Krisztina J. 2008. “Measurement of Immediate-Early Gene Activation- c-Fos and Beyond.” *Journal of Neuroendocrinology* 20 (6): 665–72. <https://doi.org/10.1111/j.1365-2826.2008.01734.x>.

Krabbe, Sabine, Enrica Paradiso, Simon D’Aquin, Yael Bitterman, Julien Courtin, Chun Xu, Keisuke Yonehara, et al. 2019. “Adaptive Disinhibitory Gating by VIP Interneurons Permits Associative Learning.” *Nature Neuroscience* 22 (11): 1834–43. <https://doi.org/10.1038/s41593-019-0508-y>.

Lashley, K S. 1929. *Brain Mechanisms and Intelligence: A Quantitative Study of Injuries to the Brain. Brain Mechanisms and Intelligence: A Quantitative Study of Injuries to the Brain.* Chicago, IL, US: University of Chicago Press. <https://doi.org/10.1037/10017-000>.

- Lee, Candice, Sandrine L. Côté, Nima Raman, Hritvic Chaudhary, Bryan C. Mercado, and Simon X. Chen. 2023. “Whole-Brain Mapping of Long-Range Inputs to the VIP-Expressing Inhibitory Neurons in the Primary Motor Cortex.” *Frontiers in Neural Circuits* 17 (May): 1093066. <https://doi.org/10.3389/fncir.2023.1093066>.
- Lee, Soohyun, Illya Kruglikov, Z Josh Huang, Gord Fishell, and Bernardo Rudy. 2013. “A Disinhibitory Circuit Mediates Motor Integration in the Somatosensory Cortex.” *Nature Neuroscience* 16 (11): 1662–70. <https://doi.org/10.1038/nn.3544>.
- Letzkus, Johannes J., Steffen B.E. Wolff, and Andreas Lüthi. 2015. “Disinhibition, a Circuit Mechanism for Associative Learning and Memory.” *Neuron* 88 (2): 264–76. <https://doi.org/10.1016/j.neuron.2015.09.024>.
- Lu, Jian, Zhouzhou Zhang, Xinxin Yin, Yingjun Tang, Runan Ji, Han Chen, Yu Guang, et al. 2022. “An Entorhinal-Visual Cortical Circuit Regulates Depression-like Behaviors.” *Molecular Psychiatry* 27 (9): 3807–20. <https://doi.org/10.1038/s41380-022-01540-8>.
- McNaughton, Bruce L., Francesco P. Battaglia, Ole Jensen, Edvard I Moser, and May-Britt Moser. 2006. “Path Integration and the Neural Basis of the ‘Cognitive Map.’” *Nature Reviews Neuroscience* 7 (8): 663–78. <https://doi.org/10.1038/nrn1932>.
- Miao, Chenglin, Qichen Cao, May-britt Moser, and Edvard I Moser. 2017. “Parvalbumin and Somatostatin Interneurons Control Different Space-Coding Networks in the Medial Entorhinal Cortex.” *Cell* 171 (3): 1–15. <https://doi.org/10.1016/j.cell.2017.08.050>.
- Mittelstaedt, M. L., and H. Mittelstaedt. 1980. “Homing by Path Integration in a Mammal.” *Naturwissenschaften* 67 (11): 566–67. <https://doi.org/10.1007/BF00450672>.

- Miyashita, Teiko, Stepan Kubik, Nahideh Haghghi, Oswald Steward, and John F. Guzowski. 2009. "Rapid Activation of Plasticity-Associated Gene Transcription in Hippocampal Neurons Provides a Mechanism for Encoding of One-Trial Experience." *Journal of Neuroscience* 29 (4): 898–906. <https://doi.org/10.1523/JNEUROSCI.4588-08.2009>.
- Moser, Edvard I., Yasser Roudi, Menno P. Witter, Clifford Kentros, Tobias Bonhoeffer, and May-Britt Moser. 2014. "Grid Cells and Cortical Representation." *Nature Reviews Neuroscience* 15 (7): 466–81. <https://doi.org/10.1038/nrn3766>.
- Moser, Edvard I., Emilio Kropff, and May-Britt Moser. 2008. "Place Cells, Grid Cells, and the Brain's Spatial Representation System." *Annu. Rev. Neurosci.* 31: 69–89. <https://doi.org/10.1146/annurev.neuro.31.061307.090723>.
- Nilssen, Eirik S., Thanh P. Doan, Shinya Ohara, and Menno P. Witter. 2019. "A Reappraisal of the Lateral and Medial Entorhinal Subdivisions Mediating Parallel Cortical Pathways." *Hippocampus* in press (June): 1–17. <https://doi.org/10.1002/hipo.23145>.
- O'Keefe, J., and J. Dostrovsky. 1971. "The Hippocampus as a Spatial Map. Preliminary Evidence from Unit Activity in the Freely-Moving Rat." *Brain Research*. [https://doi.org/10.1016/0006-8993\(71\)90358-1](https://doi.org/10.1016/0006-8993(71)90358-1).
- O'Keefe, John, and Lynn Nadel. 1978. *The Hippocampus as a Cognitive Map*. Oxford; New York: Clarendon Press ; Oxford University Press.
- Paspalas, Constantinos D., and Georgios C. Papadopoulos. 2001. "Serotonergic Afferents Preferentially Innervate Distinct Subclasses of Peptidergic Interneurons in the Rat Visual Cortex." *Brain Research* 891 (1–2): 158–67. [https://doi.org/10.1016/S0006-8993\(00\)03193-0](https://doi.org/10.1016/S0006-8993(00)03193-0).

- Pastoll, Hugh, Helen L. Ramsden, and Matthew F. Nolan. 2012. “Intrinsic Electrophysiological Properties of Entorhinal Cortex Stellate Cells and Their Contribution to Grid Cell Firing Fields.” *Frontiers in Neural Circuits* 6 (April): 1–21. <https://doi.org/10.3389/fncir.2012.00017>.
- Pi, Hyun-Jae, Balázs Hangya, Duda Kvitsiani, Joshua I. Sanders, Z. Josh Huang, and Adam Kepecs. 2013. “Cortical Interneurons That Specialize in Disinhibitory Control.” *Nature* 503 (7477): 521–24. <https://doi.org/10.1038/nature12676>.
- Poulter, Steven, Tom Hartley, and Colin Lever. 2018. “The Neurobiology of Mammalian Navigation.” *Current Biology* 28 (17): R1023–42. <https://doi.org/10.1016/j.cub.2018.05.050>.
- Prönneke, Alvar, Bianca Scheuer, Robin J. Wagener, Martin Möck, Mirko Witte, and Jochen F. Staiger. 2015. “Characterizing VIP Neurons in the Barrel Cortex of VIPcre/TdTomato Mice Reveals Layer-Specific Differences.” *Cerebral Cortex* 25 (12): 4854–68. <https://doi.org/10.1093/cercor/bhv202>.
- Prönneke, Alvar, Mirko Witte, Martin Möck, and Jochen F. Staiger. 2020. “Neuromodulation Leads to a Burst-Tonic Switch in a Subset of VIP Neurons in Mouse Primary Somatosensory (Barrel) Cortex.” *Cerebral Cortex (New York, N.Y. : 1991)* 30 (2): 488–504. <https://doi.org/10.1093/cercor/bhz102>.
- Ramón y Cajal, Santiago. 1909. *Histologie Du Système Nerveux de l'homme & Des Vertébrés* . Ed. française. Vol. v. 1. Paris: Maloine.
- . 1968. *The Structure of Ammon's Horn. TA - TT* -. Springfield, Ill. SE - xxii, 78 pages illustrations 24 cm: C.C. Thomas.

- Ramsden, Helen L, Gülşen Sürmeli, Steven G McDonagh, and Matthew F Nolan. 2015. "Laminar and Dorsoventral Molecular Organization of the Medial Entorhinal Cortex Revealed by Large-Scale Anatomical Analysis of Gene Expression." *PLoS Computational Biology* 11 (1): e1004032. <https://doi.org/10.1371/journal.pcbi.1004032>.
- Rhomberg, Thomas, Laura Rovira-Esteban, Attila Vikór, Enrica Paradiso, Christian Kremser, Petra Nagy-Pál, Orsolya I Papp, et al. 2018. "VIP-Immunoreactive Interneurons within Circuits of the Mouse Basolateral Amygdala." *The Journal of Neuroscience* 38 (31): 2063–17. <https://doi.org/10.1523/JNEUROSCI.2063-17.2018>.
- Roth, Bryan L. 2016. "DREADDs for Neuroscientists." *Neuron* 89 (4): 683–94. <https://doi.org/10.1016/j.neuron.2016.01.040>.
- Rowland, David C., Horst A. Obenaus, Emilie R. Skytøen, Qiangwei Zhang, Cliff G. Kentros, Edvard I. Moser, and May Britt Moser. 2018. "Functional Properties of Stellate Cells in Medial Entorhinal Cortex Layer II." *eLife* 7: 1–17. <https://doi.org/10.7554/eLife.36664>.
- Rudy, Bernardo Rudy, Gordon Fishell, SooHyun Lee, and Jens Leffler-Hjerling. 2013. "Three Groups of Interneurons Account for Nearly 100% of Neocortical GABAergic Neurons" 71 (1): 45–61. <https://doi.org/10.1002/dneu.20853>.
- Saloman, Jami L., Nicole N. Scheff, Lindsey M. Snyder, Sarah E. Ross, Brian M. Davis, and Michael S. Gold. 2016. "Gi-DREADD Expression in Peripheral Nerves Produces Ligand-Dependent Analgesia, as Well as Ligand-Independent Functional Changes in Sensory Neurons." *The Journal of Neuroscience* 36 (42): 10769–81. <https://doi.org/10.1523/JNEUROSCI.3480-15.2016>.
- Sargolini, Francesca, Marianne Fyhn, Torkel Hafting, Bruce L McNaughton, Menno P Witter,

- May-Britt Moser, and Edvard I Moser. 2006. “Conjunctive Representation of Position, Direction, and Velocity in Entorhinal Cortex.” *Science* 312 (5774): 758–62.
- Schlesiger, Magdalene Isabell, Tobias Ruff, Duncan Archibald Allan MacLaren, Isabel Barriuso-Ortega, Khalid Magomedovich Saidov, Ting Yun Yen, and Hannah Monyer. 2021. “Two Septal-Entorhinal GABAergic Projections Differentially Control Coding Properties of Spatially Tuned Neurons in the Medial Entorhinal Cortex.” *Cell Reports* 34 (9): 108801. <https://doi.org/10.1016/J.CELREP.2021.108801>.
- Schmidt-Hieber, Christoph, and Matthew F. Nolan. 2017. “Synaptic Integrative Mechanisms for Spatial Cognition.” *Nature Neuroscience* 20 (11): 1483–92. <https://doi.org/10.1038/nn.4652>.
- Solstad, Trygve, Trygve Solstad, Charlotte N Boccara, Charlotte N Boccara, Emilio Kropff, Emilio Kropff, May-Britt Moser, May-Britt Moser, Edvard I Moser, and Edvard I Moser. 2008. “Representation of Geometric Borders in the Entorhinal Cortex.” *Science* 322 (December): 1865–68. <https://doi.org/10.1126/science.1166466>.
- Stachniak, Tevye J., Anirvan Ghosh, and Scott M. Sternson. 2014. “Chemogenetic Synaptic Silencing of Neural Circuits Localizes a Hypothalamus→Midbrain Pathway for Feeding Behavior.” *Neuron* 82 (4): 797–808. <https://doi.org/10.1016/j.neuron.2014.04.008>.
- Sürmeli, Gülşen, Daniel Cosmin Marcu, Christina McClure, Derek L F Garden, Hugh Pastoll, and Matthew F. Nolan. 2015. “Molecularly Defined Circuitry Reveals Input-Output Segregation in Deep Layers of the Medial Entorhinal Cortex.” *Neuron* 88 (5): 1040–53. <https://doi.org/10.1016/j.neuron.2015.10.041>.
- Swanson, L. W., and C. Kohler. 1986. “Anatomical Evidence for Direct Projections from the Entorhinal Area to the Entire Cortical Mantle in the Rat.” *Journal of Neuroscience* 6 (10):

3010–23. <https://doi.org/10.1523/jneurosci.06-10-03010.1986>.

Sziklas, V. 1999. “The Effects of Lesions to the Anterior Thalamic Nuclei on Object-Place Associations in Rats.” *European Journal of Neuroscience* 11 (2): 559–66. <https://doi.org/10.1046/j.1460-9568.1999.00448.x>.

Tang, Qiusong, Andrea Burgalossi, Christian Laut Ebbesen, Saikat Ray, Robert Naumann, Helene Schmidt, Dominik Spicher, and Michael Brecht. 2014. “Pyramidal and Stellate Cell Specificity of Grid and Border Representations in Layer 2 of Medial Entorhinal Cortex.” *Neuron* 84 (6): 1191–97. <https://doi.org/10.1016/j.neuron.2014.11.009>.

Taube, J S, Robert U Muller, and J B Ranck. 1990. “Head-Direction Cells Recorded from the Postsubiculum in Freely Moving Rats. I. Description and Quantitative Analysis.” *The Journal of Neuroscience: The Official Journal of the Society for Neuroscience* 10 (2): 420–35. <https://doi.org/10.1212/01.wnl.0000299117.48935.2e>.

Taube, Jeffrey S. 1998. “Head Direction Cells and the Neurophysiological Basis for a Sense of Direction.” *Progress in Neurobiology* 55 (3): 225–56. [https://doi.org/10.1016/S0301-0082\(98\)00004-5](https://doi.org/10.1016/S0301-0082(98)00004-5).

Tennant, Sarah A, Lukas Fischer, Derek L F Garden, Klara Zsofia Gerliei, Cristina Martinez-Gonzalez, Christina McClure, Emma R Wood, and Matthew F Nolan. 2018. “Stellate Cells in the Medial Entorhinal Cortex Are Required for Spatial Learning,” 1313–24. <https://doi.org/10.1016/j.celrep.2018.01.005>.

Tolman, E C, B F Ritchie, and D Kalish. 1946. “Studies in Spatial Learning. II. Place Learning versus Response Learning.” *Journal of Experimental Psychology* 36 (3): 221–29. <https://doi.org/10.1037/h0060262>.

- Topolnik, Lisa, and Suhel Tamboli. 2022. “The Role of Inhibitory Circuits in Hippocampal Memory Processing.” *Nature Reviews Neuroscience* 23 (8): 476–92. <https://doi.org/10.1038/s41583-022-00599-0>.
- Tremblay, Robin, Soohyun Lee, and Bernardo Rudy. 2016. “GABAergic Interneurons in the Neocortex: From Cellular Properties to Circuits.” *Neuron* 91 (2): 260–92. <https://doi.org/10.1016/j.neuron.2016.06.033>.
- Tsoi, Sau Yee, Merve Öncül, Ella Svahn, Mark Robertson, Zuzanna Bogdanowicz, Christina McClure, and Gulşen Sürmeli. 2022. “Telencephalic Outputs from the Medial Entorhinal Cortex Are Copied Directly to the Hippocampus.” *ELife* 11: 1–19. <https://doi.org/10.7554/ELIFE.73162>.
- Turi, Gergely Farkas, Wen Ke Li, Spyridon Chavlis, Ioanna Pandi, Justin O’Hare, James Benjamin Priestley, Andres Daniel Grosmark, et al. 2019. “Vasoactive Intestinal Polypeptide-Expressing Interneurons in the Hippocampus Support Goal-Oriented Spatial Learning.” *Neuron* 101 (6): 1150-1165.e8. <https://doi.org/10.1016/j.neuron.2019.01.009>.
- Tyan, L., S. Chamberland, E. Magnin, O. Camire, R. Francavilla, L. S. David, K. Deisseroth, and L. Topolnik. 2014. “Dendritic Inhibition Provided by Interneuron-Specific Cells Controls the Firing Rate and Timing of the Hippocampal Feedback Inhibitory Circuitry.” *Journal of Neuroscience* 34 (13): 4534–47. <https://doi.org/10.1523/JNEUROSCI.3813-13.2014>.
- Urban, Daniel J., and Bryan L. Roth. 2015. “DREADDs (Designer Receptors Exclusively Activated by Designer Drugs): Chemogenetic Tools with Therapeutic Utility.” *Annual Review of Pharmacology and Toxicology* 55 (1): 399–417. <https://doi.org/10.1146/annurev-pharmtox-010814-124803>.

- Wall, Nicholas R., Mauricio de la Parra, Jordan M. Sorokin, Hiroki Taniguchi, Z. Josh Huang, and Edward M. Callaway. 2016. "Brain-Wide Maps of Synaptic Input to Cortical Interneurons." *Journal of Neuroscience* 36 (14): 4000–4009. <https://doi.org/10.1523/JNEUROSCI.3967-15.2016>.
- Wehner, R. 2003. "Desert Ant Navigation: How Miniature Brains Solve Complex Tasks." *Journal of Comparative Physiology A: Neuroethology, Sensory, Neural, and Behavioral Physiology* 189 (8): 579–88. <https://doi.org/10.1007/s00359-003-0431-1>.
- Wickersham, Ian R., David C. Lyon, Richard J O Barnard, Takuma Mori, Stefan Finke, Karl Klaus Conzelmann, John A T Young, and Edward M. Callaway. 2007. "Monosynaptic Restriction of Transsynaptic Tracing from Single, Genetically Targeted Neurons." *Neuron* 53 (5): 639–47. <https://doi.org/10.1016/j.neuron.2007.01.033>.
- Wiegert, J Simon, Mathias Mahn, Matthias Prigge, Yoav Printz, and Ofer Yizhar. 2017. "Silencing Neurons: Tools, Applications, and Experimental Constraints." *Neuron* 95 (3): 504–29. <https://doi.org/10.1016/j.neuron.2017.06.050>.
- Winter, Shawn S., Benjamin J. Clark, and J S Taube. 2015. "Disruption of the Head Direction Cell Network Impairs the Parahippocampal Grid Cell Signal." *Science* 347 (6224): 1–6. <https://doi.org/https://doi.org/10.1126/science.1259591>.
- Winterer, Jochen, Nikolaus Maier, Christian Wozny, Prateep Beed, Jörg Breustedt, Roberta Evangelista, Yangfan Peng, Tiziano D'Albis, Richard Kempter, and Dietmar Schmitz. 2017. "Excitatory Microcircuits within Superficial Layers of the Medial Entorhinal Cortex." *Cell Reports* 19 (6): 1110–16. <https://doi.org/10.1016/j.celrep.2017.04.041>.
- Witter, Menno P., Thanh P. Doan, Bente Jacobsen, Eirik S. Nilssen, and Shinya Ohara. 2017.

“Architecture of the Entorhinal Cortex A Review of Entorhinal Anatomy in Rodents with Some Comparative Notes.” *Frontiers in Systems Neuroscience* 11 (June): 46. <https://doi.org/10.3389/fnsys.2017.00046>.

Zong, Weijian, Horst A. Obenaus, Emilie R. Skytøen, Hanna Eneqvist, Nienke L. de Jong, Ruben Vale, Marina R. Jorge, May Britt Moser, and Edvard I. Moser. 2022. “Large-Scale Two-Photon Calcium Imaging in Freely Moving Mice.” *Cell* 185 (7): 1240-1256.e30. <https://doi.org/10.1016/j.cell.2022.02.017>.

Zutshi, Ipshita, Maylin L Fu, Varoth Lilascharoen, Jill K Leutgeb, Byung Kook Lim, and Stefan Leutgeb. 2018. “Recurrent Circuits within Medial Entorhinal Cortex Superficial Layers Support Grid Cell Firing.” *Nature Communications* 9 (1). <https://doi.org/10.1038/s41467-018-06104-5>.